Supraspinal activity patterns underpinning locomotor diversity in larval zebrafish

Joanna Yen Na Lau

A dissertation submitted in partial fulfilment
of the requirements for the degree of
Doctor of Philosophy

Department of Neuroscience, Physiology & Pharmacology
University College London

September 13, 2019

I, Joanna Yen Na Lau, confirm that the work presented in this thesis is my own. Where information has been derived from other sources, I confirm that this has been indicated in the work.

Abstract

How do supraspinal circuits produce the diversity of locomotor outputs needed for an animal's survival? To answer this question, I study the reticulospinal (RS) system of larval zebrafish, as these cells provide the main source of descending motor control. I combine two-photon calcium imaging of RS neurons with high-speed behavioural tracking to study RS activity across a range of kinematically distinct swim types.

Examination of reticulospinal recruitment across different swim types has revealed unique, but partially overlapping activity patterns, suggesting that some cells encode kinematics common to multiple swim types, while others encode kinematics which are characteristic of a specific swim type. By developing regression-based encoding models which describe a cell's activity using low-level tail kinematics, we identify "kinematic modules". These modules contain cells with similar kinematic encoding and thus represent the core combinations of kinematic features encoded by RS activity. I find that laser ablation of cells within a module produce specific kinematic deficits without affecting shared elements of locomotion. This data suggest a circuit architecture where kinematic modules can be differentially combined to produce locomotor diversity through the context-specific recruitment of particular groups of RS neurons.

I also describe a novel preparation for the imaging of fluorescent activity indicators in larval zebrafish using an acousto-optic lens microscope. This methodology allows for rapid 3D point scanning of the entire reticulospinal complex during visual stimulus presentation and behavioural tracking. The improved temporal resolution and sampling across the whole population provides an opportunity to examine the relative timing of activity between reticulospinal neurons.

Impact Statement

To study how a defined population of neurons encode a range of locomotor kinematics, I used modern optical techniques to record neural activity during high-speed behavioural tracking. Together with collaborators, I performed an unsupervised classification of larval zebrafish behaviour to identify distinct swim types, developed predictive models which describe supraspinal neural activity using a multitude of features, and adapted a 3D imaging system for use in larval zebrafish.

The classification of partially-restrained larval zebrafish behaviour is of great relevance to researchers using larval zebrafish as a model organism to study the relationship between neural activity and behaviour. The identified swim classes indicate the behavioural diversity which can be produced under these conditions, and act as a reference point for comparison with the behaviours characterised in freely swimming larvae. In addition to this, I describe a protocol enabling the use of high-speed, two-photon AOL microscopy and rapid, online, 3D movement correction with larval zebrafish. This work provides two main benefits to the neuroscientists: The first is that high-speed random access point scanning methods allow the sampling of disparate neuronal populations, and provide a foundation upon which researchers can use optical activity indicators with faster kinetics. The second is that larval zebrafish provide a major challenge to online movement correction, and adapting such a system for use in zebrafish does not only enable its use in this model organism, but also improves the stability of its use in other species.

The analyses described in this thesis will also be useful beyond neuroscience and have applications across various disciplines. Datasets with a large number of predictors which show high collinearity are a common challenge which needs to be overcome when developing predictive models. The solutions presented in this thesis will be useful to those looking to solve these problems.

By applying these various techniques, I describe a circuit architecture to explain how a neuronal population can support diverse motor outputs in a vertebrate

species. This consolidates the present literature and presents new avenues for researchers to explore supraspinal control of locomotion.

Acknowledgements

Firstly, I must thank my supervisor Isaac. I am honoured, and perhaps still disbelieving that you invited me to join your lab. You have been a remarkable teacher throughout, always ready to offer guidance when I needed it most. I feel very lucky to have received your supervision, whether it was advice on analysis, the navigation of various political issues, or even brunch, I cannot thank you enough.

Both this PhD and my own brain has benefited greatly from the expertise of Dr James Fitzgerald. Thank you for your invaluable insight, constant curiosity and patient explanations during all of our meetings.

I have also had the great fortune to have been a part of a truly excellent lab. It has been a privilege to have worked alongside such clever and kind people. Thank you Pedro for welcoming and supporting me; my "acquaintance" Paride for his unwavering kindness and wisdom; Asaph for his intelligence and humour (and for being a fellow admirer of the Desserts™); and Charlie for quick wit, good ideas and tea breaks. I must also acknowledge our lab meeting additions: Eirinn, Chintan, Renato, and Meg for advising on all manner of topics ranging from statistics to electrical circuits, and most importantly for helping to pad out the lab meeting rota.

I also wish to thank Professor Angus Silver and the talented scientists in his lab. Thank you George for helping with various fish illumination designs and to Vicky for valiant reprogramming of the FPGAs. A special *merci beaucoup* to Antoine, a MATLAB extraordinaire. I am so grateful for your selflessness, generosity, and all the Thursday afternoons you donated for the sake of fish.

Thank you also to my secondary supervisor Professor Steve Wilson, I am sure I do not speak for myself when I say that the First Floor is a truly special place to work. Thank you to all members of the First Floor, past and present, for your part in making our working environment what it is today. I am especially grateful to my PhD relations: Renato for his trusted advice and invaluable friendship, Anya for making me laugh until I cried and treasured Southwold adventures, my inspiring desk neighbour Ingrid, MK for all manner of advice, Lisa for her caring nature, and

Shannon for always seeing and hearing me where I was. I must also mention some wonderful post-docs: my snack/distraction neighbour Gaia, and Declan for being my confidant.

A very big thank you to everyone in the excellent UCL Fish Facility. Thank you for your attention and care (both to me and the fish) over the years.

My time at UCL has been greatly improved by the various friends I have made over the years. These include Patrick and Holly, whom despite slipping through the First Floor net, I still value dearly. This also features my fantastic PhD support network of talented individuals: (Drs!) Charlotte Arlt, Lloyd Russell, Henry Dalgleish, and Oli Gauld.

I must also thank some very special supervisors I have had over the years. Drs Amy Milton, Jenn Murray, Dawn Eagle, and Christoph Schmidt-Hieber went above and beyond to help me. Without their teaching and guidance, I would not have been able to embark on a PhD, let alone be completing one today.

To my dear friends, I do not only owe you my endless gratitude for supporting me and saving my sanity, but also an apology for all the times you agreed to meet around weird work hours, and usually somewhere close to the lab. What did I ever do to deserve you all? I am very grateful to have lived with my best friends, Kate and Sean. Thank you for looking after me. And I am happy to have kept such close and true friends as Jynsym, Farzhana, and Siu-Teing for all these years. You are all very special people without whom this PhD would surely not exist.

Last but not least, thank you to my family. I am glad to have had the backing of a family who always supported my education with their selfless spirit. I thank my many talented and kind relatives who have helped me in many ways over the years. I am very grateful to my grandparents, particularly my grandmothers, whom I owe so very much. A final thank you to my parents and brother, for being there all this time.

Table of Contents

List of figures

Chapter 1 Introduction

Whether it is moving towards a valued resource or away from an unpleasant stimulus, all animals need to move within their environment in order to survive. How animals produce and control these movements in a way suited to their surroundings requires the integration of various sensory and internal factors, together with the synergistic control of many muscle groups. This is an undoubtedly complex feat and requires the involvement of many different brain regions, as summarised in Figure 1.1. However, despite the evolutionary separation across vertebrate species, there are some common, basic elements to locomotion, such as the patterned alternation of limbs and muscles, suggesting the possibility of conserved neural mechanisms underlying locomotor control. Here I will describe some of the key findings of vertebrate locomotor control from the bottom-up with a particular focus on the role of the reticular formation and how "simpler" vertebrate species allow the study of locomotor control across defined neural populations.

1.1 Control of rhythmic motor outputs

1.1.1 Spinal cord circuits

How the nervous system generates and controls the rhythmic patterns of motor output observed in vertebrate locomotion has been a constantly evolving area of research in neuroscience. As all vertebrates show a rhythmic, coordinated use of different muscle groups, conserved nervous system elements such as the spinal cord are an attractive place to start one's search for the basis of locomotor control. One early hypothesis of how these behaviours might arise was developed by Charles Sherrington. In his famous work titled "The integrative action of the nervous system", he proposed the reflex-arc as the unit of nervous system motor control. These "simple reflexes" were defined as stereotyped actions initiated by sensory receptors, and

Sherrington posited that “The main secret of nervous co-ordination lies evidently in the compounding of reflexes” (Sherrington, 1911).

Graham Brown went on to disprove Sherrington’s reflex chaining hypothesis by identifying the production of rhythmic motor outputs in the absence of sensory inputs (Graham Brown, 1911). In experiments conducted in cats, Graham Brown transected the dorsal roots innervating the limbs, thus removing sensory input to the spinal cord. Following this transection, Graham Brown found that the ankle flexor and extensor muscles could still produce rhythmic alternating contractions. This demonstrated that the isolated spinal cord can generate reciprocal activity between these muscles without any sensory inputs. Ultimately, this led him to develop the half-centre hypothesis, which proposed the existence of two neuronal networks (half-centres) which mutually inhibit each other to produce alternating contractions in opposing muscle groups. This formed the basis for our current-day understanding of central pattern generators (CPGs) in spinal cord.

Studies in lower vertebrates were critical to the characterisation of these circuits in the spinal cord, and also indicated the presence of descending control from upstream brain regions. In particular, lamprey have proved to be an excellent model organism in which to study spinal circuits due to their greater CNS simplicity in comparison to mammals, and amenability to *in vitro* experimentation. Studies by Grillner et al., found that spinal CPGs feature commissural and local inhibitory interneurons which ensure that only muscles on one side of the network are active at a time (Grillner *et al.*, 1987). In addition to this, the authors also found that bath application of excitatory amino acids, such as glutamate and kainate, to the isolated lamprey spinal cord was able to evoke rhythmic motor outputs as measured from the ventral roots. This observation of spinal CPG activation via excitatory amino acids was supported by studies conducted in other vertebrates, such as tadpoles (Dale and Roberts, 1984). This suggested that while spinal CPGs are able to produce the rhythmic motor patterns of locomotion, the locomotor commands themselves may stem from descending glutamatergic pathways (Grillner and Wallén, 1984).

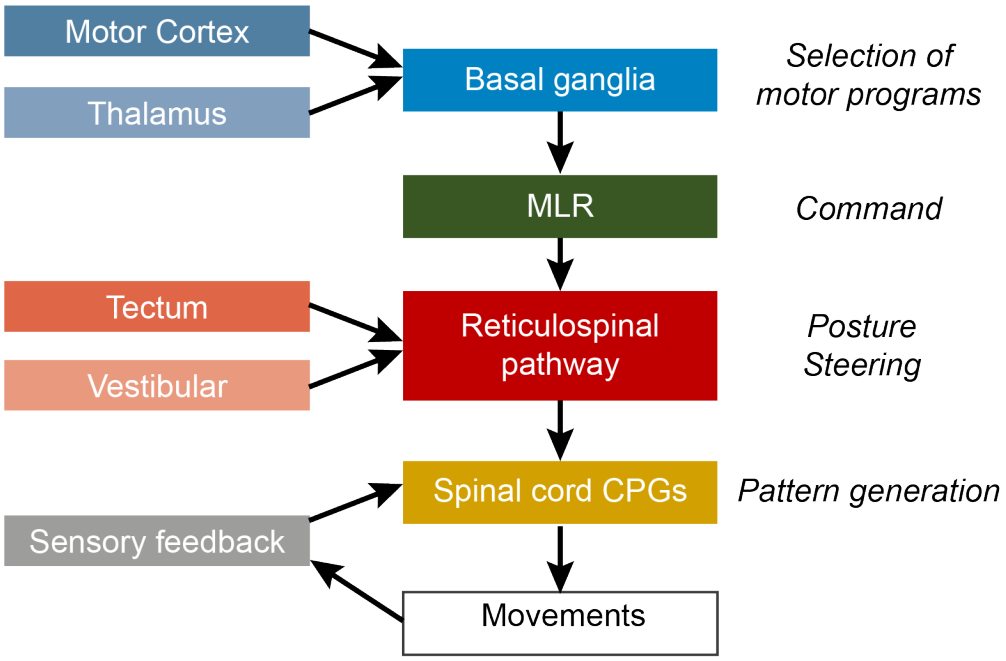

Figure 1.1 Summary of the subsystems involved in locomotor control
Adapted from Grillner et al., 2007. Motor programs selected in the basal ganglia are conveyed to the mesencephalic locomotor region (MLR). Locomotor commands elicit patterned motor output via reticulospinal (RS) projections to spinal cord central pattern generators (CPGs). The RS neurons in the brainstem can act as a site for integration of sensory information.

1.2 Supraspinal motor systems

1.2.1 The mesencephalic locomotor region

Which brain regions provide this descending glutamatergic input for the initiation and control of spinal cord circuits? As shown in Figure 1.1, we now know that there are many levels in the motor hierarchy above the spinal cord, however in the interest of discussing highly conserved regions across vertebrates, I will focus on midbrain and hindbrain regions such as the mesencephalic locomotor region (MLR) and reticular formation. Influential studies by Shik et al., used decerebrate preparations to reveal that these spinal locomotor systems are influenced by the activity of specific brainstem areas, such as the MLR (Shik, Severin and Orlovsky, 1969). In these experiments, the brainstem was transected at the level of the midbrain, resulting in the removal of descending inputs from rostral brain areas to spinal cord

circuits. Shik et al., found that electrical stimulation of a midbrain region, the MLR, in decerebrate cats was capable of producing locomotion. The MLR is defined as a site at which the intensity of electrical stimulation is proportional to the strength of the induced locomotion, and lacks direct projections to the spinal cord. This region has since been identified in numerous vertebrate species including rats (Skinner and Garcia-Rill, 1984), salamanders (Cabelguen, Bourcier-Lucas and Dubuc, 2003), lamprey (Sirota, Di Prisco and Dubuc, 2000), and carp (Kashin, Feldman and Orlovsky, 1974), thus establishing the MLR as a conserved functional element in vertebrate locomotor control.

Since its discovery, the mammalian MLR has been found to be a complex structure consisting of distinct sub-regions and contains cells with different neurotransmitter expression. Two major regions of the mammalian MLR are the cuneiform nucleus (CnF) and the pedunculopontine nucleus (PPN) (Skinner and Garcia-Rill, 1984). Advances in viral and genetic techniques in mouse models have allowed researchers to selectively examine the functions of different neurotransmitter populations within these regions. This has revealed intricate functional diversity within the MLR that was not originally evident from electrical stimulation experiments.

Different neurotransmitter populations within the MLR exert opposing effects on locomotion. By using Cre-inducible viruses in mice, researchers have found that specific optogenetic stimulation of glutamatergic cells in the MLR is capable of eliciting locomotion in mice (Lee *et al.*, 2014; Roseberry *et al.*, 2016). This induced locomotion could reach speeds similar to those achieved through unrestricted electrical MLR stimulation. On the other hand, optogenetic stimulation of GABAergic or cholinergic MLR cells produced no observable behavioural effects when the mouse was stationary, but did produce a respective deceleration or acceleration when the mouse was running (Roseberry *et al.*, 2016). This illustrates the functional complexity within the MLR, and suggests an important need to examine the functions of populations of neurons with the same neurotransmitter expression.

There is further functional diversity within the mouse glutamatergic MLR population. Localised viral injections and optical fibre placement has enabled functional comparisons of the glutamatergic CnF and the glutamatergic PPN. Josset et al., used optogenetic stimulation to specifically attribute initiation of locomotion to

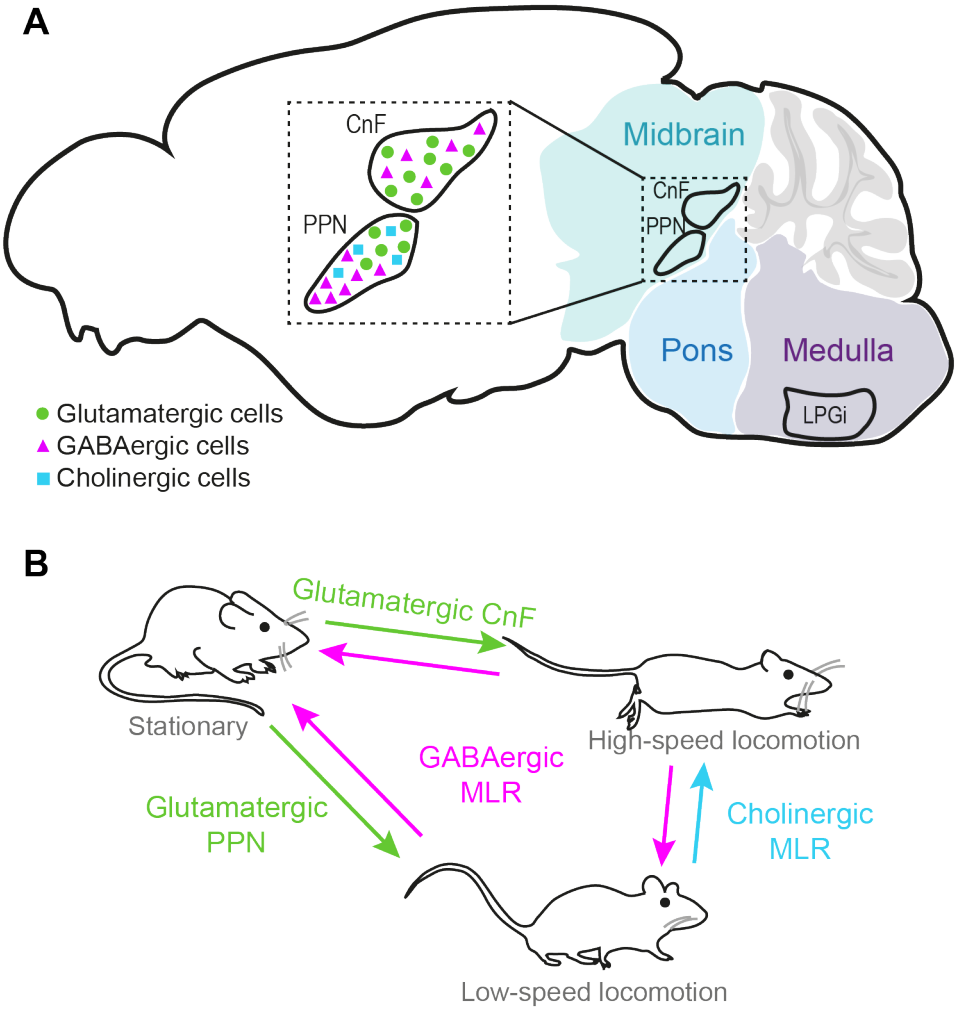

Figure 1.2 Functional diversity of different neurotransmitter populations exemplified by the MLR
A. Sagittal view of the mouse brain featuring supraspinal regions described in this chapter. Inset, the locations and neurotransmitter diversity of MLR nuclei. CnF, cuneiform nucleus; PPN, pedunculopontine nucleus; LPGi, lateral paragigantocellular nuclei.
B. Schematic summarising the locomotor functions of these neurotransmitter populations as described by targeted optogenetic photostimulation. Figure reproduced from Lau, Bianco, & Severi, 2019.

glutamatergic CnF neurons, but not glutamatergic PPN neurons (Josset *et al.*, 2018). In contrast, Caggiano et al., found that the glutamatergic PPN could elicit locomotion, but only through high frequency stimulation (Caggiano *et al.*, 2018). Caggiano went on to find that the induced locomotion from these two separate glutamatergic populations was also different: CnF stimulation induced locomotion with shorter latency and greater speeds than measured for PPN-evoked locomotion. Chemogenetic inhibition and extracellular recordings further implicated the glutamatergic CnF in high speed locomotion, and the glutamatergic PPN in low speed locomotion associated with exploratory behaviours (Caggiano *et al.*, 2018). These studies

illustrate the diverse functional roles that can only be identified through progressively focussed investigation of individual cell groups (Figure 1.2), and also how context-specific locomotor outputs could be produced through separate neuronal circuits.

1.2.2 The reticular formation

While the MLR can initiate and modulate the speed of locomotion, how are these motor commands or instructions transmitted to the spinal cord? As the MLR lacks direct projections to the spinal cord, motor commands must be relayed by intermediate structures. Tracing experiments in cats revealed the presence of efferent projections from the CnF and PPN to various regions within the pontomedullary reticular formation (PMRF) (Steeves and Jordan, 1984; Nakamura *et al.*, 1989). These areas of the reticular formation were also considered likely to contain neurons which project to the spinal cord via the ventrolateral funiculus (Valverde, 1961; Steeves and Jordan, 1980). Therefore, these structures within the PMRF are a strong candidate to serve as the conduit between the upstream MLR and downstream spinal CPGs.

The structure of the mammalian reticular formation is complicated and it has been difficult to ascribe specific functions to particular nuclei. The reticular formation extends through the midbrain, pons and medulla and contains many nuclei with indistinct borders between regions. Comparisons between studies of the reticular formation are further complicated by variations in nomenclature across the literature (Brownstone & Chopek, 2018). Furthermore, many early studies were conducted in cats, and translation of identified regions to other mammalian species is not always obvious; even the open-access Allen Brain Atlases for mice lack information on the boundaries of various reticular structures across coronal and sagittal views (Lein *et al.*, 2007). Bearing these complications in mind, a study by Takakusaki and colleagues examined the functions of different PMRF regions in cats and made an effort to reconcile findings across the literature (Takakusaki *et al.*, 2016). In doing so they chiefly describe the presence of functional topographical organisations within the PMRF which regulate postural muscle tone and locomotion. Control of posture is linked to locomotion, as animals must be able to adjust for changes in equilibrium associated with locomotion. In particular, they identify that stimulation of the dorsomedial PMRF, specifically the nuclei reticularis pontis oralis, pontis caudalis,

and gigantocellularis (NRPo, NRPc, NRGi), exert an inhibitory effect on muscle tone, while stimulation of the ventromedial PMRF, including the ventral NRPc and nucleus reticularis magnocellularis (NRMc) exerts an excitatory effect. This suggests a diversity of motor functions within the reticular formation, and it would be interesting to determine whether these opposing functions are associated with projections from MLR cell groups with similar functions.

Only recently can researchers examine the specific functional roles of neuronal subtypes within a reticular formation region. Mice are a more amenable model system for this cellular-level approach than cats. Recent work from Silvia Arber's laboratory has identified a reticular structure well-suited to influence locomotion, and found diverse functions produced by neuronal sub-populations within this region. Trans-synaptic tracing using rabies viruses revealed that the NRGi and NRMc show similar connections to both forelimbs and hindlimbs, suggesting that they might have a particularly important role in locomotor control (Esposito, Capelli and Arber, 2014). A subsequent study by Capelli et al. went on to investigate the functions of different neurotransmitter populations within the NRGi (Capelli *et al.*, 2017). Localised viral injections and Cre lines selective to individual neurotransmitters were used to confine the expression of the optogenetic activator ReaChR to specific neural populations (Capelli *et al.*, 2017). They found that widespread optogenetic simulation of the entire lateral paragigantocellular nucleus (LPGi) failed to induce or modulate locomotion, but that photoactivation of glutamatergic LPGi neurons initiated locomotion, whilst photoactivation of glycinergic LPGi neurons produced locomotor arrest. In addition to this, the authors found that ablation of glutamatergic LPGi neurons attenuated locomotion following glutamatergic MLR stimulation, thus providing evidence for the glutamatergic LPGi population to act as a relay for locomotion-promoting MLR commands. These technical advances available in other model organisms have thus provided greater insight into the operation of select neuronal populations in the reticular formation.

Selective examination of a particular neuron class has revealed an interesting locomotion terminating effect of glutamatergic cells within the rodent reticular formation. In this study, selective optogenetic activation of the glutamatergic V2a neurons in the NRGi and NRMc of mice were found to stop locomotor-like activity in an *in vitro* preparation (Bouvier *et al.*, 2015). The functions of these brainstem V2a neurons were also tested in freely-moving mice. Optogenetic photoactivation of these

neurons evoked a profound halting response, while blocking the synaptic output of these neurons resulted in increased mobility. This study shows a surprising locomotion-terminating effect of glutamatergic reticular neurons, in contrast to what has been typically described for glutamatergic hindbrain neurons. Studies such as these again highlight the utility of studying specific groups of neurons, in this case those that show expression of the same transcription factor, to develop an understanding of supraspinal motor control.

1.3 The reticular formation in lower vertebrates

With a growing focus on studying the functions of individual groups of cells, lower vertebrates provide neuroscientists with the opportunity to closely examine the role of specific hindbrain neurons in behaviour. Here I focus on lamprey and larval zebrafish as two model organisms which have been invaluable in this effort.

1.3.1 Lamprey reticular formation

Lamprey offer many benefits to the study of supraspinal motor control. Although simpler in comparison to mammals, lamprey possess basic structures of the vertebrate brain (Murakami and Kuratani, 2008). Additionally, the lamprey nervous system is robust to *in vitro* preparations, with easily identifiable, large neurons in the hindbrain which are highly suitable for microelectrode experiments (Figure 1.3). In addition to this, the motor outputs of lamprey are well characterised (Grillner and Wallén, 1984), altogether making them an excellent system in which to study the relationship between brainstem neurons and locomotion.

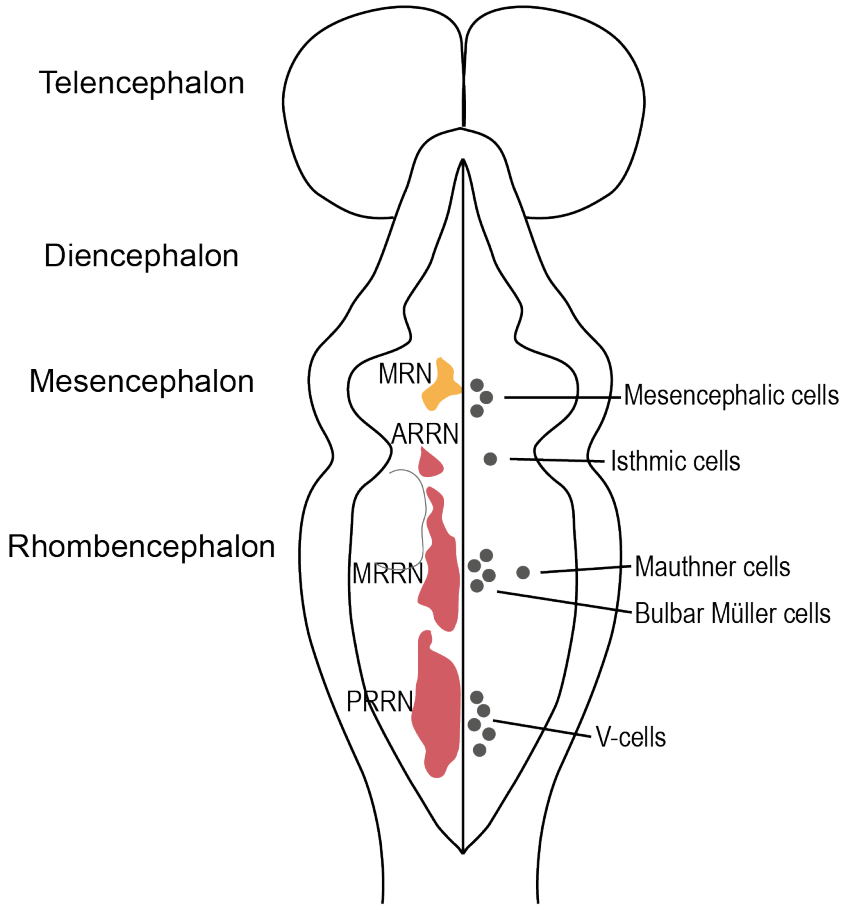

Figure 1.3 Schematic of lamprey reticular formation
Left, the reticular formation. This extends from the rostral mesencephalon to the caudal rhombencephalon (medulla) and consists of separate sub-regions. Right, the large, identifiable reticulospinal neurons. MRN, mesencephalic reticular nucleus; ARRN, anterior rhombencephalic reticular nuclei; MRRN, middle rhombencephalic reticular nuclei; PRRN, posterior rhombencephalic reticular nuclei. Adapted from Brodin *et al.*, 1988.

The reticular formation of lamprey has been well described, and parallels have been made with other vertebrate hindbrain structures. The lamprey reticular formation consists of four major nuclei: the posterior (PRRN), middle (MRRN), anterior (ARRN) rhombencephalic nuclei, and the mesencephalic reticular nucleus (MRN) (Figure 3). In addition to this, there are large identifiable reticulospinal (RS) neurons located in each of these regions, such as the bulbar Müller cells and the Mauthner cells (Brodin *et al.*, 1988). These large cells can act as key anatomical landmarks, and also allow for reliable comparisons of these cells across individual animals. In addition to this, the ARRN and MRRN are considered to be homologous to the superior and middle reticular nuclei of fish, amphibians and reptiles, or the NRPo and NRPc in mammals. Meanwhile the PRRN is homologous to the inferior reticular nuclei in fish,

amphibians and reptiles, and the NRGi, NRMc, and nucleus reticularis ventralis in mammals (Daghfous *et al.*, 2016). Overall, studies have established that the descending control of locomotion in lamprey share common principles to higher vertebrates, as exemplified by the identification of an MLR in lamprey (Sirota, Di Prisco and Dubuc, 2000).

The lamprey reticular formation also appears to mediate similarly complex locomotor effects to those described in mammal studies. As described earlier, recent work has shown that specific populations of hindbrain neurons have roles in terminating locomotion (Bouvier *et al.*, 2015). Neurons which have similar halting effects on locomotion have also recently been identified in lamprey. In these experiments, a functional group of RS neurons termed "stop cells", located in the caudal PRRN were found to show increased activity at the beginning and end of locomotor bouts (Juvin *et al.*, 2016). This suggests that lamprey RS neurons also show varied roles in locomotor control in a way similar to mammals.

Studies in lamprey have also identified that the reticular formation acts as a site where the information from various sensory modalities can be integrated to shape motor output. Studies have identified projections to the MRRN from visual processing regions such as the optic tectum (Zompa and Dubuc, 1996). Other sensory modalities which have been found to interact directly with RS neurons include vestibular (Deliagina *et al.*, 1992) and trigeminal inputs (Ray *et al.*, 2010). Altogether this research emphasises how the reticular formation represents a key region where multiple sensory inputs can converge to shape locomotor output.

1.3.2 Larval zebrafish reticulospinal cells

Larval zebrafish are also a highly useful model organism in which to study the relationship between single reticulospinal cells and precise aspects of behaviour. In addition to a well-characterised RS population and a developing understanding of locomotor output, researchers can also apply modern genetic and optical techniques to larval zebrafish experiments. The genetic tractability offered by this model organism allows for an examination of genetically defined cell populations, which as described earlier, has been critical in mammalian studies aiming to elucidate the motor functions of various brain areas.

The RS cells in larval zebrafish have been identified by retrograde labelling from the spinal cord. In this method, the RS axons are severed in order to take up a dye. Despite this technique failing to label all of the spinally projecting RS neurons, particularly those with small axons (Kimura *et al.*, 2013), researchers have still been able to conduct an in-depth examination into the morphology of the large, canonical RS neurons across early stages of development (Metcalfe, Mendelson and Kimmel, 1986). As a result, it is generally understood that the larval zebrafish RS system is a highly stereotyped population, consisting of ~150 anatomically distinct neurons which are symmetrical about the midline (Kimmel, Powell and Metcalfe, 1982) (Figure 1.4). The majority of these RS neurons reside in the hindbrain, however a bilateral group of cells, known as the nucleus of medial longitudinal fascicle (nMLF) are found in the mesencephalon. In addition to this, Kimmel and colleagues developed a nomenclature system where each of these cells is given a unique name that reflects its location in the hindbrain and relative position to the other RS cells (Figure 1.5). This stereotypy across animals and standardised nomenclature has allowed researchers to consistently identify and study the functions of the same neurons across larvae.

Close examination of the morphology and projection patterns of the RS neurons has led to the identification of serial families of cells (Metcalfe, Mendelson and Kimmel, 1986). The projection pathways of different RS neurons are diverse. RS neurons either project ipsilaterally or contralaterally, and the caudal extent of these projection pathways varies between neurons (Metcalfe, Mendelson and Kimmel, 1986). The RS axons descend into the spinal cord along two major pathways: the medial and the lateral longitudinal fascicle (mlf, llf). The mlf contains the axons of reticulospinal cells, vestibulospinal cells and reticular interneurons, and goes on to form the ventromedial fascicle. The llf, on the other hand, contains RS axons together with ascending fibers and descending sensory fibers and forms the dorsolateral fascicle. Comparisons of the dendritic arbors and projection pathways of the RS neurons led Metcalfe et al., to propose that RS neurons across different levels of the hindbrain form serially repeated groups. Examples of such groups include the Mauthner, MiD2cm, and MiD3cm cells, which are all contralaterally projecting and show extended lateral dendrites, or the ventromedial RoV3, MiV1, and MiV2 cells which are groups of small, ventral, ipsilaterally projecting neurons. Due to these morphological variations across serial RS groups, particularly their differing spinal cord targets, it is likely that different RS groups occupy different functional roles.

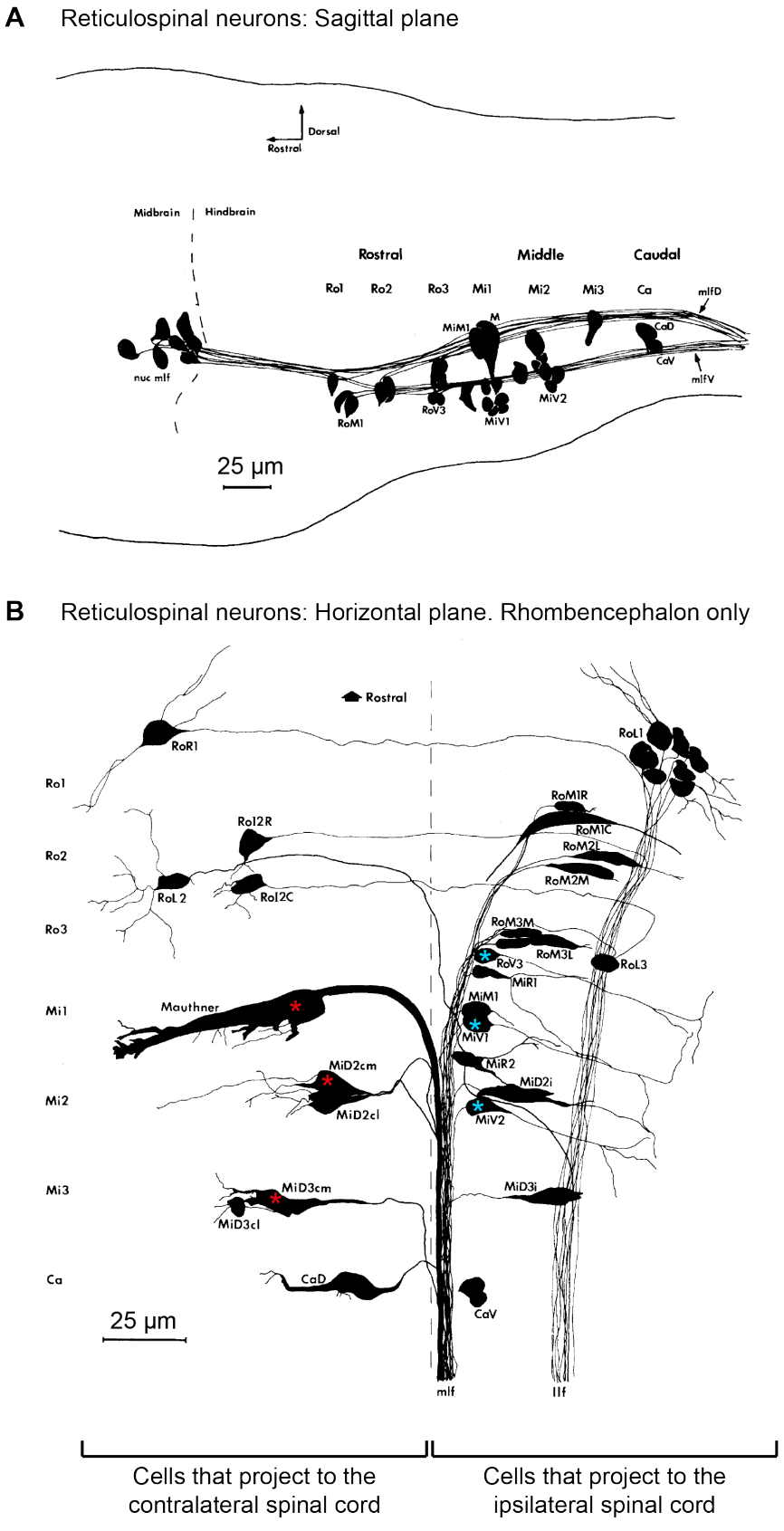

Figure 1.4 Drawings of the larval zebrafish reticulospinal neurons
A. Sagittal view displaying the dorso-ventral extent of the RS neurons.
B. Horizontal view of RS neurons, separated into those that project contralaterally (left), and those that project ipsilaterally (right). Asterisks denote serial families of cells; red: Mauthner cell and segmental homologs (Mauthner cell, MiD2cm, MiD3cm); blue: ventromedial cells (RoV3, MiV1, MiV2). Adapted from Metcalfe, Mendelson and Kimmel, 1986.

Less is known about other hindbrain neurons beyond the large canonical RS neurons. Yet it is important to consider their roles in behaviour as not all spinally projecting cells are labelled by backfill, and they could also interact with the identified RS neurons by forming local circuits. One example of spinally projecting neurons not labelled by backfill are some of the hindbrain V2a neurons which are capable of eliciting swimming upon selective photostimulation (Kinkhabwala *et al.*, 2011; Kimura *et al.*, 2013). In addition, some neurons are not spinally projecting but can still shape motor output by coordinating RS activity. An example of these are the "feedforward inhibitory neurons" identified by Koyama et al. which allow only one Mauthner cell to be active at a time (Koyama *et al.*, 2016). Therefore, the cells surrounding the RS neurons in the hindbrain can also be behaviourally relevant and warrant investigation.

1. Cell location	2. Location in zone	3. Axial level in segment	4. Detailed location of individual cells
Mesencephalon	**D**orsal		*Relative location*
Rostral Rhombencephalon	**V**entral **M**edial	Level **1**	**L**ateral **M**edial
Middle Rhombencephalon	**I**ntermediate	Level **2**	*Axonal projection*
Caudal Rhombencephalon	**L**ateral **R**ostral	Level **3**	**i**psilateral mlf
	Caudal		**c**ontralateral **l**lf **c**ontralteral **m**lf

Figure 1.5 Schematic explaining the nomenclature system used to identify larval zebrafish reticulospinal neurons
Emphasised characters indicate those that are used in the short identity code. Nomenclature developed by Kimmel et al., 1982; Metcalfe et al., 1986.

1.3.3 Larval zebrafish locomotion

Key to understanding the relationship between RS neurons and behaviour is a good characterisation of the behaviour repertoire itself. The use of high-speed cameras has allowed researchers to resolve detailed tail kinematics and additionally study the movements of the eyes, jaw and pectoral fins (McClenahan, Troup and Scott, 2012; Mearns *et al.*, 2019). In the larval stages starting from 4 days post fertilisation (dpf), zebrafish swim in a "beat-and-glide" fashion, where brief periods of swimming, known as "bouts", are separated by a short period of quiescence commonly referred to as the inter-bout-interval (Buss and Drapeau, 2001). High-resolution tracking has revealed that each individual bout is composed of a series of tail oscillations about the

midline known as individual “half beats”. A whole cycle of the tail refers to the period between two peaks on the same side of the midline, and half beats refer to the period between the peak on one side of the midline, and the next peak on the contralateral side. These bouts often occur with a simultaneous movement of the eyes. These eye movements can be used to identify distinct behavioural routines such as hunting, which is characterised by a nasal rotation of both the left and right eyes in a convergent saccade (Bianco, Kampff and Engert, 2011).

Over the years, various researchers have tended to focus on the stereotyped swims evoked by a particular stimulus, leading to a somewhat fragmented description of larval zebrafish swimming. The names assigned to these stimulus-evoked swims typically reference the shape of the tail during the behaviour. Popular examples include: escape “C-starts” in response to aversive stimuli, such as a cutaneous touch or a mechanoacoustic stimulus (Kimmel, Patterson and Kimmel, 1974), the “O-bends” associated with whole-field luminance changes (Burgess and Granato, 2007), and the “J-turns” observed during hunting routines (McElligott & O’Malley, 2005). However, due to this focus on stimulus-evoked bouts, considerably less is known for normal swimming beyond the term “slow” swims and turns (Budick and O’Malley, 2000).

Recent work by Marques et al sought to provide an unsupervised classification of the larval zebrafish locomotor repertoire, and thus unify previous findings and provide a framework for future experiments to build upon (Marques *et al.*, 2018). In this impressive work, larvae were presented with a wide range of stimuli to evoke the full behavioural diversity. The tail movements during these bouts were recorded and described by a multitude of kinematic features. Subsequent unsupervised classification of this data resulted in 13 kinematically distinct bout types. These bouts could largely be likened to previously described bout types and showed similar deployment to specific contexts. This study also included a characterisation of natural swimming in the absence of any obvious stimuli, and identified multiple “slow” and “routine” swim types. This provided a valuable reconciliation of earlier published work and also highlighted the presence of kinematic distinctions between bout types.

1.3.4 Roles of larval zebrafish reticulospinal neurons in locomotion

How does the activity of larval zebrafish RS neurons produce this locomotor diversity? Due to the detailed characterisation of larval zebrafish RS neurons, and the ability to reliably evoke specific swims using stimuli, neuroscientists have worked to establish the functional roles of individual RS neurons. This avenue of research has benefitted greatly from the optical transparency of zebrafish larvae, enabling researchers to employ techniques such as calcium imaging, optogenetic stimulation, and targeted laser ablations. This field has moved from identifying RS cells important for large scale behaviours, such as the production of a bout type or for prey capture, to examining how these cells relate to lower-level behavioural kinematics.

One of the most well-known RS functions is that of the Mauthner cell in C-starts, a function supported by research in other teleost fish species (Zottoli and Faber, 2000). Calcium imaging of RS cells in larval zebrafish revealed that the Mauthner cell and its segmental homologs, MiD2cm and MiD3cm (Metcalfe, Mendelson and Kimmel, 1986), showed differential activity to taps directed to either the head or tail (O'Malley, Kao and Fetcho, 1996). In particular, all three cells showed activity in response to head taps, whilst only the Mauthner cell was active for tail taps. Subsequent loss-of-function experiments confirmed that larvae could still respond to head-directed taps following Mauthner cell ablation, whilst ablation of the entire array abolished short-latency escape responses (Liu and Fetcho, 1999). These experiments revealed that there are functional groups of RS neurons, which when ablated can greatly affect locomotor outputs, and in this case remove the production of a bout type.

A recent study examined the role of the Mauthner cell in escape behaviours elicited by a visual looming stimulus, which is likely to resemble an oncoming predator. The authors of this study found that fish tended to perform a low-latency, stereotyped, escape response in response to a fast approaching looming stimulus, and a slow, more kinematically variable response to slow approaching stimuli (Bhattacharyya, McLean and MacIver, 2017). They found that the Mauthner cell was frequently recruited during responses to fast-approaching stimuli, and much less likely to be recruited during in response to a slow-approaching stimulus. For responses

where the Mauthner cell was inactive, other RS neurons, such as ventromedial MiV1 and MiV2 showed increased recruitment, suggesting that these cells are capable of driving an alternative, long-latency response swim towards stimuli that appear less urgent and threatening. This study provided insights into the differential recruitment of neurons for non-Mauthner evoked escapes.

Further selective RS ablations produced profound effects on different large-scale behaviours. Gahtan et al., bilaterally ablated two large cells in the nMLF (MeLr and MeLc) which appeared to be tectorecipient. As the authors suspected these cells might mediate the integration of visual inputs, they examined the effects of these cells on hunting and prey capture, a visually-dependent behaviour (Gahtan, Tanger and Baier, 2005). Larvae with MeLr and MeLc ablations showed deficits in orienting towards prey and overall prey capture. From this it is clear that other individual RS cells beyond the long-studied Mauthner cell also have important roles in behaviour, although how these behavioural deficits manifest with regard to low-level behavioural features is unknown.

More recent studies have focused on the relationship between RS neurons and specific behavioural features. Importantly, these studies build upon one another and nicely illustrate how the progressive emphasis on precise behavioural features has been aided by technical and analytical advances. For example, following on from the finding that the bilateral removal of two large nMLF cells can profoundly affect behaviour, several studies have examined what precise behavioural features these nMLF cells might encode to produce this effect. Thiele and colleagues conducted calcium imaging and optogenetic stimulation of nMLF cells while recording tail movements (Thiele, Donovan and Baier, 2014). In this study, they found that many nMLF neurons show activity during swims, and that differential photoactivation of the left/right nMLF regions produced an ipsilaterally biased “steering” tail movement. Another study conducted by Severi et al. focused primarily on the large nMLF cells, and examined how the activity and ablation of these cells related to swim kinematics associated with forward swimming (Severi *et al.*, 2014). Interestingly, electrical stimulation of these cells evoked swims with a duration and intensity proportional to the strength of stimulation. Although this is a quality reminiscent of the MLR, nMLF cells are spinally projecting and so do not meet the criteria described earlier. Ablation of these cells also produced reductions in locomotor kinematics such as bout speed and tail beat frequency. Overall, both studies identified specific roles of nMLF cells

in key features of swimming, such as postural adjustment and swim vigour. One can imagine that impairments in the production of these behavioural outputs could underlie the poor orientation towards prey identified by Gahtan et al..

A further example of the advances made in identifying the relationship between specific RS neurons and locomotor kinematics is exemplified by study of the ventromedial cells, RoV3, MiV1 and MiV2. The activity of these cells as measured by calcium imaging, was found to increase when zebrafish larvae were presented with a visual stimulus that evoked turn swims towards a specific direction (Orger *et al.*, 2008). Specifically, the ventromedial cells on each side of the midline showed an increase in calcium indicator fluorescence for stimuli which elicited turns towards the ipsilateral side. The authors of this study went on to show that ablation of these neurons produced a profound deficit in turning towards the ablated side. Whether this represented the loss of an entire bout type, such as a routine turn towards one side, or the inability to produce kinematics critical to this motor output was subsequently examined by Huang and colleagues (Huang *et al.*, 2013). In these experiments the authors found that ablation of these neurons produced a specific kinematic deficit where the high-amplitude tail bend of the first half beat towards the ablated side was lost. Furthermore, Huang also identified a higher fraction of symmetrical forward swims following ventromedial cell ablation. This suggested that other swimming patterns are supported by the remaining RS population, and that the ventromedial cells serve to produce a kinematic that “transforms” symmetrical swims into asymmetrical turns.

1.4 Neural coding strategies underlying motor control

What is the functional architecture of supraspinal motor systems? Neuroscientists have been captivated by this question, and various circuit architectures have been proposed to explain the relationship between neuronal populations and behaviour. These circuit architectures describe how a specific role or function is produced by neurons; functions could be widely spread across many hundreds of neurons, or could be more discrete and modular, involving only small numbers of neurons. In this section I describe some popular circuit architectures, and

consider what motor representations could be supported or coded by these frameworks.

1.4.1 Possible circuit architectures

At one end of the spectrum is a population code, sometimes also known as a "distributed" circuit architecture (Morton and Chiel, 1994). In such a system, the collective activity of a large number of broadly tuned neurons is used to perform a specific function. A notable example of such a coding strategy is seen in the coding of hand movement direction across cells in primate motor cortex (Georgopoulos, Schwartz and Kettner, 1986). In this study, Georgopoulos et al. found that individual motor cortical neurons were broadly tuned across movement directions, and represented each neuron by a vector. The angle of these individual neuron vectors described the preferred tuning direction of the neuron, and the length of the vector described the neuron's change in firing rate from baseline. The authors then developed a population vector calculated from the average of all the individual vectors recorded, and found that it had a direction similar to that of the observed hand movement. This suggested that the overall activity of motor cortical neurons could encode hand movement direction.

The other extreme alternative would be a single-neuron coding strategy, where a complex event is signalled or produced by the activity of a single cell with sharp tuning. Such a strategy has been described for so-called "command neurons", first described in crayfish (Wiersma and Ikeda, 1964). This term arose when Wiersma and Ikeda found that the stimulation of any one of five interneurons was capable of eliciting a swimming response. However, the concept of a command neuron has been adapted over the years, most notably by Kupfermann and Weiss who set strict necessity and sufficiency criteria for this label, and extended this definition to include multiple "homogeneous neurons" (Kupfermann and Weiss, 1978). This rigorous definition has made it hard to identify true command neurons, as even the Mauthner cell, often viewed as an archetypal command neuron, would fail to meet this criteria in larval zebrafish (Liu and Fetcho, 1999).

Similar to this single-neuron coding strategy, is a "dedicated" circuitry, where a dedicated group of neurons act in concert to produce a particular output. Unlike the

definition set out by Kupfermann and Weiss, these neurons do not necessarily need to be "homogeneous" to one another, and thus do not require "virtually identical inputs and outputs" (Kupfermann and Weiss, 1978). In this case, the larval zebrafish Mauthner cell and segmental homologs, MiD2cm and MiD3cm, could be interpreted as a type of dedicated circuit for short-latency high-angle escape swims to head-directed tap stimuli (Liu and Fetcho, 1999). However, it is not how clear how the application of this circuitry across all motor outputs would be able to produce a continuum of varying and flexible behaviours.

To account for this, Morton and Chiel also presented a "reorganising circuitry" as an intermediary between population and dedicated coding strategies (Morton and Chiel, 1994). Under this definition, circuits are more flexible, with different behavioural responses being produced by the addition or removal of neurons, and even changes in effective synaptic connections. They propose that these circuit changes could be dependent on factors such as the behavioural state of the animal, thus resulting in context-specific behaviours.

1.4.2 Motor representation

These different circuit architectures support various motor representations. For example, it is easier to imagine how dedicated circuits could underlie highly stereotyped behaviours, such as an escape behaviour, whilst population coding might better suit flexible, continuous behaviours, such as hand movement direction, which would vary depending on the circumstances.

Identifying which motor features are present in the activity of a supraspinal neural population can be achieved through predictive modelling. Under this umbrella term, there are two complementary types of model commonly used in neuroscience: "encoding" models which would predict neural activity from the motor features, and "decoding" models which use the neural activity to predict these features.

What would these models tell us about the motor representation or computations described by the activity of a neuronal population? The prevailing view is that only the model operating in the direction of information flow can provide an insight into the computations employed by the neurons being studied, i.e. a decoding model for examining how supraspinal neurons produce a motor output (Kriegeskorte

and Douglas, 2019). Under these circumstances, an encoding model would provide insight into the motor features represented by the measured neural activity. Consider the study described earlier by Georgopoulos et al. which examined the activity of neurons in primate motor cortex during hand movements: the vectors used to describe the activity and tuning of individual neurons represent an encoding model, and the population vector used to predict the motor output from each of these individual represents a decoding model (Georgopoulos, Schwartz and Kettner, 1986). Bearing in mind the direction of information flow for this example, the computation used to produce this population vector (the decoding model) can be interpreted as a possible computation employed by the brain when making hand movements. The individual neuron vectors (the encoding models), on the other hand, would suggest that information about the angle of hand movement is present in the cell's activity.

1.5 Measuring population activity through calcium imaging

In order to understand how neuronal activity relates to behaviour, it is important to sample activity from across the population being studied. There are many ways to record the activity of multiple neurons simultaneously, such as through multi-channel recordings using electrode arrays or probes. However, these require spike-sorting methods to resolve individual units and do not provide a thorough understanding of the anatomical location of the cells being sampled.

On the other hand, two-photon (2P) population calcium imaging allows researchers to monitor the activity of visually identified neurons. In addition to this, researchers can also determine the anatomical location of each cell within a population. When this method is used in tandem with viral and genetic techniques, one could also sample a desired subgroup of cells. However, this high spatial resolution comes with the cost of a lower temporal resolution than what can be achieved through electrophysiological techniques.

It is important to note that the changes in fluorescence collected from the calcium imaging of neurons are only a proxy of neural activity. Genetically encoded calcium indicators (GECIs) such as GCaMP6f show an increase in brightness upon the binding of intracellular calcium. As action potentials and postsynaptic potentials

produce an influx of calcium into the cell primarily mediated by voltage-gated calcium channels, this produces a change in the fluorescence of the intracellular calcium indicator (Grienberger and Konnerth, 2012). In response to the influx of calcium produced from a single action potential, GECIs show a rapid rise in fluorescence, followed by a slow exponential decay (Figure 1.6). As such, this observed fluorescence can be described as a convolution of the action potential firing rate with the waveform of this unitary transient. To obtain a measure of the inferred spike rate underlying these calcium transients, one can perform a deconvolution to apply the inverse process (Yaksi and Friedrich, 2006). There are currently a range of open-source methods which neuroscientists can use to perform this computation (Pnevmatikakis *et al.*, 2016; Friedrich, Zhou and Paninski, 2017). Some of these methods also calculate the calcium indicator kinetics, such as the decay time (tau) of the exponential decay, which is useful for situations where this information cannot be provided empirically from "ground-truth" data.

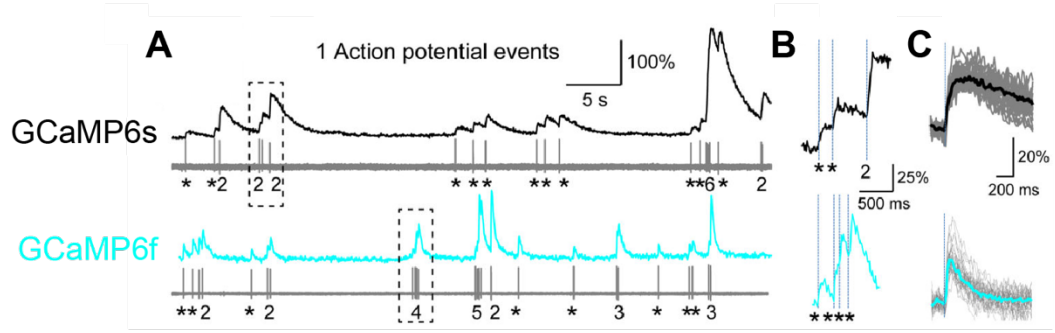

Figure 1.6 2P Calcium imaging of a single neuron with simultaneous cell-attached recordings in mouse visual cortex
A. Fluorescence time series and recorded spikes for a single neuron. Top, GCaMP6s expressing neuron; bottom, GCaMP6f expressing neuron. Single spikes are marked by *, otherwise the number of spikes for each burst is indicated.
B. Close up fluorescence time series for a burst of action potentials (grey boxes in A). Top, GCaMP6s; bottom, GCaMP6f.
C. Change in fluorescence in response to one action potential.
Figure adapted from Chen et al., 2013.

1.6 Aims of the thesis

In summary, studies in mammals have highlighted a need to consider supraspinal motor control at a cellular level. Larval zebrafish are a valuable model system in which to study this, owing to the wide range of optical and genetic tools available together with their well characterised RS population and locomotor diversity. Current studies have had success in identifying a few groups of RS cells which appear to support specific kinematic functions, but it is not yet known what locomotor features are represented by the rest of the RS population, or the nature of the coding scheme by which the full locomotor repertoire is produced. My specific aims for this thesis were to:

1. Conduct calcium imaging of RS neurons during a range of behaviours and identify the reticulospinal recruitment and activity patterns associated with distinct bout types (Chapter 2).
2. Build encoding models of RS activity to develop an understanding of the behavioural features represented by the activity of different RS neurons and identify possible functional groups of neurons. This would also provide an insight into the possible coding strategy employed by the population (Chapter 3).
3. Test the roles of functionally identified neurons on behaviour by conducting loss-of-function experiments through precise cell ablations (Chapter 4).
4. Develop a novel methodology where it is possible to study RS population activity with greater temporal resolution. This would enable examination of the relative timing of RS neurons to one another, and could lead to the eventual development of decoding models of RS activity (Chapter 5).

Chapter 2 Reticulospinal recruitment during locomotion

2.1 Introduction

As the functions of many larval zebrafish RS neurons are not known, I decided to study population activity through calcium imaging, as this would allow me to resolve and identify individual cells. To do this, I need to label or express a calcium indicator across the population in a way that minimises any effects on behaviour. Previous studies have used spinal cord injection to label RS neurons with synthetic calcium indicators and studied the activity of these neurons in relation to behaviours or stimuli (O'Malley, Kao and Fetcho, 1996; Orger *et al.*, 2008). However, the number of neurons labelled is highly variable, and the procedure is invasive as RS axons are severed by the injection in order to take up the dye. This is a particular concern when studying RS activity with regard to motor outputs, as there could be potential compensatory effects within the RS population, or alterations to behaviour. This means that the traditional backfill method of RS labelling is not ideal for the combined study of RS activity and behaviour.

Recent methodological advances have enabled researchers to use genetically encoded calcium indicators and Gal4/UAS systems to flexibly label specific cells with a variety of fluorescent proteins. Gal4/UAS and the improved KalTA4/UAS, is a bipartite system consisting of a Gal4 or KalTA4 transcription factor and its DNA binding site (upstream activator sequence, UAS). Expression of Gal4/KalTA4 can drive the expression of any protein whose coding sequence is linked to the target UAS. Whilst enhancer trap lines using the Gal4/UAS system have provided a less invasive way to examine the activity of particular RS regions than with backfill labelling (Thiele, Donovan and Baier, 2014), at present there does not exist a transgenic line

which labels the majority of the RS population with minimal expression and overlap of undesired regions. Indeed, even so-called “pan-neuronal” lines which can express various fluorophores under the endogenous *elavl3* promoter to label the majority of neurons still fail to completely label the RS population (Vladimirov *et al.*, 2018). Ultimately, this means that there is currently no published transgenic zebrafish in which it is possible to express fluorophores across the majority of the RS population.

In order to conduct calcium imaging while recording locomotor output, it is necessary to head fix or restrain the animals and evoke behaviours under these conditions. Some studies have used fictive recordings to complement their calcium imaging, a procedure where the fish is paralysed and the occurrence of swims and their laterality decoded from ventral root recordings (Ahrens *et al.*, 2012). However, this approach lacks the kinematic complexity of whole-tail tracking. Instead, partially restrained or “tethered” preparations, where the eyes and tail are free to move have been successfully introduced (Bianco & Engert, 2015), but it is not clear what behavioural diversity is achievable in this preparation. Whilst a tethered preparation allows for combined calcium imaging and detailed behavioural tracking along the length of the tail, it is already evident that tethered behaviours can be different or absent in comparison to freely swimming fish (Severi *et al.*, 2014).

In this chapter I conducted calcium imaging of larval zebrafish RS cells while they performed a range of locomotor outputs in order to study the RS activity patterns relating to these behaviours. I also present a novel transgenic line which enables the flexible expression of GECIs across RS neurons, and describe an assortment of behaviours which can be elicited under partially restrained conditions. Examination of the RS recruitment towards these different bout types help to reveal which of the circuit architectures proposed by Morton and Chiel best describe motor-related RS activity.

2.2 Results

2.2.1 The majority of RS cells are reliably labelled by *KalTA4u508*

Examination of transgenic driver lines generated by the lab identified a transgene, *KalTA4u508*, which labelled hindbrain neurons similar to those labelled by backfill (Figure 2.1A; Kimmel et al., 1982). To confirm this, I backfilled RS neurons with Texas Red-dextran dye in *KalTA4u508;UAS:GCaMP6f* larvae (Figure 2.1B). I found that many of the Texas Red labelled neurons were also colabelled by GCaMP6f, indicating that *KalTA4u508* labels RS neurons. I also noticed that *KalTA4u508;UAS:GCaMP6f* labelled some neurons which were not labelled by backfill. I term these as putative non-reticulospinal neurons (non-RS for brevity), as it is known that some spinally projecting neurons are not always labelled by backfill (Kimura *et al.*, 2013). As the RS neurons have unique names (Kimmel, Powell and Metcalfe, 1982; Metcalfe, Mendelson and Kimmel, 1986), I also produced labels for these non-RS cells which reports their location relative to the predefined RS cell types (Figure 2.1C; grey outlines represent non-RS cells, and black outlines represent RS cells). From this, it appears that *KalTA4u508;UAS:GCaMP6f* larvae could be a useful tool in which to study the activity of the RS neurons together with neighbouring non-RS neurons.

KalTA4u508;UAS:GCaMP6f labelling of RS neurons is consistent across fish. I backfilled the RS neurons in multiple *KalTA4u508;UAS:GCaMP6f* larvae and found that there is a reliable, symmetric labelling of RS cells via *KalTA4u508* across fish (Figure 2.1D). Of the singly occurring cell types, such as the Mauthner cell or large cells of the nMLF, the majority are reliably labelled in more than 90% of fish (blue coloured cells, Figure 2.1D). However, for labels which refer to groups of cells it is difficult to determine the exact number of cells within a group due to variations in the expression of *KalTA4u508;UAS:GCaMP6f* larvae and the backfill labelling method. By summing the number of cells labelled in each cell group and dividing by the total number of fish, I present a measure of the likely number of cells labelled per fish (red cells, Figure 2.1D). One should note that while some cell groups appear to contain fewer cells than others, this could reflect a small cell group rather than a lack

of sufficient labelling. Overall this shows that the majority of RS cells are labelled in each fish, and only the lateral RS cells are infrequently sampled.

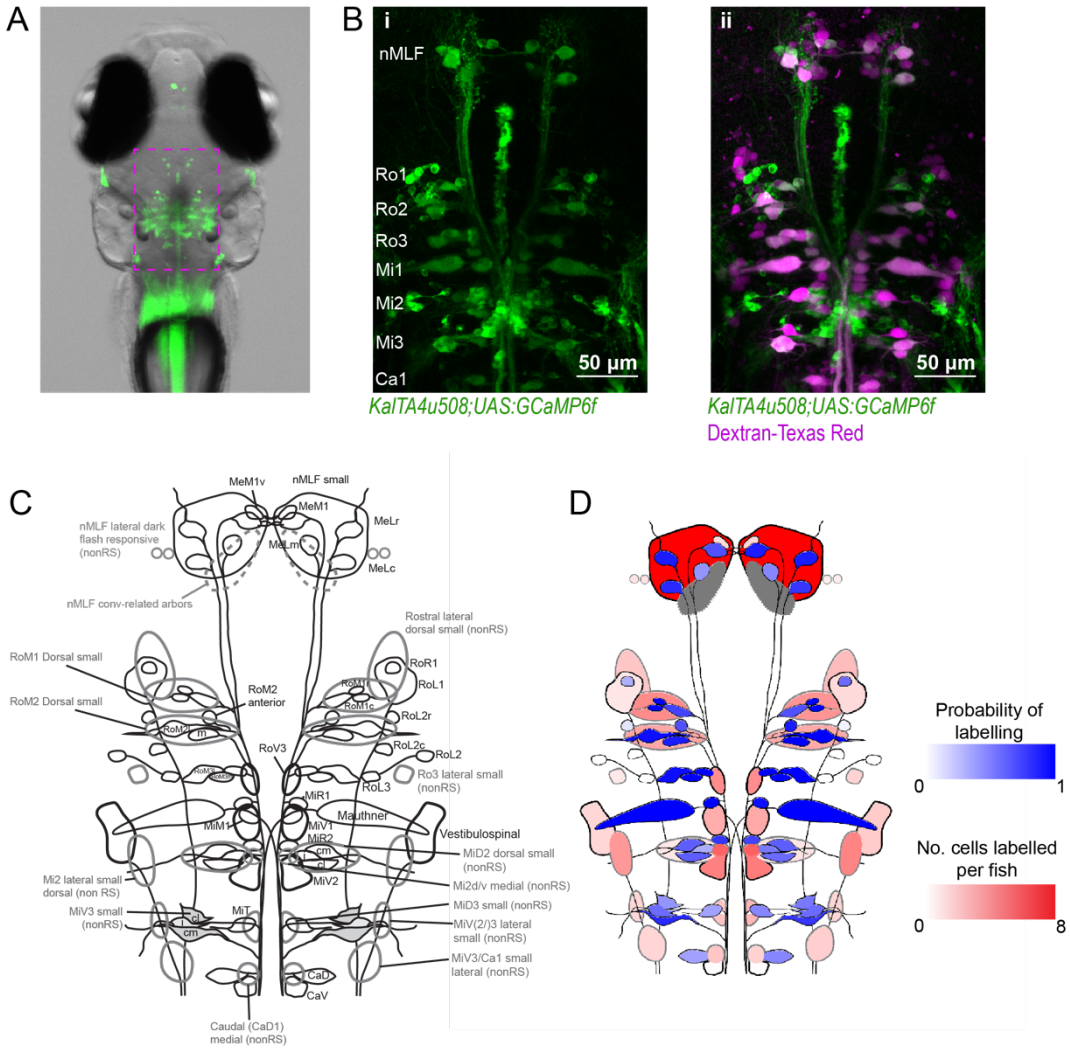

Figure 2.1 The *KalTA4u508* labels the majority of reticulospinal neurons.
A.Fluorescent micrograph of a *KalTA4u508;UAS:GCaMP6f* larva at 5 dpf. Pink box indicates the location of the RS population and the imaging window used for all experiments. Note that there is some fluorescence reflection on the body.
B.*KalTA4u508;UAS:GCaMP6f* expression and spinal cord backfill colabelling of RS neurons
i. *KalTA4u508;UAS:GCaMP6f* larva at 5 dpf. Green are cells labelled with GCaMP6f
ii. *KalTA4u508;UAS:GCaMP6f* as in i but with spinally projecting reticulospinal cells labelled with Texas Red dextran in magenta.
C.Schematic of spinally projecting RS neurons in black and putative non-spinally projecting neurons (non-RS) in grey. Thicker lines indicate cell labels which refer to groups of cells.
D.Frequency of cell labelling in *KalTA4u508;UAS:GCaMP6f* larvae (N = 19 fish). Singly labelled cells are coloured by their probability of labelling, and cell groups are coloured by the mean number of that cell type. Greyed out cell types indicate no data because the structures were never labelled by backfill.

One of the non-RS labels refers to cell arbors only detectable during calcium imaging. These denote a bilateral collection of arbors in the posterior nMLF. These arbors were identified by increases in calcium fluorescence from the calcium imaging experiments discussed later in this chapter. As they are not visible during anatomical imaging with backfill labelling, the corresponding soma are not known, and these cells have been coloured grey (Figure 2.1D).

2.2.2 Identification of novel RS cells

Close examination of the cells colabelled in *KalTA4u508;UAS:GCaMP6f* larvae and by backfill allowed me to identify cells with unique morphologies that do not currently have an individual class label (Metcalfe, Mendelson and Kimmel, 1986). In the vicinity of Ro2, I have identified a single novel cell with a small, circular soma. This cell is present on both sides of the midline and is clearly distinguishable from nearby RS cells as it is located ~30 µm dorsal to the predefined RoM1c and RoM1r cells (Figure 2.2A). These cells are also frequently labelled in *KalTA4u508;UAS:GCaMP6f* larvae; left side labelled 13/19 larvae, right side labelled 17/19 larvae (Figure 2.1D, Figure 2.2B). In keeping with the existing nomenclature (Kimmel, Powell and Metcalfe, 1982), I propose the label "Rostral Rhombencephalon, Level 2, Anterior" (RoM2a) for this novel cell.

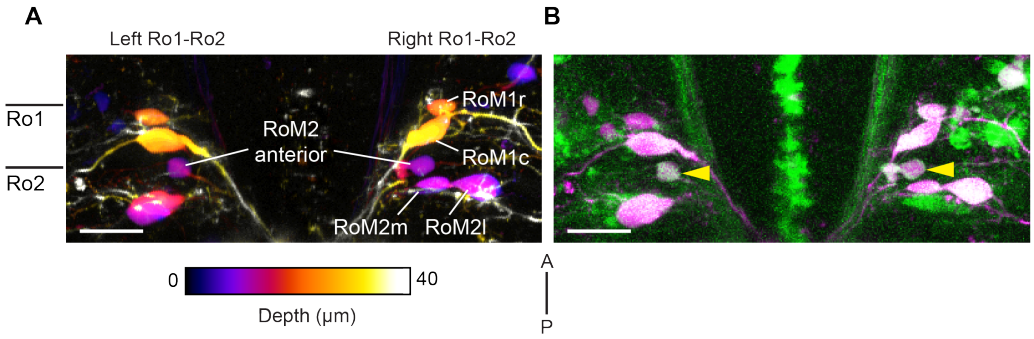

Figure 2.2 Novel RS cell type identified by backfill and *KalTA4u508;UAS:GCaMP6f* labelling
A. Maximum projection over a select z-range of RS cells in Ro1-Ro2. Cells were labelled by spinal cord backfill with dextran-conjugated Texas Red dye. Image is colour coded by depth.
B. Maximum projection of the same fish as in A. Cells are labelled with *KalTA4u508;UAS:GCaMP6f* (green) and dextran-conjugated Texas Red dye (magenta). Yellow arrowheads indicate colabelling of novel cell type RoM2a. Green midline labelling represents some labelling of structures in or near the floorplate by *KalTA4u508.*
Scalebars are 20 µm.

2.2.3 Combined two-photon calcium imaging and behavioural tracking

To study the activity of RS neurons, I used a raster-scanning 2P microscope where a partially-restrained *KalTA4u508;UAS:GCaMP6f* larva can undergo calcium imaging whilst the eyes and tail are simultaneous tracked (Figure 2.3A). As RS cells are not located superficially at the dorsal surface of the brain, 2P microscopy allows for imaging of these neurons with minimal interference from the biological tissue above. In addition to this, as the RS population spans ~150 μm in depth, images were acquired at individual z-planes separated by 5 μm steps. GCaMP6f was selected due to its faster kinetics in comparison to other available GCaMP6 variants (Chen *et al.*, 2013), which would be useful in examining neural activity in relation to behaviours that can be produced in quick succession.

In order to evoke a variety of locomotor outputs during imaging, two projectors were used to present visual stimuli and a solenoid-controlled water puff provided a mechanosensory stimulus. Visual stimuli included prey-like moving spots, moving black and white gratings in different directions (optomotor gratings), looming spots, and whole-field dark flashes. Multiple repeats of each stimulus were presented in a pseudo-random order for one imaging plane, before being repeated again for the next imaging plane. This allowed me to continuously evoke behaviours across all z-planes of calcium imaging acquisition.

In response to these varied stimuli, tethered zebrafish perform a range of swimming bouts. Variations in the behaviours produced can already be seen upon examination of the cumulative tail angle in response to different stimuli (Figure 2.3B). For example, swims in response to a forward grating are more symmetrical about the midline than those to a rightward grating, prey-like stimulus or water puff. This suggests that the choice of stimuli in these experiments is capable of eliciting diverse behaviours.

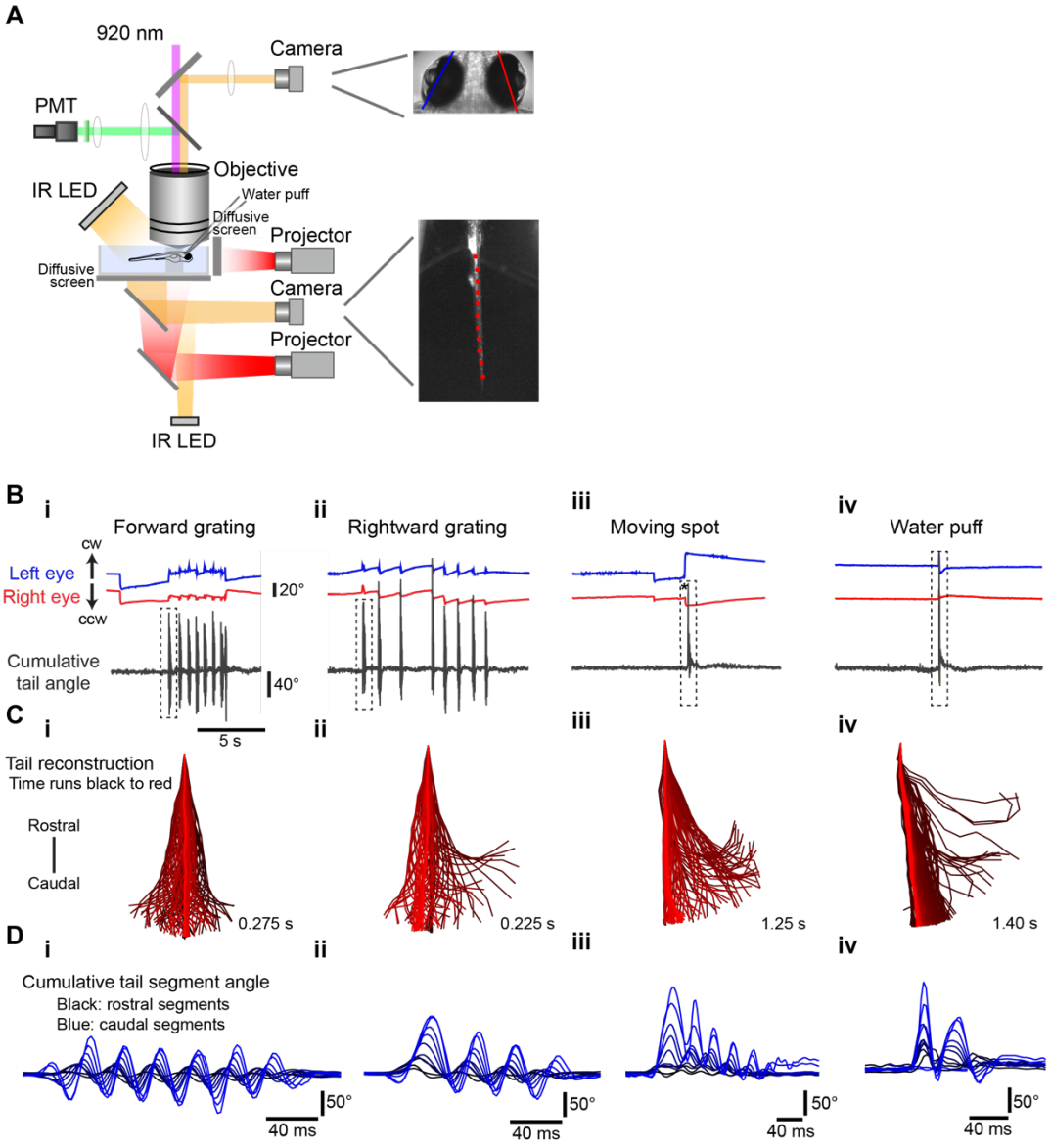

Figure 2.3 Combined 2P calcium imaging and behavioural tracking

A. Schematic of the experimental setup and behavioural tracking. Left illustrates how a partially-restrained larva is positioned underneath the objective with visual stimuli presented in front of and below the fish. Infrared LEDs allow for online eye and tail tracking, representative images of which are shown on the right. Overlaid are the vectors used for calculation of eye angle (blue for left eye, red for right eye), and the markers for tail segments.

B. Examples of eye and tail tracking for different stimuli presentations. Left eye angles in blue, right eye angles in red, and cumulative tail angle in grey. Asterisk denotes a convergent saccade.

i. Forward moving grating presented beneath the fish which typically evokes forward swims.

ii. Rightward moving grating presented beneath the fish which typically evokes turns towards the right.

iii. Moving spot presented in front of the fish which typically evokes hunting routines and hunting related swims.

iv. Water puff directed to the fish's left ear which typically evokes an escape "C-start".

C. Overlaid tail reconstruction of a single bout from the cumulative tail angle traces in B (dashed box). i-iv as in B.

D. Cumulative tail segment angles of the bouts in C. i-iv as in B.

2.2.4 Classification of frequently occurring bout types in a tethered preparation

These stimulus-evoked bouts show kinematic differences. For example, swims that look similar at the level of the cumulative tail angle in response to a moving spot and water puff (Figure 2.3Biii, iv), show more obvious differences when looking at the cumulative angles of individual tail segments (Figure 2.3-Diii, iv). In particular, the moving spot swim shows a greater curvature in caudal tail segments, whilst the water puff swims show additional bending of the tail in very rostral segments. Thus, by describing behaviour in terms of detailed tail kinematic features, it is possible to identify unique characteristics between the swims evoked through different stimuli.

Bouts in freely swimming fish have recently been categorised by their kinematic features (Marques *et al.*, 2018), and we wanted to develop a similar categorical description of tethered behaviour for comparison. It is important to note that due to the use of a tethered preparation, we do not have measurements of larval displacement for these swims. Displacement measures have been used to describe bouts in multiple studies, and also feature prominently in the bout classification by Marques et al., meaning that it cannot be directly applied to these experiments (Borla *et al.*, 2002; McElligott and O'Malley, 2005; Marques *et al.*, 2018). As we found that bouts evoked from different stimuli show different tail kinematics, we first described the bouts from 51 tethered fish through a range of kinematic features (see Appendix A). These features include those that are descriptive of the whole bout, such as overall asymmetry index, as well as features specific to individual half beats at different lengths of the tail, such as the peak angle (θn) or velocity (vel n) (Figure 2.4Ai). Once this kinematic representation of all bouts was collected, I used a bout clustering procedure that was developed by Dr Isaac Bianco. In brief, PCA was performed on the bouts in kinematic features space, and the resulting first 20 PCs were then used in a clustering procedure to produce 9 distinct bout types (see Methods; Figure 2.4B). We found three symmetrical bout types under the "forward swim" (FS) category, and three bout types under the turn category, each with a left and right direction.

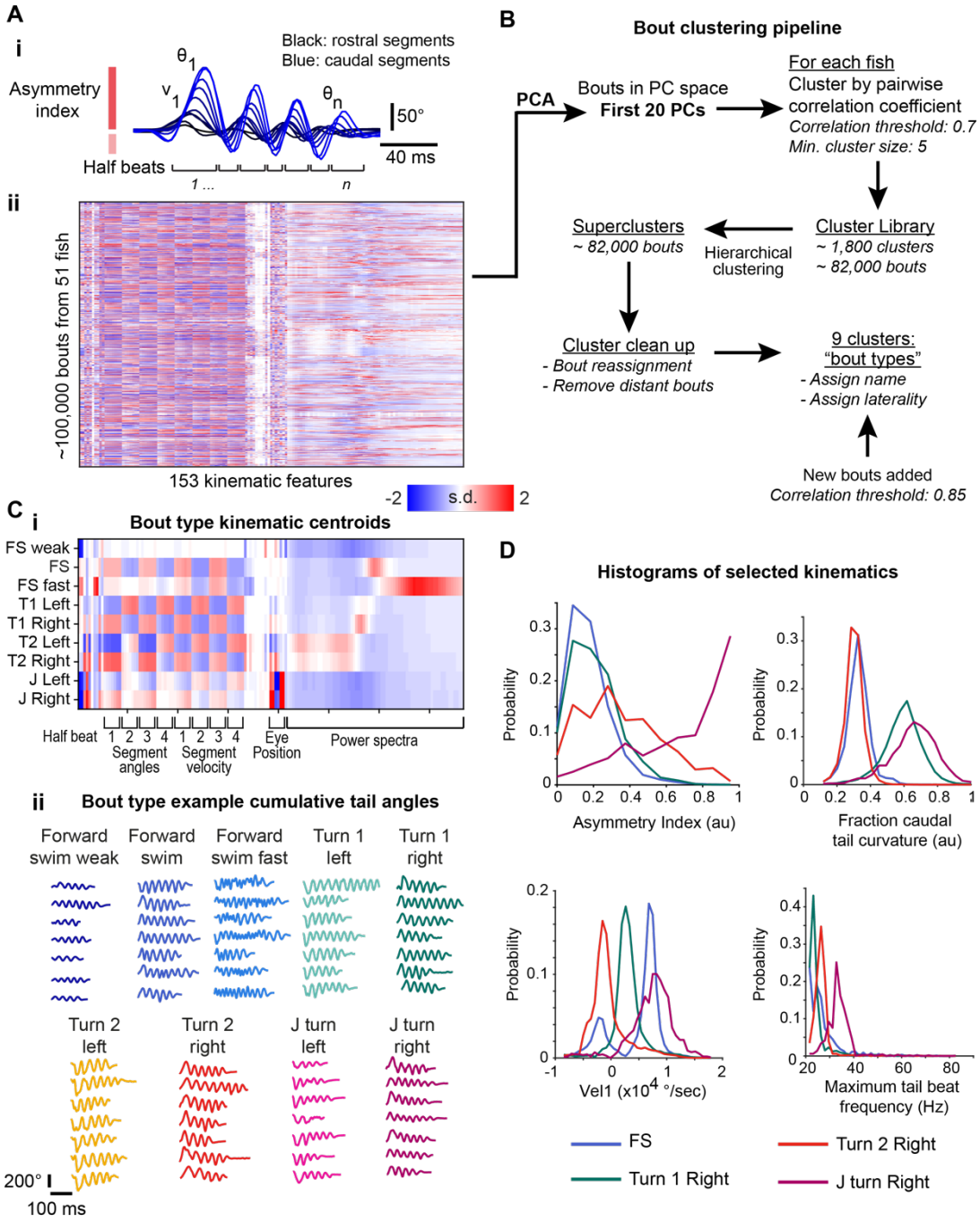

Figure 2.4 Unsupervised clustering identifies 9 bout types based on motor kinematics
A. Bouts can be described in terms of various kinematics.
i. Illustrative example of the kinematic information obtained from tail tracking. Parameters can be at the bout level (asymmetry index, maximum angle etc.), whilst others are specific to each cycle of the tail ("half-beat") and include measurements for each tail segment. See Appendix A for full list.
ii. Matrix of bouts from 51 fish described by their intrafish z-score to 153 kinematic features.
B. Unsupervised clustering pipeline to identify distinct bout types.
C. Kinematic centroids and cumulative tail angle for each of the identified bout types.
i. Kinematic centroids for each bout type, calculated as the median values across all bout types. Same scale as in A ii. Bouts were randomly selected and equally sampled from 5 different fish.
ii. Example cumulative tail angles for each bout type. Bouts were selected randomly from 5 different fish.
D. Histograms of selected tail kinematics for selection of bout types. Only forward swim and right turn bout types are displayed for easier visual comparison.

2.2.5 Bout types are kinematically distinct

The FS bouts are akin to the approach and slow swims categorised by Marques et al., (Marques *et al.*, 2018). The three FS bout types are: FS weak, FS, and FS fast. Progression from FS weak to FS fast demonstrates an increase in high power tail movements (Figure 2.4C). These bouts are largely symmetric about the midline, except for FS bouts which show a slight bias towards rightward swims, as demonstrated by positive segment angles in the first half beat. As the bout types have been calculated from many bouts across many fish, this slight rightward bias is likely to be common to many fish. Possible causes for this systematic effect might be due to experimenter handling or the layout of the microscope.

Under the turn category, there are 3 types, each with a left and right direction: Turn 1 (T1), Turn 2 (T2), and J turns. All turn types show greater segment angles and velocities towards the direction of turning for the first half beat (Figure 2.3C). T2 bouts are separable to T1 bout types largely due to their higher amplitude segment angles in the first and third half beats, as well as their lower frequency tail oscillations. J turns are kinematically distinct to both T1 and T2 turns. J turns have higher values for eye position kinematics reflecting convergence of the eyes during these bouts. As J turns are a bout common to hunting routines, and hunting routines are defined by periods where the eyes are converged, this suggests that these are bouts used when hunting has been evoked. In addition, unlike the other turn types, these identified J turns show particularly high tail bending of only the caudal segments, which is also a characteristic of these swims as described in the previous literature (McElligott and O'Malley, 2005).

Some kinematics show similar distributions across the different identified bout types, whilst others show more obvious differences and represent features that are characteristic of that bout type. As there are symmetrical left/right pairs of bout types, I selected only the rightward turns and FS bouts for easier comparison (Figure 2.4D). One can see that while FS and T2 right bouts show similar fractions of caudal curvature, they are more distinguishable from their vel1 values. Similarly, FS and T1 right bouts show a similarly low asymmetry index, but can be easily differentiated from their distributions for other kinematics such as fraction of caudal tail curvature, vel1 or maximum tail beat frequency. Again, the J turns identified here show several kinematic differences to the other bout types, such as greater asymmetry values,

caudal tail curvature and tail beat frequency. These have also been identified as key kinematics for this bout type in other studies (Borla *et al.*, 2002; McElligott and O'Malley, 2005). This indicates that bout types are not necessarily distinguishable from single kinematics, and that their differences are a result of a combination of kinematics.

Aside from kinematic distinctions, the different bout types also show some context-specific deployment (Figure 2.5). For moving gratings, the most common bout type is the one that produces swimming in the direction of that grating: forward swims for forward gratings, T2 left for leftward gratings, and T2 right for rightward gratings (Figure 2.5A,B,C). Looming, and prey-like spots elicit a higher fraction of J turns than the other stimuli (Figure 2.5D,E,F). As J turns are common to hunting routines, this suggests that these particular stimuli are capable of evoking a hunting response in larval zebrafish. While this is unusual for a looming stimulus, I suspect that early into the expansion of the looming spot, when the spot size is small, that it may resemble a prey and thus elicit a hunting response in the fish. Dark flash stimuli elicit a range of turns, which suggests an attempt to re-orient (Burgess and Granato, 2007). Finally, the water puff stimulus evokes a very high fraction of FS fast swims, suggesting some high power avoidance swim, possibly similar to the "burst swims" described in response to a similar stimulus elsewhere (Budick and O'Malley, 2000). This context-specific occurrence of particular bouts is therefore in keeping with published results, and demonstrates the locomotor diversity that can be evoked under tethered conditions.

It is also clear that these bout types do not encompass all of the behaviours produced by larval zebrafish. For each stimulus condition, a large fraction of bouts are unclassified (Figure 2.5). Some of these unclassified bouts could be the result of tracking errors, or the production of "struggles" which can occur in tethered preparations. Under freely-swimming conditions, one would expect to identify escape-related swims such as the "Spot Avoidance Turn", "O-bend" or "C-start" in response to looming spots, dark flashes and water puffs respectively (Kimmel, Patterson and Kimmel, 1974; Burgess and Granato, 2007; Marques *et al.*, 2018). Yet this classification does not identify any bout types which are obviously similar to these labels. However, water puff stimuli evoke a high fraction of FS fast and unclassified bouts. FS fast swims might represent a secondary component to an escape behaviour, and the large fraction of unclassified bouts suggests that escape behaviours are being

evoked, but are not numerous enough in the current classification to have formed a robust bout type.

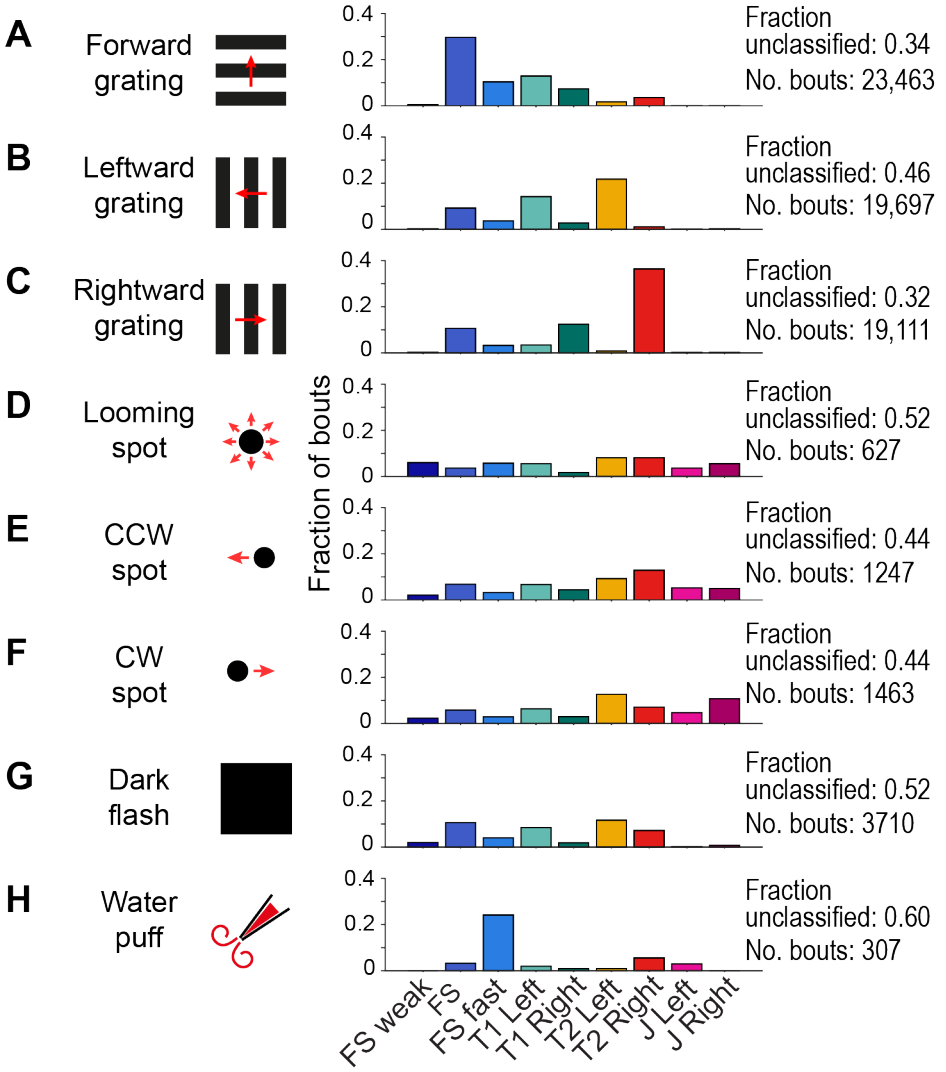

Figure 2.5 Bout occurrence for different stimuli
A-H. Fraction of each bout type which occurred for different stimuli presentations. Values were computed for bouts pooled across 67 fish in A-G, and 18 fish in H.

2.2.6 Reticulospinal activity associated with different bout types

As the different bout types are kinematically distinct, I wanted to determine if this was similarly reflected in the patterns of RS and non-RS activity associated with each bout type. If different RS and non-RS cells are active for each of the bout types, this would suggest more of a dedicated circuitry where these RS cells are highly tuned to the kinematic features associated with each bout. On the other hand, if all cells showed similar activity across these behaviours this would suggest a more distributed circuit where the cells are broadly tuned across kinematic features.

First, I had to identify and label the imaged cells, and obtain a suitable measure of activity from the calcium imaging data. After *post-hoc* movement correction, I manually segmented cells and assigned them to their appropriate RS/non-RS cell label (Figure 2.1C). While GCaMP6f offers faster kinetics than other GCaMP6 variants, it still shows a slow exponential decay which offers a low temporal resolution measure of activity. To calculate a measure of each neuron's activity I applied the OASIS deconvolution algorithm to infer spikes (Friedrich, Zhou and Paninski, 2017). This deconvolution produced activity measurements which are more temporally restricted than using the calcium transients alone. This analysis provided an inferred spike rate for each cell and therefore also offered a binary measurement of whether a cell was active or not at a given time. For each cell, I used these measurements to calculate the fraction of times it was active, i.e. its recruitment probability, and its mean inferred spike rate for each bout type.

2.2.7 Anatomical recruitment maps for different bout types

To visualise these values and combine the data from across fish, I produced anatomical maps where each RS/non-RS label is coloured by the mean recruitment probability (Figure 2.6), or the mean inferred spike rate of those cells towards each of the different bout types. I find that these maps show partially overlapping yet distinct activity patterns, suggesting that these behaviours are not produced as the result of a totally distributed circuit architecture across RS and non-RS neurons. These features can be

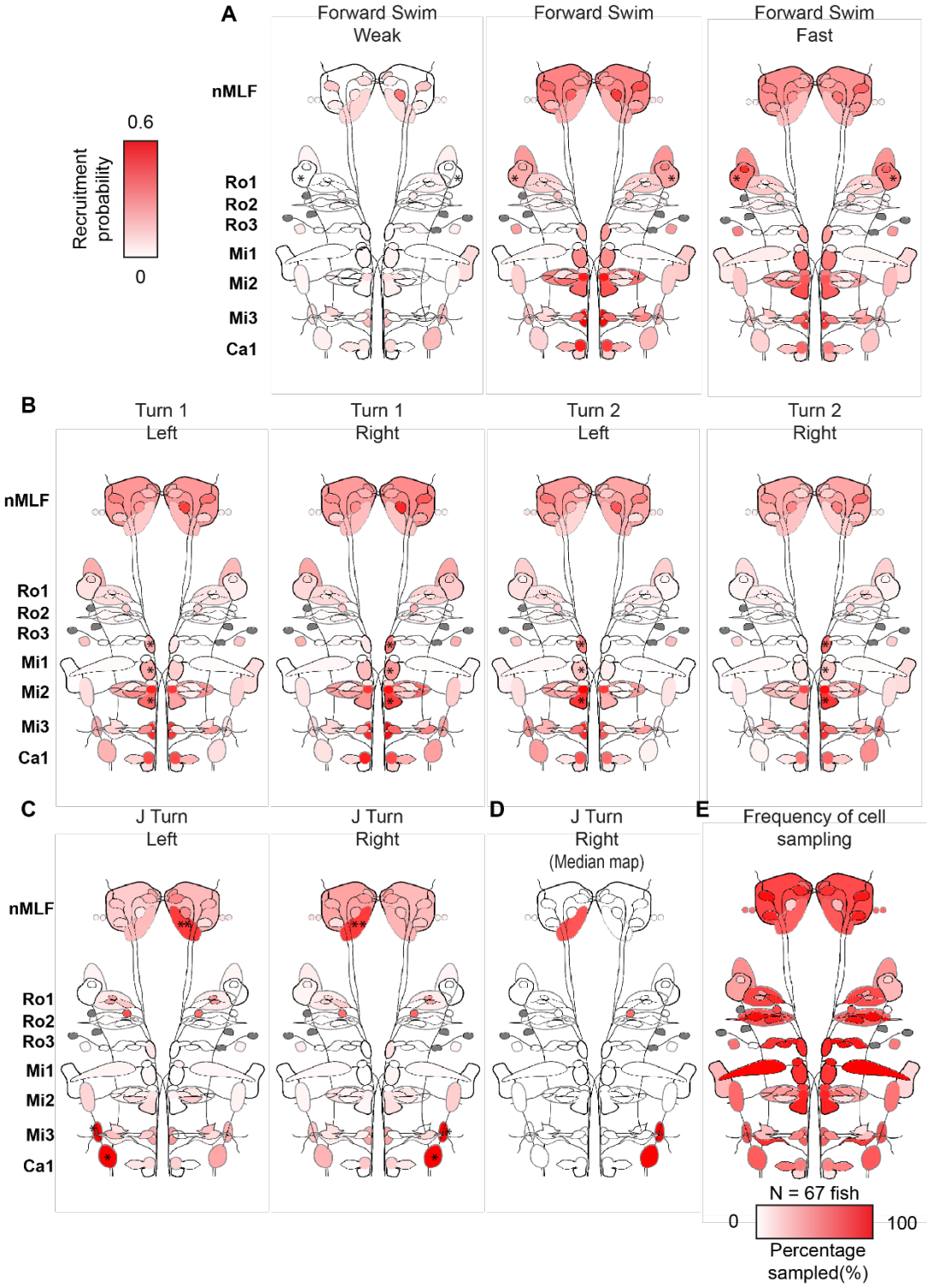

Figure 2.6 Recruitment maps: Probability of a cell label being active during different bouts
A-C Cell labels are coloured here by the mean recruitment probabilities of all cells in that label to a specific bout type. The recruitment probability for each bout type is calculated individually for each recorded cell.
A. Forward swim bout types. RoL1 cells are marked with an *.
B. Turn bout types: Turns 1 and 2. Ventromedial cells on the ipsilateral side to turn direction are marked with an *.

C. J turns. Caudal, lateral non-RS cell groups on the ipsilateral side to turn direction are marked with an *, non-RS nMLF arbors on the contralateral side to turn direction are marked by **.
D. J turn right recruitment map where cells are coloured by the median recruitment probability for all cells within that cell type.
E. Fraction of cells in each cell type labelled in these maps. Values for single cell labels are calculated as their presence in an imaging experiment divided by the total number of fish. For group cell labels are coloured by the number of cells labelled in a fish, divided by the mean of all cells of that type across all fish.
Cells marked with grey mean no measurements were collected for that cell type. Data collected from 67 fish.

seen from both comparisons across categories of bouts, such as FS versus turn bout types, as well as within these categories, for example across different turn types or FS intensities. The shared patterns of recruitment between bout types suggests that these cells could mediate a kinematic feature common to all swims, whilst the unique contributions of cells to single bout types suggests a role in producing kinematics characteristic to that bout type.

One example of shared recruitment is seen in the large nMLF cells which show spiking activity across all bout types (Figure 2.7). These neurons have previously been implicated in tail beat frequency and swim speed (Severi *et al.*, 2014), which would support a role across the various swim types observed here. In addition, for FS weak swims, only the large MeLm cells in the nMLF show a high spike rate (Figure 2.7A). As the swims become more vigorous, the other large nMLF cells show greater activity (Figure 2.7A). This is in keeping with the findings by Severi et al., where the activity of nMLF cells was found to correlate with features such as tail beat frequency (Severi *et al.*, 2014). These recruitment maps therefore identify the large nMLF cells as those which could support the production of kinematic features common to multiple bout types.

Some RS neurons which show differential recruitment between bout types are the ventromedial cells (Figure 2.6B, Figure 2.7B). These cells have been associated with turning (Orger *et al.*, 2008), and have been found to be important in producing a lateralised, high amplitude tail angle for the first half beat (θ1) (Huang *et al.*, 2013). In keeping with this, these cells show an expected symmetrical recruitment for non-lateralised behaviours such as forward swims, and an asymmetric increase in recruitment probability and inferred spike rate on the side ipsilateral to turn direction (Figure 2.6,C, Figure 2.7 B,C). Between T1 and T2 bouts, there is a relative increase in the recruitment probability and mean number of spikes for RoV3 and MiV2 cell

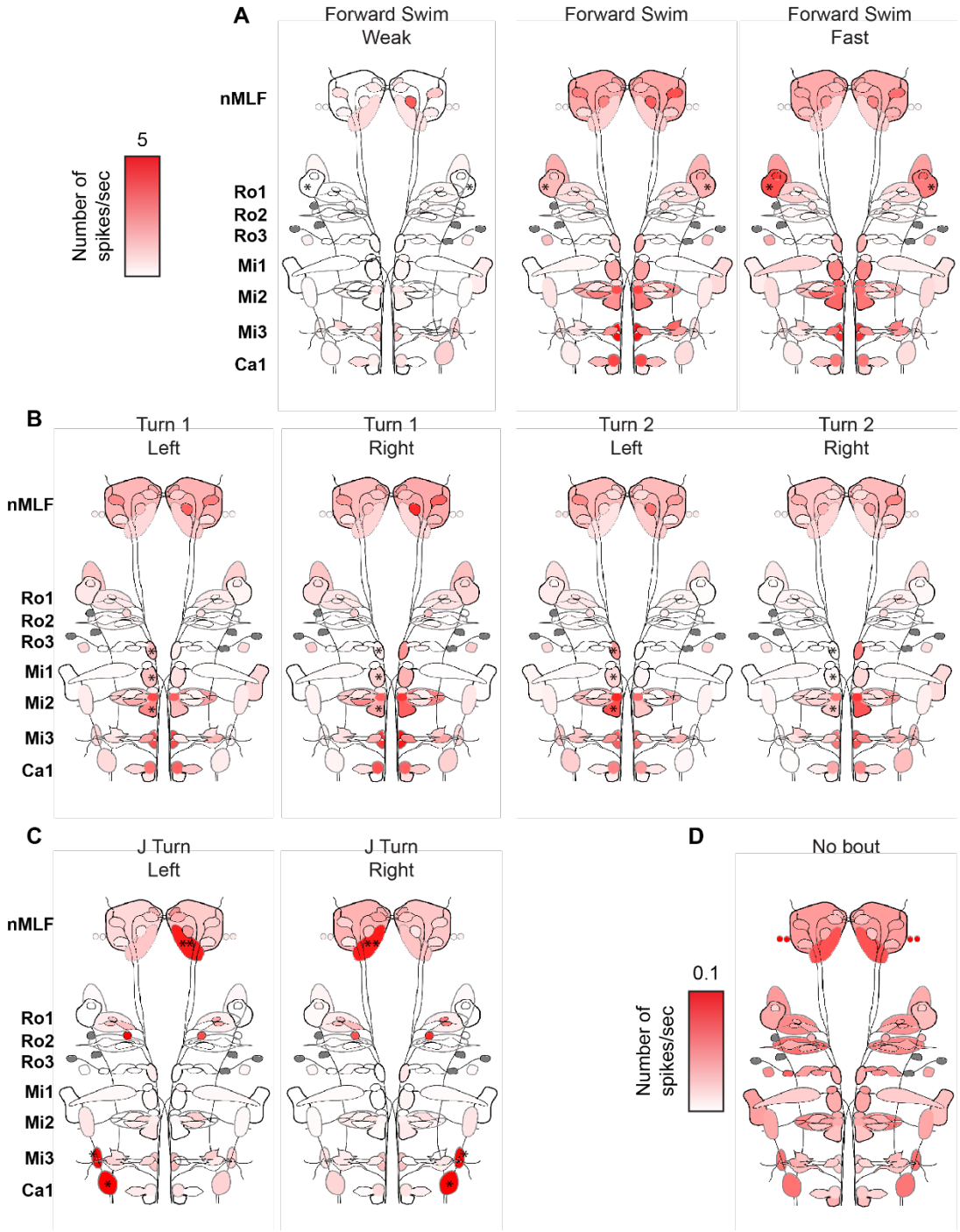

Figure 2.7 Activity maps: Mean inferred spike rate for each cell label for each bout type

A-C. Cells are coloured by the mean inferred spike rate during that bout for all cells of that cell type.

A. Forward swim bout types. RoL1 cells are marked with an *

B. Turn bout types: Turns 1 and 2. Ventromedial cells on the ipsilateral side to turn direction are marked with an *.

C. J turns. Caudal, lateral non-RS cell groups on the ipsilateral side to turn direction are marked with an *, non-RS nMLF arbors on the contralateral side to turn direction are marked by **.

D. Mean inferred spike rate calculated across periods of no swimming. Note different scale to maps in A-C.

Cells marked with grey mean no measurements were collected for that cell type. Data collected from the same 67 fish as Figure 2.6.

groups in comparison to MiV1 cells. This supports the finding that RoV3 and MiV2 cells have a stronger bias for ipsilateral turns than the MiV1 cells, which show a weaker directional bias (Huang *et al.*, 2013). It is reassuring to identify ventromedial cell activity during turns using our methodology and confirm the results in the literature.

RoL1 cells also show bout-type specific recruitment. These cells show a greater probability of recruitment and spiking during forward swims compared to other bout types. Previous studies have also associated RoL1 cells with stimuli that evoke forward swimming and forward swimming decoded from ventral root recordings (Orger *et al.*, 2008; Vladimirov *et al.*, 2018), and it is interesting to see here that their recruitment probability and inferred activity increases as the swim becomes more vigorous (Figure 2.6A, Figure 2.7A). However, these cells also show a mild recruitment for T1 bouts. As T1 bouts closely resemble FS bouts (Figure 2.4C), the bilateral recruitment of these cells for FS, FS Fast and T1 swims suggest a possible role in producing coordinated, symmetric tail beats.

Within turn types, there is a marked difference in the recruitment maps for J turns compared to T1 and T2 bouts. As described earlier, J turns are kinematically distinct to other turn types, most notably due to tail bending in the caudal segments and eye movements which produce convergence of the eyes. These kinematic distinctions could in turn be reflected by the differences in the probability and spiking maps for J turns when compared to other turn types. Notably, for the J turn maps, there is a reduction in the recruitment of the ventromedial cell groups typically associated with turns. Instead, J turn maps show prominent asymmetric recruitment patterns in non-RS cell types. These non-RS cell types which show recruitment during J-turns can be further separated into those whose recruitment is either ipsilateral or contralateral to the turn direction. There are caudal, lateral non-RS cells which show preferential activity and recruitment on the side ipsilateral to the J turn (cells marked *, Figure 2.6C, Figure 2.7C). The non-RS arbors in the nMLF however, show increased recruitment and activity on the side contralateral to turn direction (cells marked **, Figure 2.6C, Figure 2.7C). These non-RS arbors in posterior nMLF are close to the oculomotor nucleus which innervates the muscles controlling eye movements (Higashijima, Hotta and Okamoto, 2000). I suspect that the activity of these arbors during J turns reflects the high vergence angle observed in hunting routines, and as such might serve to coordinate eye and tail movements. Overall the

clear kinematic differences between J turns and other turn types appears to be reflected by distinct J turn recruitment maps which show unique involvement of different RS and non-RS cell groups

The J turn recruitment maps feature symmetrical recruitment of cells in Ro1-Ro2. In particular, RoM1c, RoM1r, and the newly described RoM2a cells show a higher probability of being active for J turns than all other bout types. The bilateral recruitment of these cells suggests that they could be involved in a symmetric feature of J turns, such as the straightening of the rostral parts of the tail such that the tail bend is limited to only caudal segments (McElligott and O'Malley, 2005).

2.2.8 Recruitment probabilities are not normally distributed

Maps coloured by the median recruitment probability of the cell types to the different bout types are sparser than those coloured by mean values. This is exemplified in Figure 2.6D which shows a median recruitment map for right J turns. The presence of more low values suggests that the overall recruitment probability of cells is very low, and that measures of recruitment probability or inferred spike rate are not normally distributed. As these measurements are collected across multiple fish, this could represent variations in the connectivity and activity of different neurons between animals. This distribution of recruitment probabilities suggests that RS neurons show aspects of a reorganising circuit architecture (Morton and Chiel, 1994), with some neurons being flexibly added or removed from the active group, while there are others which show a more reliable involvement, such as the lateral, caudal non-RS cells in this example (Figure 2.6D).

2.2.9 Baseline activity

RS cells are considered to be largely silent when there is no locomotion. To investigate this, I also produced a map of inferred spike rate for all periods where there were no recorded bouts (Figure 2.7D). Some non-RS cells near the nMLF (Figure 2.7D), show a high number of inferred spikes, however this is expected as these cells show a strong response to dark flash stimuli, regardless of any accompanying

behaviour. Otherwise, the inferred spike rate of these cells is substantially lower than the values measured in response to a bout occurring.

These inferred spike rates in the absence of swims can provide some insight into the false positives produced by the spike inference method. The Mauthner cell shows a very low firing rate in the absence of any bouts, but it is known that a single spike in one of these cells is capable of eliciting an escape swim (Eaton, DiDomenico and Nissanov, 1991). This suggests that the OASIS algorithm may therefore be detecting some spikes incorrectly. Due to the very low inferred spike rates for when there was no swim bout compared to when there was a bout, this suggests that the value of these false positives is very low and different to when the cell was likely to have been truly active. It is also reassuring to see that all cells show a similar level of spiking in the absence of behaviour, suggesting that if this value is partly due to errors in spike inference, then at least this is equal across the population.

2.3 Discussion

The distinct patterns of RS and non-RS recruitment we observe for kinematically distinct bout types indicates a dedicated or reorganising circuit architecture underlying the production of these behaviours. In support of the latter, I find that the probability of recruitment for single neurons is not normally distributed, suggesting that some neurons are added or removed from the active group. The shared elements of recruitment maps between bout types suggest that these cell groups might encode kinematic features common to these bout types, whilst the unique elements of recruitment maps between bout types might encode kinematic features that are characteristic to individual bout types.

2.3.1 Characterisation of non-RS cells and newly identified RS cells

KalTA4u508 larvae provide a valuable tool in which to study RS activity, but this transgene also labels additional non-RS cells which may be occasionally confused with RS cells. The non-RS cells are largely anatomically distinct to RS cells, but in

some areas, such as around RoL1 or around MiV2, the distinction between non-RS and RS is less clear. Throughout these experiments, I have tried to distinguish these cells by using features such as their dorsoventral positioning, but it is possible that some cells are incorrectly classified. Otherwise, by repeatedly updating the drawn ROIs throughout these experiments I believe that if there are any mis-assignments, they are at least consistent.

Many non-RS cells labelled by *KalTA4u508;UAS:GCaMP6f* show bout-related activity, but we do not know their morphology or neurotransmitter identity. To develop an idea of these cells' neurotransmitter phenotype, I could perform immunohistochemistry staining of particular neurotransmitters and look for coexpression with *KalTA4u508;UAS:GCaMP6f* . I could also compare the expression of *KalTA4u508* fish with larval zebrafish brain atlases for different neurotransmitter types, however the spatial resolution of these methodologies following might not be good enough to confidently conclude cell identities (Marquart *et al.*, 2015). To examine the morphology of individual neurons I have conducted preliminary experiments to label single cells through either focal electroporation or transient expression by microinjection of DNA constructs into one-cell stage *KalTA4u508;UAS:GCaMP6f* embryos. While both have been successful in labelling individual neurons, to develop a complete sampling of all non-RS or newly identified RS cells will take some time. Overall, by characterising these neurons we would be able to identify which are spinally projecting, and whether or not they contribute to local circuits to regulate RS activity.

2.3.2 Classification of tethered behaviour

While the bout types classified from the behavioural data described here were valuable in examining population activity across fish, these categories do not constitute the full behavioural repertoire of tethered fish. For example, there is currently an absence of "aversive" bouts, such as the "O-bends", "Spot avoidance turns" and "C-starts" in this data. It is known that some free-swimming behaviours cannot be reproduced under tethered conditions (Severi *et al.*, 2014). In the case of O-bends, where the body and tail shape resembles an "O" such that the tail almost touches the head, one can imagine that this is hard to achieve in a tethered preparation

where agarose surrounding the body and head prevent this freedom of movement. However, we do know that spot avoidance turns and Mauthner-related C-starts can be successfully evoked in tethered fish (O'Malley, Kao and Fetcho, 1996; Temizer *et al.*, 2015; Bhattacharyya, McLean and MacIver, 2017).

I suspect that an aversive "C-start"-like behaviour is present in this data, but was not able to be classified at the stage of bout clustering. For example, in these experiments I found that fish performed vigorous swims in response to water puff stimuli (Figure 2.3 BCD iv, Figure 2.5H). Furthermore, during ROI marking I was able to confirm that this happened together with Mauthner cell activity. However, a bout resembling a C-start was not found, and similarly the Mauthner cell did not appear in any of the bout recruitment maps (Figure 2.6 Figure 2.7). This is likely to be a result of an undersampling of these bouts in order for them to have formed a robust cluster. Aside from the water puff stimulus not being present for all the fish used in the bout clustering procedure (water puff present for 4/51 fish), these aversive bout types are more likely to occur singly during a single stimulus presentation, as opposed to forward or turn swims which occur repeatedly in response to a single stimulus. This means that there are likely to be fewer occurrences of these bouts in comparison to the others. Repeating the bout clustering with more fish which have received a water puff stimulus is likely to result in the identification of an aversive bout type.

2.3.3 Functional heterogeneity within RS and non-RS cell labels

It should be noted that whilst these maps offer a useful way in which to identify cell groups with behaviourally relevant activity, these recruitment maps do not sufficiently describe the distribution of each cell type's recruitment probability or inferred spike rate. A cell type's recruitment probability or spiking is often not normally distributed. Maps coloured by the median of a group's recruitment probability or median inferred spike rate appear much sparser, suggesting that many cells only have low values (Figure 2.6D). This is suggestive of several things: bout types could have merged swim types with varying RS activity patterns, there could be redundancy between cells resulting in inconsistent recruitment of cells for single behaviours, or cells could show broad behavioural tuning.

In the next chapter, I present modelling approaches we developed to examine the kinematic encoding of individual cells. This allows us to identify whether RS and non-RS neurons form functional groups corresponding to the unique and shared elements of recruitment maps towards the different bout types. Furthermore these encoding models will provide us with information about the functional heterogeneity of cells within a label.

Chapter 3 Encoding models of reticulospinal activity

3.1 Introduction

As the patterns of RS recruitment across the kinematically distinct bout types show shared and unique elements, this suggests that RS neurons could encode behavioural features that are common to multiple bout types, or which distinguish individual bout types. It also appears that neurons show varying recruitment towards single bout types, suggesting a reorganising circuit architecture where neurons could show broad behavioural tuning in order to be flexibly recruited to different bout types. To examine the motor representations encoded by RS neurons, we decided to develop encoding models which predict RS activity using these kinematic features. The use of kinematic features as predictors for these models is supported by the presence of kinematic distinctions between bout types (Chapter 2), as well as evidence from ablation studies which demonstrated that subsets of RS neurons support specific kinematic outputs (Huang *et al.*, 2013; Severi *et al.*, 2014).

We hypothesise, therefore, that RS activity can be modelled with kinematic features, and there will be functional groups of neurons with similar kinematic encoding. These functional groups should be able to relate to the identified bout types. In this chapter I describe the development and application of these encoding models to RS activity. This work has been the result of a collaboration with Dr James Fitzgerald, Janelia.

3.2 Results

3.2.1 Encoding model development

To develop encoding models of RS activity, we used a generalised linear model. As we wished to examine kinematic encoding, we wanted the model inputs to be the kinematic features described in Chapter 2. Due to high collinearity between features, for example correlations between nearby segments of the tail, we used singular value decomposition (SVD) to compute orthogonal "kinematic modes" (Figure 3.1A). These modes were then used as the model inputs. The output of this model was the inferred spike rate of each individual cell recorded from 61 fish, for every bout performed while that cell was being imaged (Figure 3.1A). As this output measurement is a rate, we used Poisson regression to relate neural activity and behaviour (Figure 3.1B).

In order to produce a sparse, interpretable model, we used elastic-net regularisation to limit both the number and magnitude of model coefficients (Zou and Hastie, 2005; Figure 3.1Ci). This produced, for each cell, a series of model coefficients corresponding to the kinematic modes. The coefficients corresponding to these modes were then mapped back to the kinematic feature space, thus providing an idea of which kinematics contribute to the activity of each cell (Figure 3.1D). The sign of the model coefficient for a specific feature indicates the direction of its contribution to the neuron's response, and the magnitude reflects the size of this contribution. Negative coefficients can be interpreted as providing a reduction or damping effect on a cell's activity. Application of these coefficients together with the behaviour from particular bouts in our generalised linear model ultimately produces the predicted activity of that individual cell, across those bouts ($\hat{y}$, Figure 3.1B).

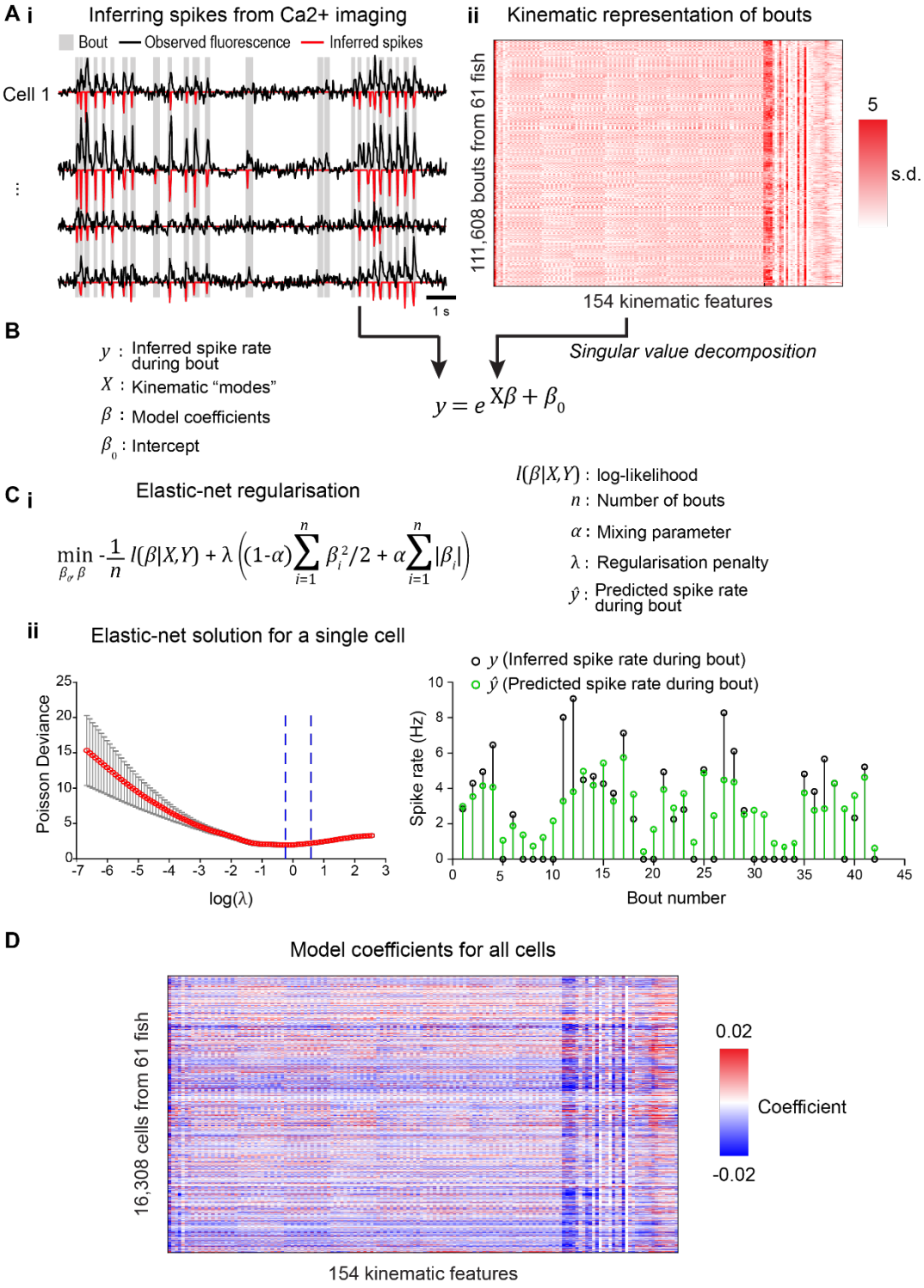

Figure 3.1 Building encoding models of RS activity
A. Input and output features for predictive modelling.
i. Predictive model output is the inferred spike rate (red). Inferred spike rate is inverted for easier visualisation.
ii. Bouts are described by a range of kinematic features. Singular value decomposition is used to represent each of these bouts in terms of "kinematic modes" which act as the input features for predictive modelling.
B. Generalised linear model used to relate RS inferred spikes to kinematic modes. As the model output is in terms of spike counts, the link function takes the form of a logarithm.

C. Example of elastic-net regularised regression for a single cell.
i. The loss function minimised by elastic-net regularisation.
ii. Model fit for a single cell. Left, selection of regularisation penalty λ. Blue lines depicts λ values which give the minimum cross-validated Poisson deviance and one standard error of this minimum. Error bars are standard deviation. Right, the model prediction and actual inferred spike rate for this cell.
D. Model coefficients for each cell converted into kinematic feature space.

3.2.2 Identification of "kinematic modules"

To identify functional groups of cells, we wanted to cluster cells with similar encoding models. However, due to remaining redundancy between predictors, we did not simply want to cluster cells by their model coefficients. Instead, we decided to cluster cells by their predicted "linear drive" to a selection of 5000 bouts sampled across all bout types and collected from the 61 fish (Figure 3.2A). By using actual recorded bouts, the combinations of kinematic features for each bout were therefore appropriately correlated in a realistic way. Furthermore, by calculating the linear drive for each cell over such a large number of bouts sampled from different fish, this meant that we predicted activity for bouts where the cell might not have been active. We then clustered cells by their linear drive values across these bouts using an agglomerative pairwise correlation algorithm (Bianco and Engert, 2015).

This clustering method produced 12 distinct clusters which we term "kinematic modules" (Figure 3.2B). Each module contains cells from multiple fish, and also contains a variety of RS and non-RS cell types. The cells forming these modules also show similar patterns of linear drive in response to a selection of novel bouts which were not used in the original clustering procedure. This indicates that the clustering is well-supported across new data, and that we have identified robust kinematic modules.

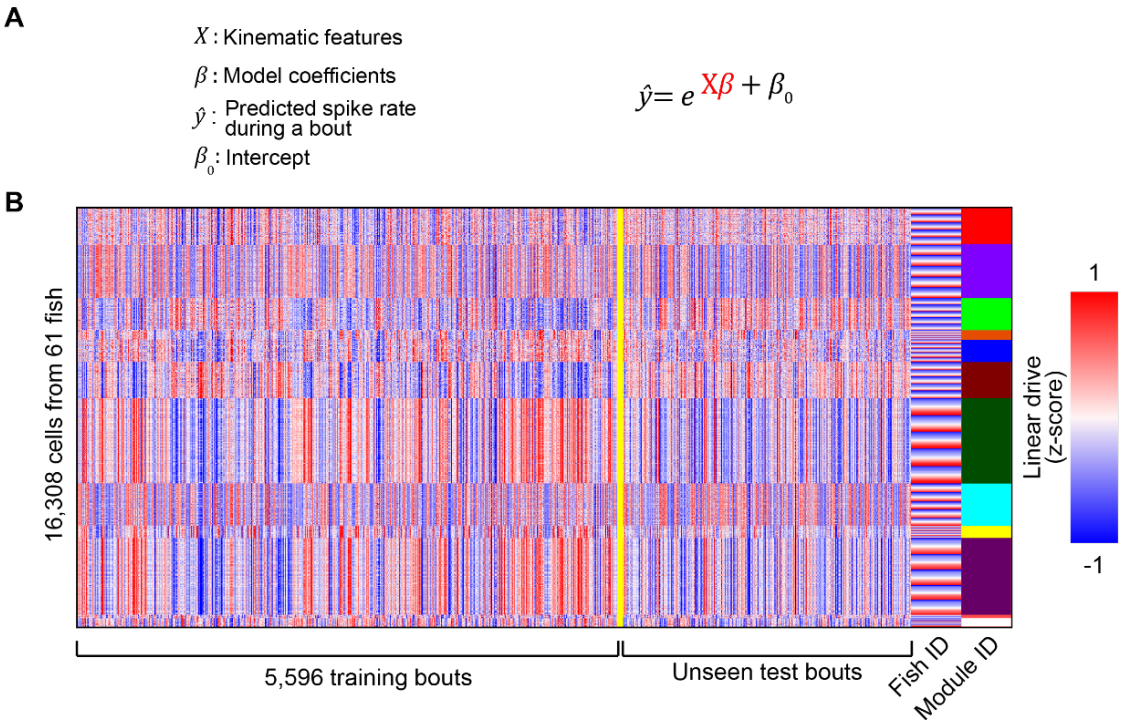

Figure 3.2 Clustering cells by their linear drive to identify "kinematic modules"
A. Generalised linear model used to relate kinematic features to neuronal activity. The $X\beta$ term coloured red is the "linear drive" value used to cluster cells calculated across a large number of bouts. B. Z-scored linear drive of cells clustered into "kinematic modules". These modules represent groups of cells with a similar linear drive, and therefore likely similar patterns of model coefficients. Cells were clustered using a selection of bouts equally collected from the 61 fish. The linear drive of these cells is also included for a group of unseen bouts which were not used in the original clustering.

3.2.3 Kinematic encoding and anatomical composition of kinematic modules

What can these kinematic modules tell us about the kinematic encoding of cells? By virtue of the clustering process, kinematic modules contain cells which have similar linear drive, and also show similar patterns of model coefficients for individual kinematic features (Figure 3.3A). This can be summarised by calculating the mean model coefficients from these cells to produce a kinematic module centroid (Figure 3.3B).

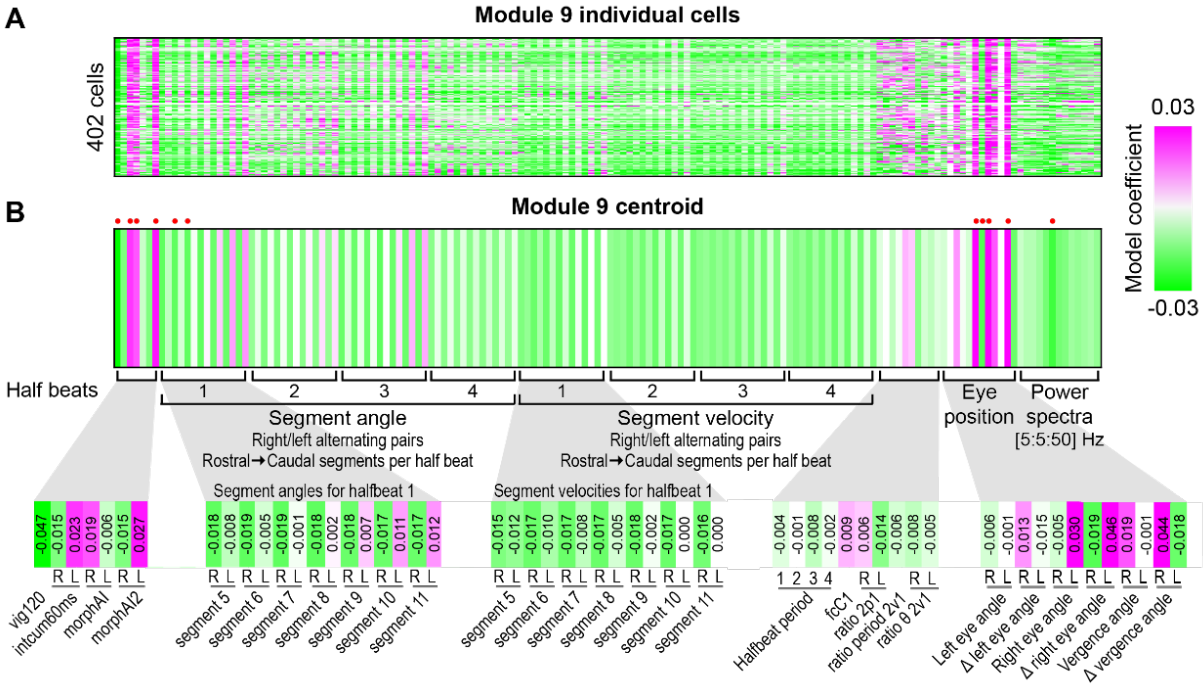

Figure 3.3 Kinematic modules are composed of cells with similar kinematic encoding
A. Model coefficients for all cells in module 9. Cells have not been clustered.
B. The kinematic module centroid of module 9 calculated as the mean of the model coefficients from all cells in A. Top: model coefficients for all kinematic features. Bottom: expanded regions with kinematic features and model coefficients labelled. Red spots indicate the kinematic features with the five highest and lowest model coefficients; R: rightward values; L: leftward values. Further details of the kinematic features can be found in Appendix A.

Examination of the kinematic features with the largest model coefficients in these kinematic modules indicate those with the greatest effect on cell activity. For example, the cells in module 9 show large positive coefficients for kinematic features relating to asymmetry, right eye position, and vergence angle (Figure 3.3B). These kinematics are relevant to the highly asymmetric J turn bouts which occur during hunting routines where the eyes are converged. In keeping with this, there are only positive coefficients for caudal segment angles towards the left, another characteristic of J turns (McElligott and O'Malley, 2005; Figure 2.4). This bias towards the left suggests that this module could contain cells which are asymmetric about the midline as observed for turn bout type recruitment maps (Figure 2.6), and also the presence of a complementary kinematic module with model coefficients favouring rightward movement.

To study the presence of such complementary left/right kinematic modules, as well as the cellular composition of each kinematic module, I produced anatomical maps coloured by the fraction of each cell type in a module, and calculated the centroid of their model coefficients (Figure 3.4). I have also highlighted some kinematic features with large model coefficients (see those marked with red spots in Figure 3.3B), and also those which showed interesting patterns of model coefficients. Overall, this allowed us to consider the anatomical arrangement of cells which show similar kinematic encoding.

Examining the kinematic modules in this way confirms that this clustering procedure has identified functional left/right pairs of modules. These functional pairs are not only complementary in terms of their model coefficients, but also in their cellular composition. Consider the pair formed by modules 2 and 8: module 2 has positive model coefficients for rightward tail angles in halfbeats 1 and 3, and contains a high fraction of ventromedial cells on the right hand side (Figure 3.4B). Module 8 neatly mirrors module 2, by having positive model coefficients for leftward tail angles in halfbeats 1 and 3, and contains a high fraction of ventromedial cells on the left hand side (Figure 3.4H). Additional functional module pairs include modules 3 and 6 (Figure 3.4C,F), and 9 and 12 (Figure 3.4I,L). Modules within a pair also contain similar numbers of cells to each other, which I think adds support to the idea of symmetric groups of cells forming functional pairs of modules.

Some modules contain high fractions of cells which showed increased activity to specific bout types (see Chapter 2). The high fraction of left/right ventromedial cells in modules 8 and 2 is reminiscent of the high recruitment probability and spiking of these cells to left and right turns respectively. These particular modules show large positive model coefficients towards left and right turn angles in the first and third half beats which supports the published result by Huang and colleagues (Huang *et al.*, 2013). This suggests that neurons belonging to these modules might contribute to these distinct kinematic aspects of routine turns.

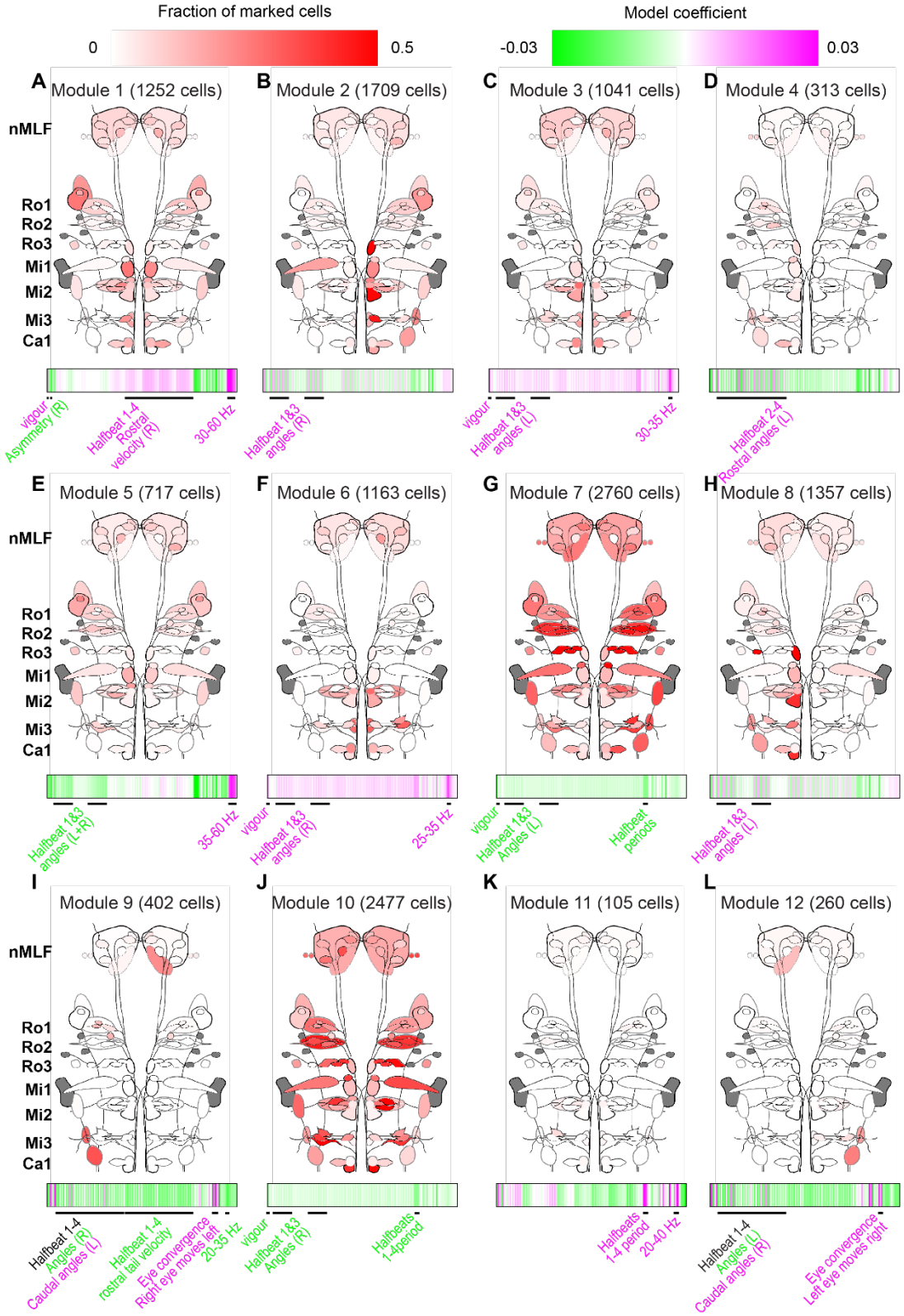

Figure 3.4 Anatomical composition of kinematic modules

A-L. Top are the anatomical maps of the cells constituting each kinematic module. Each cell type is coloured by the fraction of that cell type in a particular kinematic module.

Below are the mean model coefficients in terms of kinematic features for all cells in that module. Some kinematic features are labelled and coloured magenta for positive model coefficients, and green for negative coefficients. (L) indicates kinematics describing leftward tail movements, and (R) for rightward tail movements. The order of kinematic features is the same as in Figure 3.3.

Modules 9 and 12 also form a mirror symmetric pair which contain high fractions of cells which have a high recruitment probability towards J turns (Figure 2.6C, Figure 3.4I,L). These include asymmetric groups of neurons such as the non-RS arbors in the nMLF and the caudal, lateral non-RS cell types in Mi3 and Ca1, as well as cells within Ro1 and Ro2 bilaterally. As described earlier, module 9 contains cells with positive model coefficients towards bout asymmetry, convergent eye movements, and leftward caudal tail bend kinematics which are distinctive of left J turns (Figure 3.3). Meanwhile, the opposite is true for module 12 which contains cells that feature in the recruitment maps for right J turns and has positive weights for rightwards caudal tail angles. These modules can therefore provide an idea of the kinematic features which could be represented by these cells' activity. This is particularly useful for cells such as these whose roles in behaviour are not yet known.

The largest kinematic modules, 7 and 10, contain high proportions of many cells and also chiefly consist of negative model coefficients. These modules each contain cells from nearly all cell types. Their kinematic encoding is highly similar except that module 7 has greater negative coefficients for leftward tail angles, while module 10 has greater negative coefficients for rightward tail angles. The large number of negative coefficients in these modules suggest a reduced linear drive of these cells across many behaviours, which could result in low levels of activity during behaviour. As such high proportions of cell types contribute to these modules, especially some that we know are associated with a behaviour (e.g. the Mauthner cell), it suggests that these modules represent periods where cells were inactive during swims, the inferred spike rate was very low or perhaps true spikes were missed.

3.2.4 Cells within a cell label contribute to multiple kinematic modules

Cells from all RS and non-RS types typically contribute to 3 or more kinematic modules (Figure 3.5). The only exceptions are the RoL3 cells, of which there is only one recorded cell in this dataset. This supports the possible functional heterogeneity within cell labels described earlier from the bout recruitment maps.

Interestingly, the majority of cell types (81/89) also contain a fraction of cells which were not assigned to any kinematic module. For each cell type, this fraction of unassigned cells is less than 0.5. If unassigned cells are the result of poor model fits or noisy data, this suggests that this occurs somewhat evenly across cell types. Overall, this reveals that these kinematic modules contain the majority of sampled cells, and that they are largely composed of cells of different types.

Left/right pairs of cell types show complementary assignment to certain kinematic modules. When comparing the ventromedial cell groups (RoV3, MiV1, MiV2), which have been implicated in opposing turn directions (see Chapter 2), one can see higher fractions of cells in Module 2 for RHS cells, and higher fractions of cells in Module 8 for LHS cells (Figure 3.5). This further supports the presence of left/right functional module pairs.

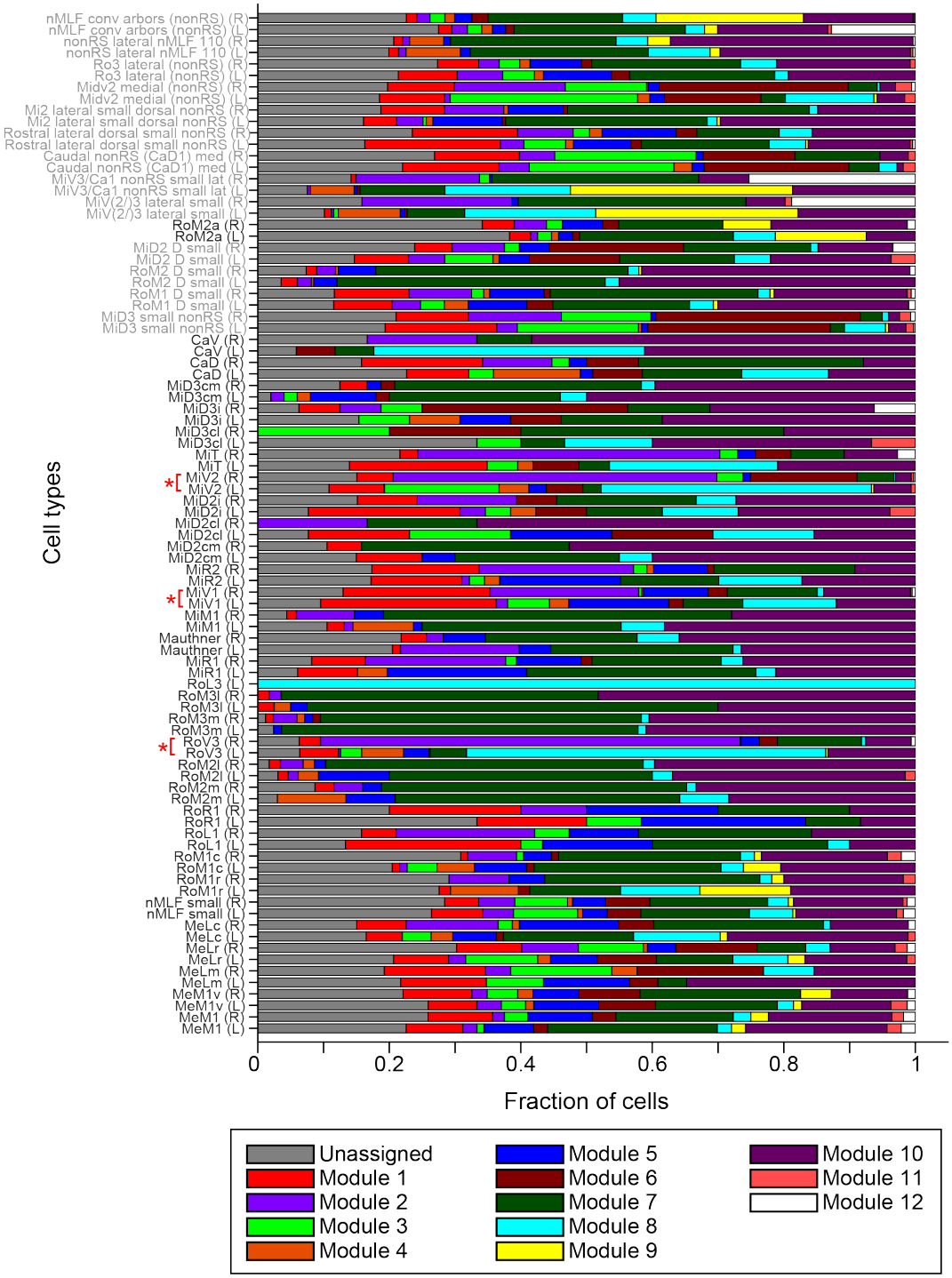

Figure 3.5 Module assignment for each RS and non-RS cell type
Bar chart showing what fraction of each cell type is in each kinematic module or unassigned. Cell types coloured grey are non-RS and those coloured black are RS. Red asterisks indicate a right/left pair of ventromedial cells.

3.2.5 Relationship between kinematic modules and bout types

It is clear when comparing module anatomical maps and bout recruitment maps that single modules do not necessarily contain all of the cells frequently recruited for a single bout. For example, Modules 2 and 8 account for the asymmetric recruitment of ventromedial cells in T1 and T2 bouts, yet there still remain other cells which show recruitment during these bouts. These other cells include ventromedial cells on the contralateral side to turn direction as well as cells in the nMLF Additionally, a fraction of Mauthner cells, typically associated with escape behaviours (O'Malley, Kao and Fetcho, 1996), appear in modules 2 and 8, and are not present for routine turn recruitment maps (Chapter 2). Overall, this suggests that multiple modules may be involved in the production of a single bout type, and also that the cells within a module are not necessarily all coactive, with cells within a module perhaps being recruited in a context-specific manner.

Similarities between bout types and kinematic modules can be seen by comparing the centroids of both in terms of kinematic features (Figure 3.6A). Left/right kinematics are separated, so the left and right kinematic pairs for the bout type centroids are mutually exclusive due to these values representing the recorded behaviour. On the other hand, kinematic module centroids represent model coefficients which can take negative coefficients for individual features. Despite this, it is evident that several bout types and kinematic modules show alternating values across left/right kinematics, reflecting an overall bias for left or right tail bends. There are also some modules and bout types which show an obvious preference for certain frequencies of tail oscillations.

To better understand the relationship between bouts and modules, we calculated the pairwise correlation coefficient between these centroids as a preliminary analysis Figure 3.6B). This analysis illustrates how some modules are correlated with multiple bout types, while others only have strong correlations with specific bout types. For example, module 6 is positively correlated with all bout types, but has higher correlations with bouts such as FS, FS fast and rightwards T1 and T2. One would thus expect cells in this module to show activity related to shared kinematics to do with propulsion and swim speed, as well as to some rightward kinematics. Indeed, this module shows positive model coefficients for features such as vigour, high frequency oscillations, and rightward tail angles (Figure 3.4). On the

other hand, modules 2 and 8, previously likened to the T1 and T2 bout recruitment maps, show large positive correlations only to turns in one direction, and negative correlations to the opposite direction (Figure 3.4B,H). Similarly, modules 9 and 12, which contain cells that show recruitment to left and right J turns respectively, also show particularly high correlations to these bout types. Furthermore, all bout types show positive correlations to at least one kinematic module. This analysis thus

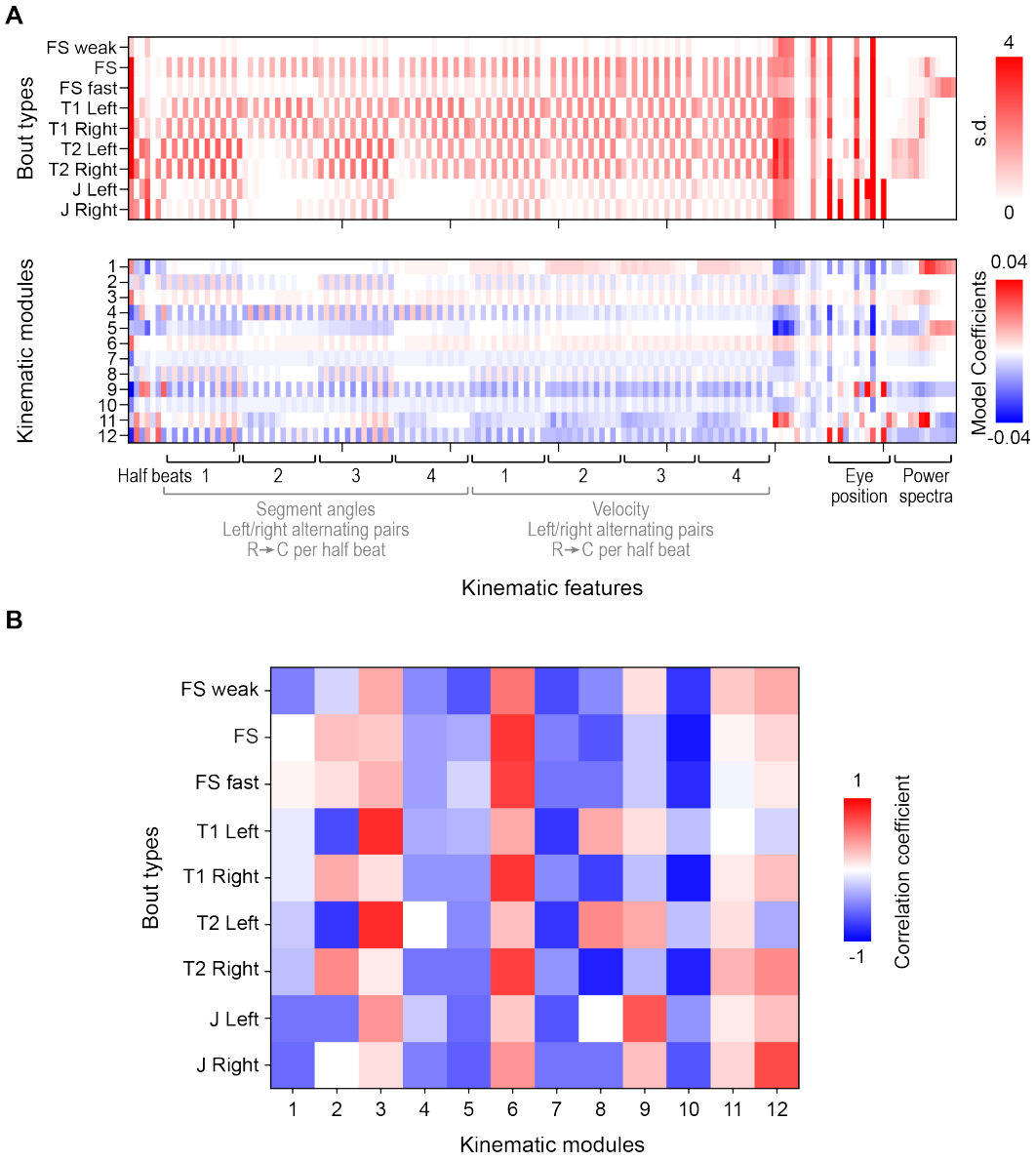

Figure 3.6 Relationship between bout types and kinematic modules
A. Comparison of bout types and kinematic modules in kinematic feature space.
Top, values for the centroids of the identified tethered bout types in kinematic features.
Bottom, values for the centroids of kinematic module coefficients, in kinematic features.
Both plots have the same kinematic features, some are labelled for reference. These match the centroids in Figure 4. R rostral, C caudal.
B. Pearson's correlation coefficient between bout type centroids and kinematic modules.

highlights modules, and therefore cells, whose kinematic encoding suggests they may underlie a subset of kinematic features of the bout types presented here.

Some modules, such as modules 4, 5, 7 and 10, are anticorrelated to all bout types, albeit with some slight differences in the magnitude of this anticorrelation. This is likely due to the majority of their model coefficients being negative, resulting in a negative correlation coefficient when compared to the bout types which have only positive values. However, for some modules, this could also be due to the absence of a bout type in this analysis. For example, Module 5 contains a fraction of Mauthner cells and shows positive model coefficients for high power tail oscillations (Figure 3.4E). As some bout types, such as aversive bout types which are Mauthner dependent, have not been identified by this bout classification, it is possible that this module represents an escape-like behaviour which does not correlate with any of the existing bout types.

3.3 Discussion

As recent studies have implicated individual RS neurons in the production of specific kinematics, and we find that there are specific RS neurons which show unique recruitment and activity toward kinematically distinct bout types, we sought to model RS activity in terms of kinematic features and thus develop encoding models. These are models which describe each neuron's activity, in terms of the kinematic features. Many cells were well-modelled by the kinematic features, which lends support to the prevailing notion that the activity of RS neurons represent motor outputs in the form of tail kinematics. By studying the sign and amplitude of the model coefficients, we can also consider which of these kinematic features appear to be most relevant to each cell's activity.

We find that many cells show similar kinematic encoding, and we cluster neurons with similar encoding model predictions to produce 12 distinct kinematic modules. These modules can be interpreted as representing separate combinations of kinematic features encoded by RS activity. Some kinematic modules contain a large fraction of cells which appear in specific bout type recruitment maps, and also have a kinematic centroid with high model coefficients for kinematic features that separate

that bout type from others. However, the cellular composition of these kinematic modules does not precisely match the bout recruitment maps, and these kinematic modules show varying correlations towards specific bout types, suggesting that multiple kinematic modules are combined to produce a bout type. Overall, we view these kinematic modules as providing a low-dimensional representation of the combinations of kinematic feature encoded by RS activity, and these could serve as building blocks which can be combined to produce different bout types, and therefore diverse behaviours.

3.3.1 Encoding model interpretation

There is debate as to the interpretability of encoding models, and their counterpart decoding models. For this data, encoding models describe the activity of neurons in terms of kinematic features, whilst decoding models would predict kinematic features and bout types from neural activity. The prevailing view is that only the model operating in the direction of information flow can provide an insight into the computations employed by the neurons in this brain region (Kriegeskorte and Douglas, 2019). Therefore, the encoding models presented here do not provide an abstraction of the neural computations responsible for generating motor output, but rather suggests that low-level behavioural kinematics are represented by RS and non-RS activity.

To identify kinematic modules, we calculated the linear drive of neurons to a series of novel bouts. It is important to note that linear drive is not the predicted spiking activity of a cell. Instead, we interpret linear drive as akin to subthreshold activity, where a negative linear drive produced by negative model coefficients reduces or dampens the activity of that cell and vice versa. In support of this, we found that clustering cells by their predicted activity produced similar results (data not shown).

3.3.2 Bouts as a combination of kinematic modules

From this analysis we cannot identify the activity relationships between modules. A model could be developed to predict bout types as a combination of

kinematic modules which could help us to understand these relationships. In addition to this, symmetric left/right functional pairs of modules are associated with opposing kinematic features, so there may be some local inhibitory circuits which prevent cells from contrasting modules being coactive. Local inhibitory interneurons have already been described in a network to prevent both Mauthner cells from being active together (Koyama *et al.*, 2016). The structured patterning of inhibitory and excitatory neurons in the hindbrain suggest that similar local inhibitory circuits could exist between the other cells of the RS population (Kinkhabwala *et al.*, 2011). These possible interactions make the understanding of how the cells within separate modules are combined to produce bout types more complicated.

3.3.3 Functional heterogeneity within RS and non-RS labels

Cells with the same RS or non-RS identity contribute to different kinematic modules, and this raises questions about functional heterogeneity within cell types. By contributing to different modules, it suggests that cells are capable of showing activity associated with different combinations of kinematic features. Some cell labels refer to groups of cells, and it is possible that there is functional diversity within these groups, as has already been observed for MiV1 neurons (Huang *et al.*, 2013). However, for cell labels which describe cells that only occur singly for a fish this is more challenging to interpret. The involvement of these singly occurring cells across multiple modules suggests that these neurons are capable of flexibly encoding a variety of kinematics and that they show broad kinematic tuning. From the recruitment maps presented in Chapter 2, we know that the distribution of a neuron's recruitment probability is not normally distributed. It may be that this variability in recruitment probability could be due to neurons' broad kinematic tuning allowing them to partially compensate for each other.

What is the importance of a single cell type to a kinematic module? As cells in a module show similar kinematic encoding, it might be that selective removal of a subset of cells within a module could be compensated for by the remaining cells. Alternatively, if only subgroups of cells within a module are active for behaviours in specific contexts, then cells of the same module would not be able to fully compensate for each other. In the next chapter I explore the effects of ablating cells which

contribute strongly to a kinematic module on naturalistic behaviour, low-level kinematic features, and overall performance of the module.

Chapter 4 Precise cell ablations produce specific kinematic deficits

4.1 Introduction

The previous chapter identified kinematic modules which indicate key combinations of kinematic features encoded by RS and non-RS activity. In order to test whether cells within a module can compensate for each other and be flexibly recruited across behaviours, I decided to remove specific cells within a module and examine the effects on behaviour. In addition, bout recruitment maps and modules identified some newly identified cells with activity related to J turns. I therefore wanted to test the functional roles of these cells by ablating them.

Laser ablation of specific RS neurons has been a widely used technique to determine how these cells are associated with various behaviours in larval zebrafish. Early ablation experiments found that certain RS cells, had significant effects on behaviours. For example, ablations of the Mauthner cell together with its segmental homologs was found to abolish the startle response towards head-directed stimuli (Liu and Fetcho, 1999). Similarly, ablations of the large nMLF cells was found to produce a profound impairment to larval zebrafish prey capture (Gahtan, Tanger and Baier, 2005).

In this chapter I conducted laser ablations of specific RS neurons whose putative functions have been indicated by the bout recruitment maps and encoding models presented earlier. By considering changes in behaviour at higher levels, such as fish orientation changes, and at the level of individual kinematics, I hoped that these ablations would enhance our understanding of the interplay between higher level behaviours, individual kinematics and kinematic modules.

4.2 Results

4.2.1 Selection of cells for ablation

In order to examine how groups of RS and non-RS cells influence behaviour, I conducted precise laser ablations of specific cells and compared larval zebrafish swimming pre- and post-ablation. In these experiments, I studied the behaviour of freely swimming larvae exploring a circular arena as this would enable the study of naturalistic behaviours such as prey capture (Henriques *et al.*, 2019). To encourage a variety of behaviours, larvae were presented with visual stimuli such as looming spots and optomotor gratings, and they were provided with live *Paramecia* to hunt (Figure 4.1Ai). Behaviour was recorded prior to the ablation at 6 dpf, and the following day post-ablation at 7 dpf (Figure 4.1Aii). In this free swimming preparation, I was able to track the larva's position, as well as the movements of the eyes and tail (Figure 4.1B). This enabled me to examine behaviour at a similar level of kinematic detail as described in previous chapters, and this allowed me to identify subtle alterations to locomotor output following cell ablations.

I conducted two major groups of cell ablations. The first ablation group was an ipsilateral ventromedial cell ablation, in which I targeted only the ventromedial cells on the LHS (Figure 4.1C). Ventromedial cells consist of RoV3, MiV1, and MiV2 cell labels. These cells appear in recruitment maps to T1 and T2 left bouts (Chapter 2), and the majority of these cells are in kinematic module 8 (Chapter 3). From the present literature, ablation of these cells is expected to produce a specific reduction in the amplitude of the tail bend during the first half beat (θ1, Huang *et al.*, 2013), and this reduction should be selective to the side of the ablation (i.e. leftwards θ1 values in these experiments). From the kinematic centroid of module 8, I would expect for these ablations to additionally alter leftward bending and velocity for the third half beat too. These results from the current literature thus allows these ventromedial cell ablations to act as a positive control to confirm the success of this methodology, as well as potentially identify additional kinematic alterations indicated from the kinematic modules.

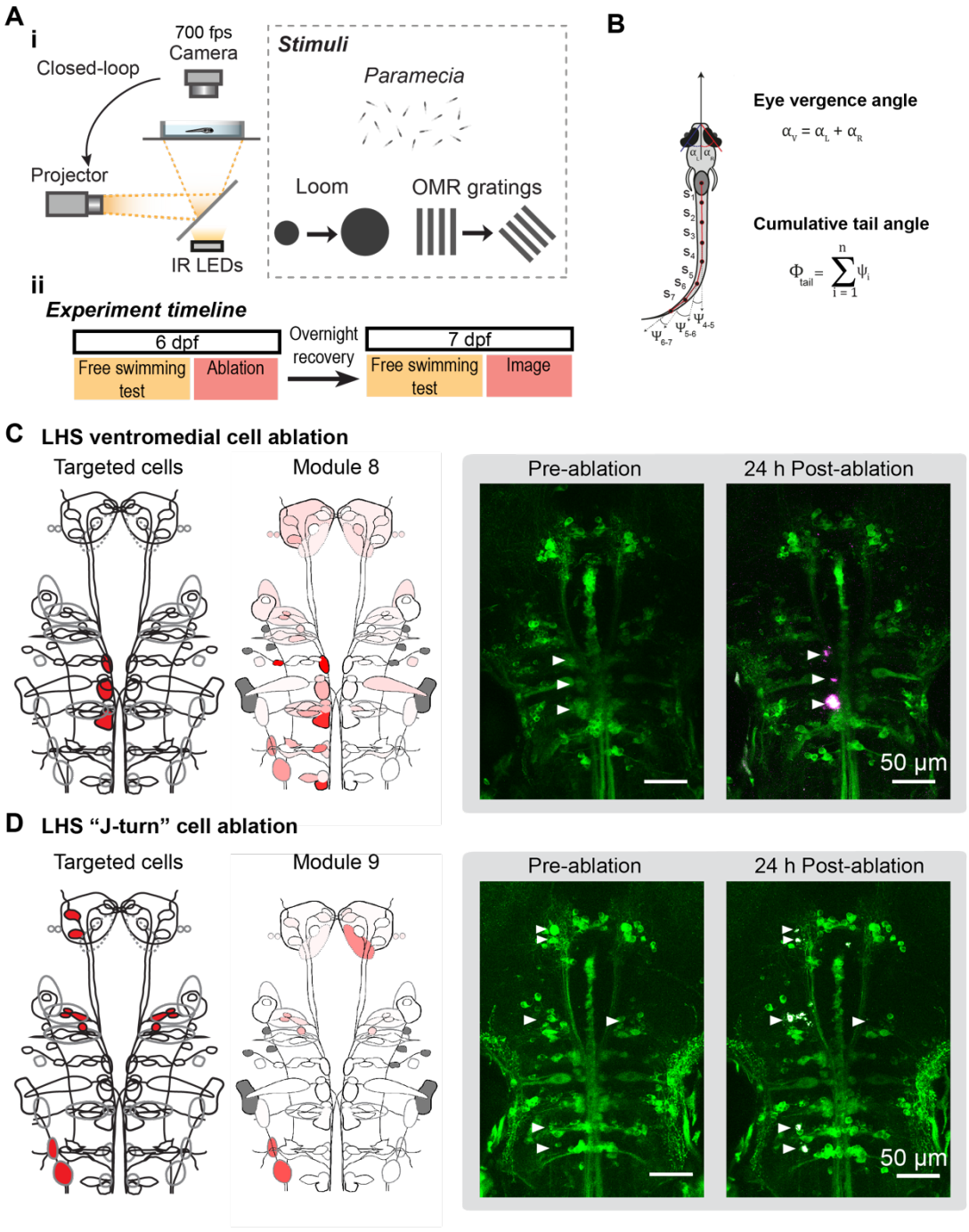

Figure 4.1 Precise cell ablations and analysis of free-swimming behaviour
A. Schematic of experiments.
i. Left, schematic of free swimming rig where single fish are recorded with a high-speed camera. Right, stimuli available to the fish. These include live *Paramecia* as prey and visual stimuli which are presented egocentric to the larva's position.B. Schematic of eye and tail tracking adapted from (Henriques *et al.*, 2019).
C-D. Examples of ablations. Left, schematic of targeted cells. Right, maximum z-projections of a *KalTA4u508); UAS:GCaMPf* larva, before and 24 h post ablation of the cells on the left. In post-ablation imaging, the presence of bright, auto-fluorescent "scars" indicate a successful ablation
C. Ablation of "J-turn" cells. On the left hand side: MeLc, MeLr, and caudal, lateral non-RS cell groups. Bilaterally: RoM1c, RoM1r and RoM2a cells.
D. Ablation of ventromedial cells on the left hand side

For my second ablation group, I chose cells which appear relevant to hunting routines and more specifically J turns (Figure 4.1C). I refer to this group as an ablation of "J cells". This group contained RS cells which had been previously implicated in prey capture, as well as novel RS and non-RS cells whose functions are unknown. I ablated two large nMLF cells (MeLr and MeLc) on the left hand side, as their ablation had been associated with reduced prey capture (Gahtan, Tanger and Baier, 2005). Guided by the recruitment maps to J turns (Figure 2.6), I also performed a bilateral ablation of RoM1c, RoM1r and the novel RoM2a cells. In addition to this, I also ablated the caudal, lateral non-RS cells on the side ipsilateral to turn direction. These RS cells in Ro1-Ro2 together with the non-RS cells contribute to Module 9. Following ablation, I would expect to see alterations to kinematic features such as caudal tail angle following ablation (see Chapter 3).

Together with the ventromedial and "J cells" ablation groups I also included control larvae. Control larvae underwent the same experimental procedures as ablated larvae save for the ablation itself. Control larvae were thus mounted in agarose and imaged for a pre-ablation z-stack using a 2P microscope.

4.2.2 Larvae are healthy after ablation

Before examining changes in low-level kinematics following ablation, I wanted to confirm that general swimming was unaffected and that larvae were largely healthy. To confirm that fish were not paralysed and capable of navigating the arena I examined the average speed and rate of swim bouts produced by larvae across all experimental conditions. I found that larvae from all groups behaved similarly between pre- and post-ablation conditions for both average speed (Figure 4.2A, control pre: 2.8±1.1, post: 2.3±0.72 p=0.074; ventromedial ablation pre: 2.4±0.67, post: 2.5±0.83, p=0.70; "J cells" ablation pre: 2.6±0.43, post: 2.7±1.0, p=0.86), and rate of swim bouts (Figure 4.2B, control pre: 1.5±0.44, post: 1.5±0.37, p=0.58; ventromedial ablation pre: 1.6±0.40, post: 1.4±0.30, p=0.11; "J cells" ablation pre: 1.3±0.12, post: 1.7±0.44, p=0.11). This indicates that neither the mounting and imaging procedure, nor the ablation of these particular RS cells produce severe deficits to general locomotion.

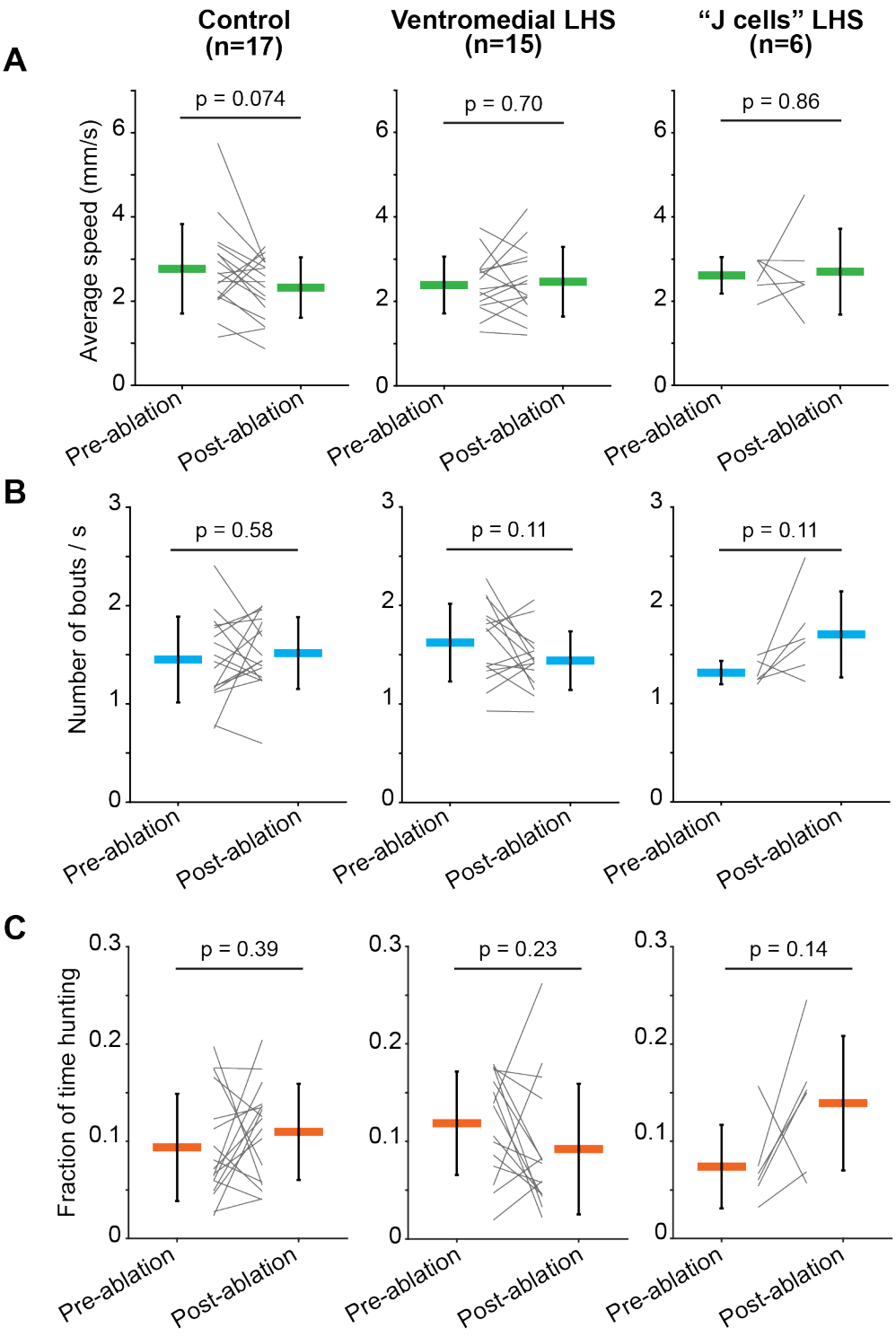

Figure 4.2 Basic swim parameters are largely unaffected following ablations
A. Average swim speed before and after ablations.
B. Average bout frequency before and after ablations.
C. Average fraction of time spent hunting before and after ablations.
Error bars are standard deviation. Statistical tests are paired t-tests.

As one of my ablation groups included cells implicated in hunting and prey capture, I also examined the fraction of time spent hunting by each larva. Hunting was defined as a period where the eyes were converged resulting in a high vergence angle (Bianco, Kampff and Engert, 2011). While this measure was not significantly different between pre- and post-ablation conditions for all groups (Figure 4.2C, control pre: 0.094±0.055, post: 0.11±0.049, p=0.39; ventromedial ablation pre: 0.12±0.053, post: 0.092±0.067, p=0.23; "J cells" ablation pre: 0.074±0.043, post: 0.14±0.069, p=0.14), suggesting that larvae were still capable of hunting prey, "J cell" ablated larvae did show a trend for an increase in the fraction of time hunting post-ablation. One hypothesis is that this effect in larvae with ablated "J cells" might reflect prolonged or increased numbers of hunting routines, perhaps due to difficulties in orienting appropriately.

4.2.3 Turning is affected in ventromedial cell ablations

As ablation of ventromedial cells has been found to produce a severe deficit in turning to the ablated side (Orger *et al.*, 2008; Huang *et al.*, 2013), I wanted to confirm that this result was achievable using *KalTA4u504* larvae. Previous experiments have labelled and targeted RS cells to ablate via spinal cord backfill, and I wanted to determine that sufficient cells were labelled by *KalTA4u508* that these experiments could be reproduced. In these experiments I ablated a slightly larger number of cells than in the experiments described by Orger et al. (Orger *et al.*, 2008); On average 5 RoV3 cells, 3 MiV1 cells, and 4 MiV2 cells in my experiments, versus the 2-4 cells ablated from each ventromedial cell group in Orger et al..

To evoke prolonged periods of turning, I presented larvae with either left- or rightward moving gratings, the locations of which were continuously updated in a closed-loop to remain egocentric to the fish's position. This encouraged larvae to repeatedly perform turn bouts to follow the direction of the grating as illustrated by plotting their cumulative orientation change during presentation of these optomotor gratings (Figure 4.3A). To compare OMR performance across fish which received gratings for different durations, I calculated the rate of orientation change across the stimulus duration (Figure 4.3B). As leftwards orientation changes have negative

values, I have shown here the corrected turn gradient (sign-inverted) for easier comparison with the values measured for rightward gratings.

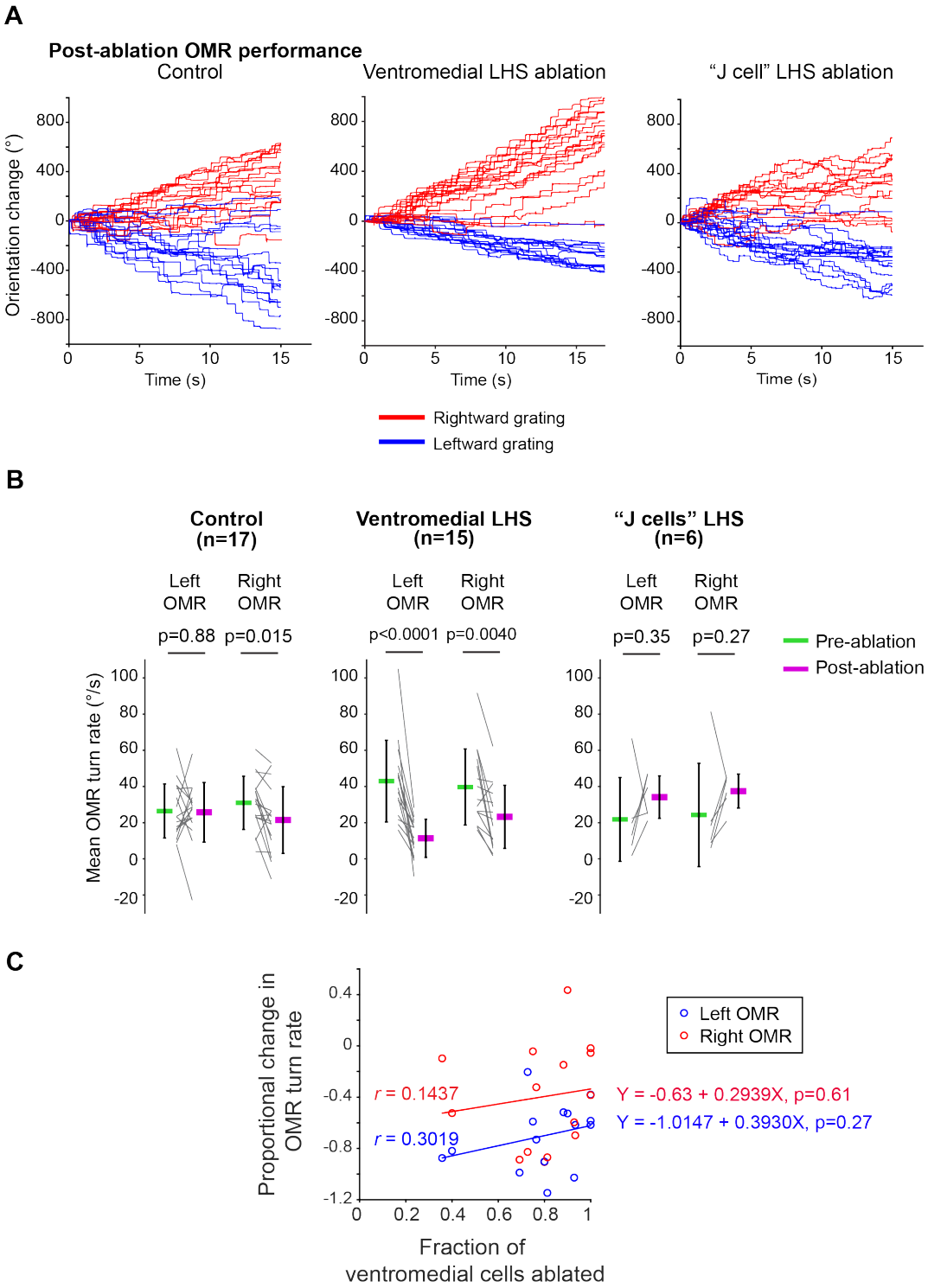

Figure 4.3 Performance during optomotor gratings is affected by ventromedial cell ablations
A. Orientation changes for single fish in each ablation group during the presentation of a leftward (blue) or rightward (red) moving grating. Each trace is a single trial.
B. OMR performance before and after ablations. Performance is quantified by the rate of reorientation to either a leftward or rightward moving grating. Left OMR measurements are corrected to positive values for easier comparison with right OMR measures. Error bars are standard deviation, statistical tests are paired t-tests.

C. Relationship between fraction of ventromedial cells ablated and proportional change (pre- and post-ablation) in OMR turn rate for left and rightward gratings. There are two values for each fish: a measure for the left OMR (blue) and a measure for the right OMR (red). Line fit by simple linear regression, r is the correlation coefficient.

Examination of OMR turn rates for control fish indicate potential behavioural changes without RS or non-RS cell ablations (Figure 4.3B). Although control fish showed no significant difference between pre and post OMR performance towards leftwards gratings (pre: 26.4±15, post: 25.7±16.5, p=0.88), they did display a reduction in turn rate towards rightward gratings (pre: 30.9±14.7, post: 21.4±18.5, p=0.015). It is possible that larvae show a change in OMR responses between 6 and 7 dpf as part of developmental differences, but it is not clear why this would be specific to only one side and could instead reflect a slight bias in experimenter handling.

Ventromedial cell ablations affect turn rate to both left and right moving gratings (Figure 4.3B). As expected from the present literature, larvae with ventromedial cell ablations show a clear reduction in turn rate towards leftwards gratings following ablation (pre: 43.0±22.6, post: 11.3±10.6, p<0.0001). However, they also show an unexpected deficit in turning towards rightward gratings following ablation (pre: 40.0±21.0, post: 23.2±17.5, p=0.0040). This is unusual because Orger et al., did not describe reduced turning towards the contralateral side (Orger *et al.*, 2008), however the data presented by Huang et al., indicates that there can be slight reductions in orientation to the contralateral side (Huang *et al.*, 2013). In addition to this, the recruitment maps I present in Chapter 2 indicate how ventromedial cells also show activity during turns to the opposite side. While this explains how these ablations could also produce mild changes to contralateral turns (Huang *et al.*, 2013), I suspect that when I ablate ventromedial cells in *KalTA4u508* larvae that I may also remove some non-RS cells in the vicinity. Most likely to be affected are the "Mi2d/v" non-RS cells which are directly adjacent to MiV2 neurons. I therefore think that my ventromedial cell ablations remove enough ventromedial cells to reproduce the published phenotypes of impaired turning towards the ipsilateral side, but may also include some non-RS cells which could exacerbate what would otherwise be a mild impairment in turning to the contralateral side.

Although "J turn" ablated larvae do not show any significant changes in turn rate between pre and post ablation conditions to left or rightward gratings, there is a

general trend for "J cell" ablated larvae to show an overall increase in turn rate following ablation (Figure 4.3B). This could be due to the ablated cells, specifically the non-RS, MeLr and MeLc cells which appear in routine turn recruitment maps, affecting the control of turn production or amplitude. Together with the prolonged hunting routines for "J cell" ablated fish, this suggests that these larvae may have overall issues with appropriate orientation.

The rate of orientation change for single fish indicates fish-to-fish variability. This can be seen both for pre-ablation conditions between experimental conditions, as well as within an ablation group. Although this has not been formally tested, it appears that larvae which received ventromedial ablations show higher pre-ablation OMR turn rates than the larvae in other groups. I always included control larvae while conducting cell ablations, however the majority of ventromedial cell ablations were conducted months prior to the "J cell" ablations. Due to the time between these experiments, the larvae used in these experiments have been collected from different generations of *KalTA4u504* fish, and I wonder if this could have produced systematic changes in behaviour such as this. To address this, I primarily focus on comparing individual fish pre and post ablation rather than comparing post ablation values between ablation conditions.

One can also see that the change in mean OMR turn rate following ventromedial cell ablation varies greatly between fish, which is an observation also described in other studies (Orger *et al.*, 2008). Orger et al hypothesise that this variability might reflect the number of cells ablated. To examine this, I used simple linear regression to calculate the proportional change in OMR turn rate based on the fraction of ventromedial cells ablated (Figure 4.3C). I found that there was no significant relationship between the fraction of cells ablated and proportional change in OMR turn rate to either left (R^2=0.091, p=0.27) or rightward moving gratings (R^2=0.021, p=0.61).

Overall these results reveal the ability to reproduce and detect a locomotor deficit at the gross behavioural level of turning for ventromedial cell ablations using *KalTA4u508* larvae. This indicates that a comparable number of RS cells are labelled in *KalTA4u508* as by spinal cord backfill in previous studies. However, this analysis does not reveal the changes in behavioural kinematics underlying these high-level behavioural changes. In order to study this, I decided to conduct a closer examination of behaviour at the level of individual kinematic differences for single fish.

4.2.4 Kinematic-level examination of individual fish

To identify differences in behavioural kinematics following ablation, I described the recorded behaviour in the same kinematic features as used in previous chapters, and conducted one-tailed comparisons for each kinematic feature between pre and post ablation conditions. This is illustrated in Figure 4.4, where I show these p values for a single fish example from each ablation condition. For this analysis, I only selected bouts that occurred during left optomotor gratings in order to select for a behaviour in which I have found a gross behavioural deficit (Figure 4.3). From these representative examples it is possible to see that at the kinematic level, there are shifts in the distributions of values following ablations.

The patterns of kinematic distribution shifts are different between control fish and the ablated larvae. The example control fish shows overall increases across right and leftward kinematics, suggesting symmetrical increases in amplitude and velocity between these developmental stages (Figure 4.4A). The example J cell ablated larva also shows overall increases in the values of left and rightward kinematics, but this change appears to be more significant for leftward kinematics. This supports the observed trend of J cell ablated fish to show increased turns to leftward gratings. In contrast to the control and J cell examples, the fish with a ventromedial cell ablation shows large decreases primarily in leftward kinematics, reflecting an asymmetric alteration to behavioural kinematics following ablation.

The example ventromedial cell ablated larva shows large reductions for kinematics associated with left turns (Figure 4.4B). As expected both from the literature and from the kinematic modules, there is a large reduction in leftward θ1 and vel1 values across all segments (Huang *et al.*, 2013). As kinematic module 8 also shows positive model coefficients towards left θ1 values for the third half beat, I expected these values might also show a reduction post-ablation. However, this does not appear to be true for this fish, which suggests that not all kinematics within a module are equally affected by ablation of the same cells. Instead, this fish shows an increase in leftward kinematics for the other half beats. This might represent an attempt to behaviourally compensate through alterations of other leftward kinematics. Low frequency oscillations, which are typical of turn swims, also show a severe reduction, but there is an increase in middle-high frequency oscillations which suggests more forward-like swims, a feature similarly described by Huang et al.

(Huang *et al.*, 2013). From this analysis, therefore, we can confirm published kinematic deficits for a single fish, as well as identify possible compensatory shifts in behaviour following ablation.

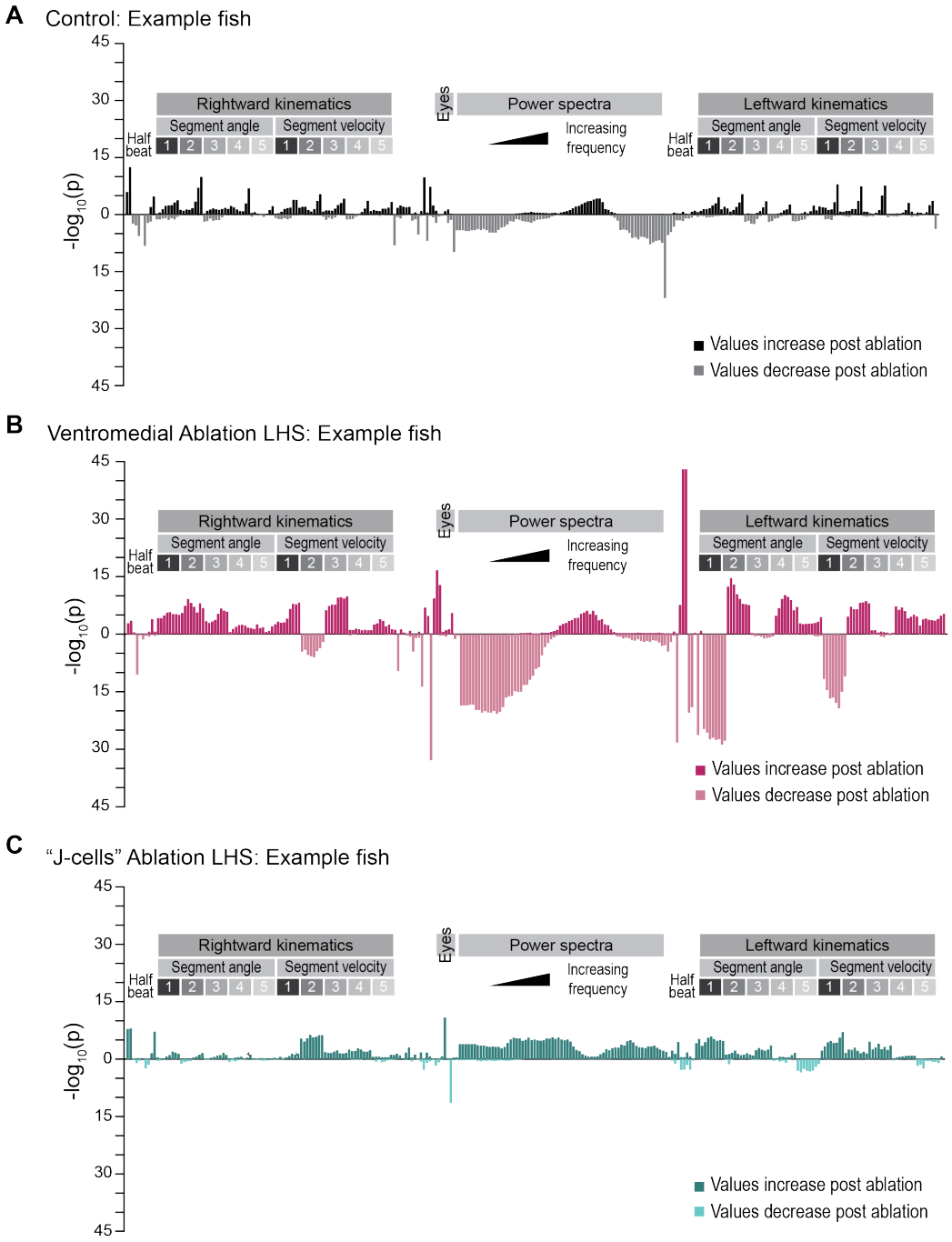

Figure 4.4 Changes in kinematic feature distributions for single fish
Pre- and post-ablation changes in the distributions of individual kinematics for all bouts that occur during the left OMR for a single fish from each ablation condition. P values are calculated by one-tailed Kolmogorov-Smirnov tests between pre- and post-ablation data.
A. Control fish.
B. Fish with ablation of LHS ventromedial cells.
C. Fish with ablation of LHS "J cells".

4.2.5 Relating behaviour to kinematic modules

As the selected RS and non-RS cells for ablation contribute to specific kinematic modules, I wanted to examine the effects of ablations in terms of these modules. To examine the effects of ablations in this way, I projected the bouts from each fish onto individual kinematic modules. Bouts recorded from free-swimming larvae were first described in the same kinematic features as used to define tethered behaviour and kinematic modules (Figure 4.5A). I then calculated the dot product between bouts and each kinematic module centroid, and normalised this value by the magnitude of each bout and module to produce a cos(θ) value for each bout (Figure 5B). These values represent the angle between each bout and the module centroid. Subsequent separation into either pre- or post-ablation bouts produced two histograms of cos(θ) values (Figure 4.5C).

To determine how well separated these histograms are, I performed a ROC analysis which asks how well pre/post conditions can be classified using these values. A higher AUC value calculated from this ROC analysis indicates that pre/post bouts are distinguishable when projected onto this module. As a preliminary way to assess the significance of this value from chance, I used a permutation test to collect AUC values calculated from shuffled class labels (Britten *et al.*, 1993), and present in red the AUC values which lie outside the central 95% of the shuffled AUC values. I expected that scores for modules which feature high fractions of the ablated cells will show greater separation between pre/post conditions than those that do not.

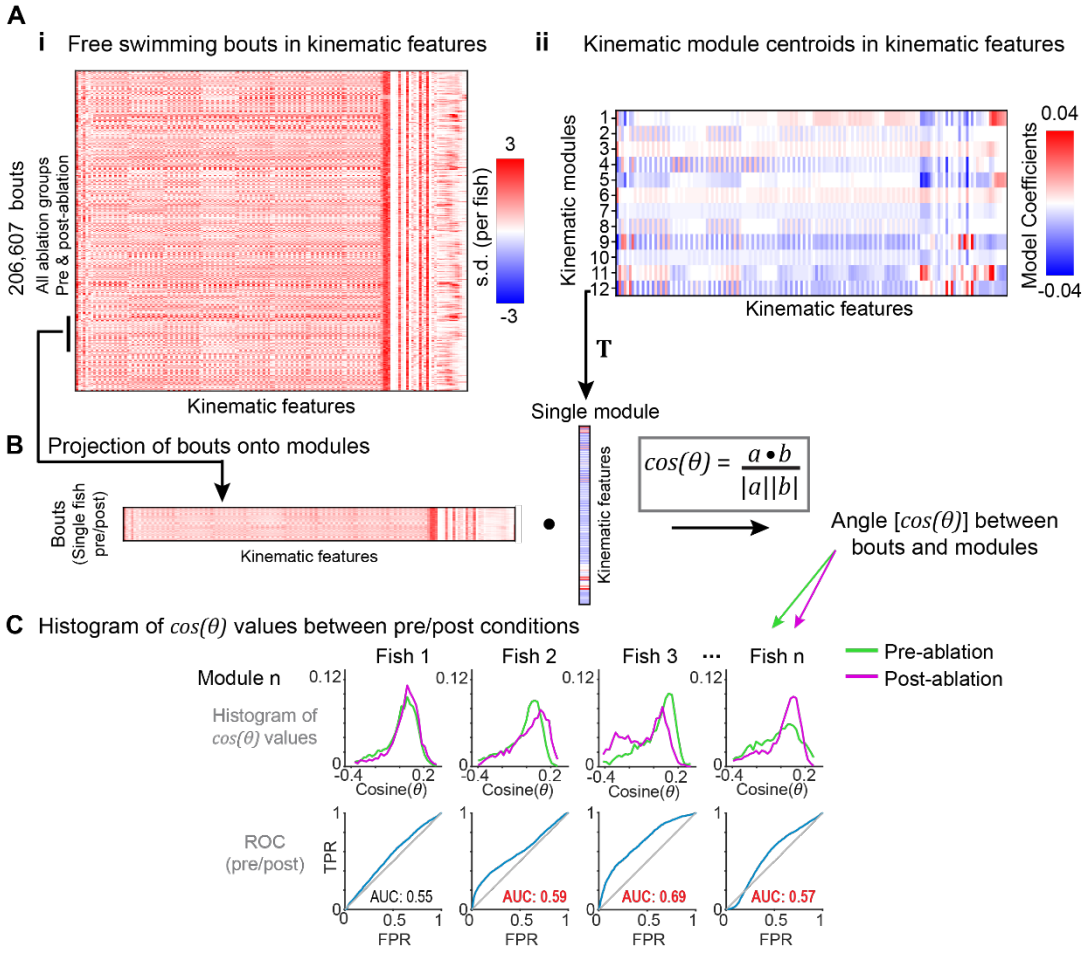

Figure 4.5 Process of projecting bouts onto kinematic modules
A. Bouts from free-swimming data are described using the same kinematic features as the kinematic modules.
i. Kinematic representation of all bouts.
ii. Kinematic centroid of each kinematic module.
B. Normalised dot product between a single fish's bouts and a kinematic module to produce a cos(θ) measure of the separation between bouts and the module.
C. Histogram and receiver operating characteristic (ROC) analysis for pre- and post-ablation cos(θ) values, calculated individually for each fish.
Top, Histogram of pre- and post-ablation cos(θ) values
Bottom, ROC analysis and corresponding area under the curve (AUC) value. AUCs in red indicate they are significant as determined by permutation test using shuffled data.

4.2.6 Ventromedial cell ablations show a graded alteration to modules

To provide a representative example for this analysis in larvae with ventromedial cell ablations, I selected larvae with different phenotype severities. To calculate phenotype severity, I took the difference between the pre-/post-ablation rate of orientation change to rightward gratings from the pre-/post-ablation rate of

orientation change to leftward gratings. This allowed me to identify larvae with a specific alteration to turning toward the left rather than those which showed a similar change in turning to both sides, which I suspected to represent larvae which also had a higher level of non-RS cells ablated. I then selected the fish with the “best” phenotype (ranked 1/15 ; Figure 4.6A), the fish with an “intermediate” phenotype (ranked 8/15; Figure 4.6B), and the fish with the “poorest” phenotype (ranked 15/15; Figure 4.6C), and one control fish (Figure 4.6D). As the ventromedial cells feature strongly in the bout recruitment maps to leftward turns, and these occur more often during left optomotor gratings, I selected only bouts which occurred during the presentation of leftwards moving gratings to better reveal the difference between pre and post ablation behaviour.

All examples show a significant separation between pre and post-ablation bouts projected onto module 8 (Figure 4.6A). As the control fish show a significant separation this suggests the presence of developmental effects on behaviour when comparing bouts projected onto module 8. However, the AUC value and degree of separation is largest for the ventromedial cell ablated larva with the “best” and “intermediate” phenotypes. For these two examples, the post-ablation cos(θ) values show a shift to the left, closer to 0 than the pre-ablation cos(θ) values. This suggests that the values of kinematics with high model coefficients in module 8, such as leftward tail angles in halfbeats 1 and 3, are reduced for post-ablation bouts. This is because low values for these kinematics would result in the dot product of the bouts and this kinematic module to tend towards 0. This is confirmed by low p values for one-tailed comparisons between pre- and post-ablation leftward tail angles during the first half beat for the fish with the “best” and “intermediate” phenotypes (Figure 4.6A,B). Accordingly, the “poorest” phenotype and control fish which have low AUC values do not show these similar patterns of kinematic alterations following ablation.

For a module where there are little to no ventromedial cells one expects to see poor separation between pre- and post-ablation for bouts projected onto this module. I tested this by projecting bouts from these example fish onto kinematic module 9, which contains mostly the cells ablated in the “J cell” group and shows preferential tuning towards leftward caudal tail movements and convergent eye positions. I found that there was indeed poor separation for bouts projected onto this module across these

example fish, except for the “intermediate” phenotype fish, which shows a leftward shift in the distribution of post-ablation cos(θ) values to more negative values

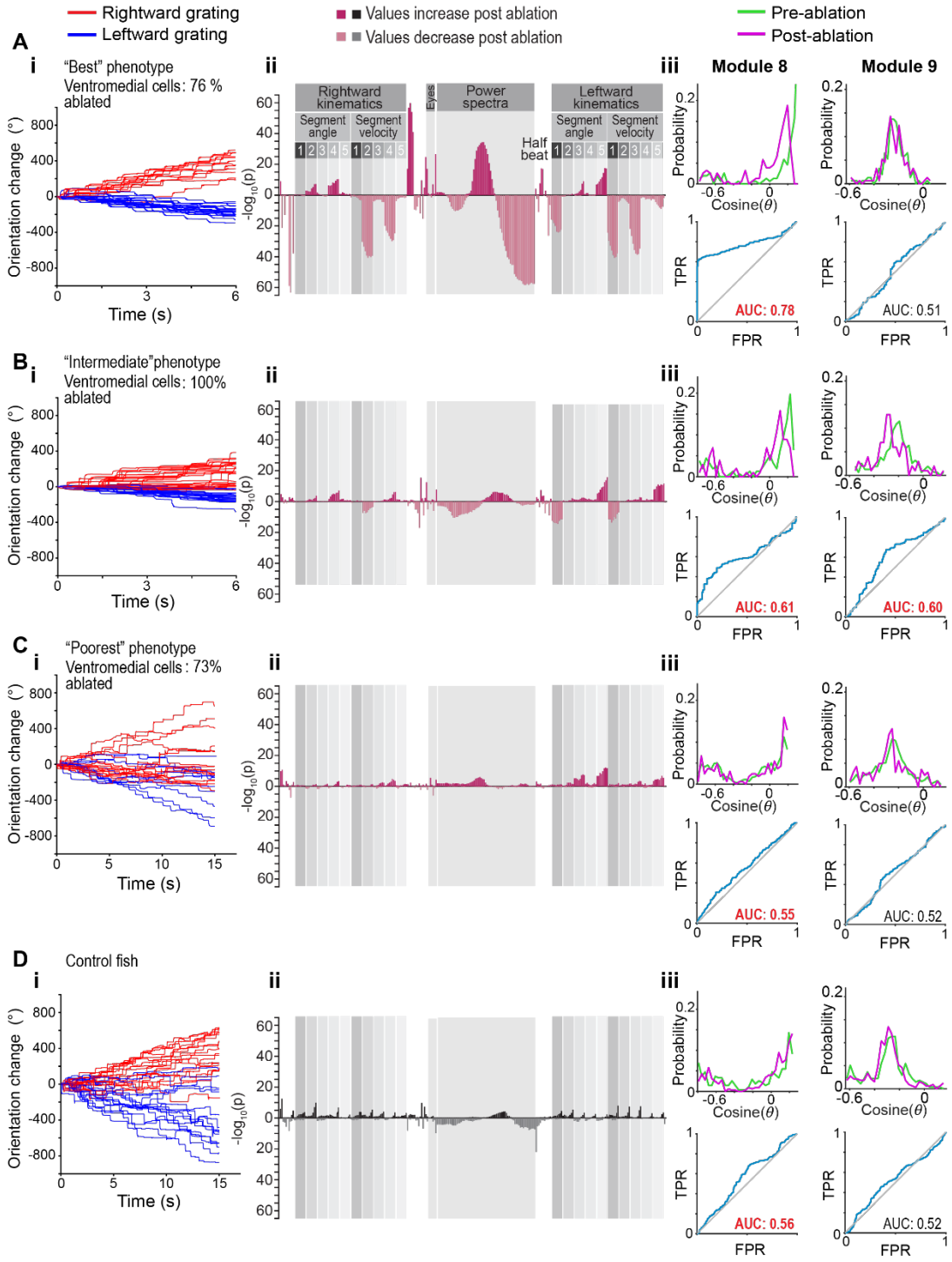

Figure 4.6 Kinematic and module projection analysis for ventromedial cell ablations
Gross behaviour, kinematic alteration, and module projection shifts for all bouts that occurred during a leftward grating presentation for different example fish.
A. LHS ventromedial cell ablation. “Best phenotype”.
B. LHS ventromedial cell ablation. “Intermediate phenotype”.
C. LHS ventromedial cell ablation. “Poorest phenotype”.
D. Control fish
i. Cumulative orientation change towards left (blue) and right (red) optomotor gratings. Each line is a separate response.

ii. p-values from one-tailed Kolmogorov-Smirnov tests between pre- and post-ablation values for each individual behavioural kinematic.
iii. Top, pre- and post-ablation histograms of cos(θ) values for bouts projected onto module 8, which contains a large fraction of ventromedial cells, and module 9, which contains a large fraction of "J cells". Bottom, the corresponding ROC curves for these values.

(Figure 4.6A-C). This would indicate increases in the values of kinematics which have negative model coefficients, such as velocity kinematics and turn angles in late half beats, and/or decreases in the values of kinematics with positive model coefficients. In keeping with this, the "intermediate" fish shows increases in velocity kinematics. Although it is not clear how ventromedial cell ablations produce this effect for only the "intermediate" fish, the increased separation for this module highlights kinematic features which are altered following ablation.

This analysis allows the examination of larval zebrafish swimming at the gross behavioural level, single kinematic level, and module level (Figure 4.6). By examining behaviour in terms of module 8, which contains a large fraction of ventromedial cells, I find that larvae which show greater pre- and post- ablation differences for this module also show appropriate shifts in the values of kinematics which have high model coefficients in this module. This indicates that ablation of cells which greatly constitute a module can produce a corresponding alteration to that module's highly weighted kinematic features. In addition to this, I find that changes in the distribution of pre and post ablation values towards different modules helps to identify altered kinematics not expected from the ablation itself.

4.2.7 Applying these analyses to a novel ablation group: "J Cells"

To study the behavioural effects of "J cell" ablations, I first examined some variables related to the first bout in a hunting routine, as this is the bout where larvae are most likely to perform J turns and thus reorient towards a prey (McElligott and O'Malley, 2005). This is because these cells were chosen due to their association with prey capture and J turns, and also from the identified trend for fish with "J cell" ablations to spend a greater fraction of time hunting (Figure 4.2C). I found that fish which received ventromedial and J cell ablations appear to show an increase in the duration of these bouts. Interestingly, this is opposite to controls where there appears to be a decrease in the duration of these bouts between 6 and 7 dpf (Figure 4.7A).

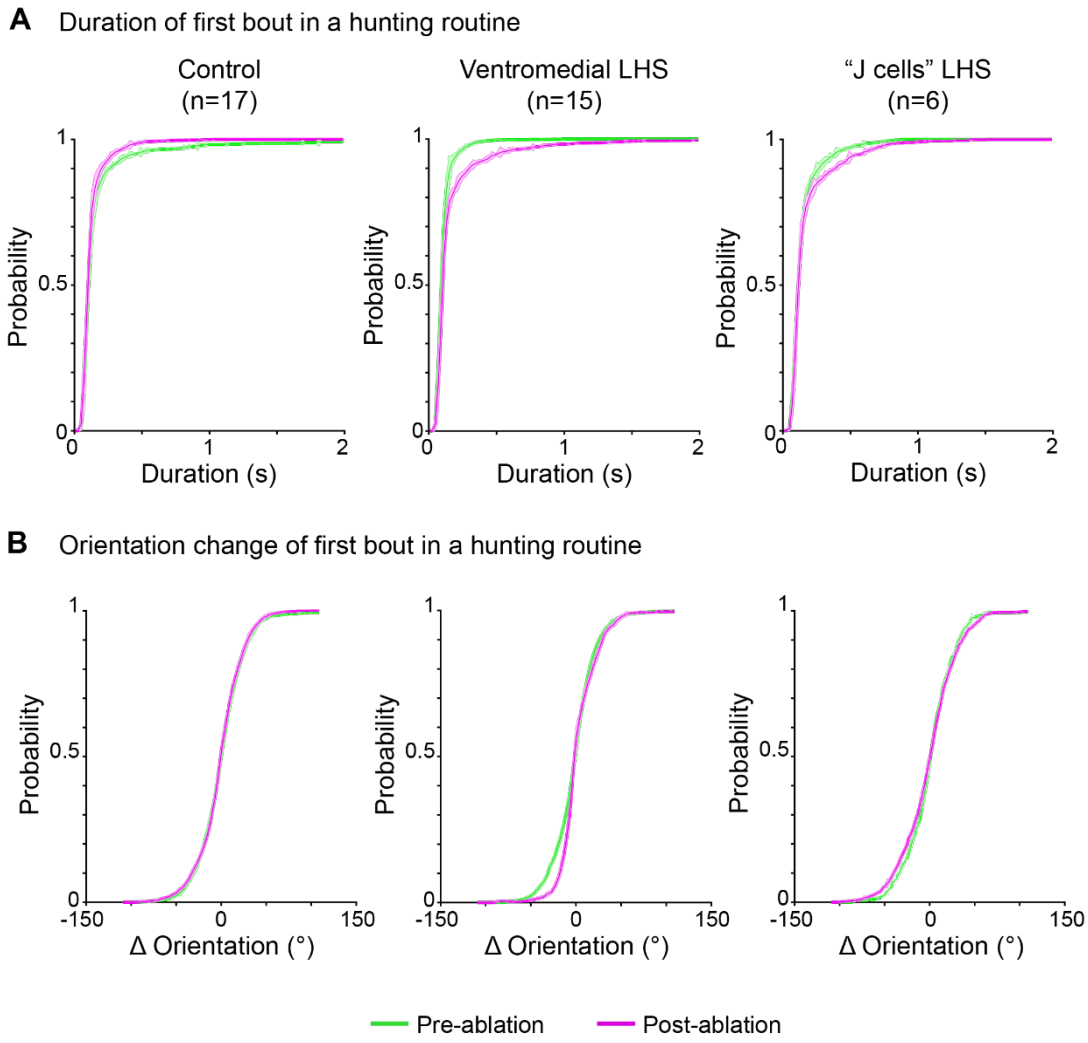

Figure 4.7 Gross behavioural measures for the first bout in a hunting routine
A. Average CDFs for pre- and post-ablation measurements of bout duration for each ablation group. Shaded regions are standard deviation error bars.
B. Average CDFs for pre- and post-ablation measurements of orientation change for each ablation group. Shaded regions are standard deviation error bars.

I also examined the orientation change of this first bout, as I suspected this might be affected if fish have impaired turning following ablation. Control fish were largely unchanged, however ventromedial cells showed a reduction in large orientations towards the side ipsilateral to ablation, while "J cell" ablated larvae appear to show a slight increase in these higher angle orientations (Figure 4.7B). While the role of ventromedial cells in hunting routines has not been described, there is some evidence to suggest that turns other than J-turns can be produced when the eyes first converge (Marques *et al.*, 2018), and therefore the deficit in high angle reorientation towards the ablated side is in keeping with the reduced ability to perform high angle tail deflections and other turn swim types following ventromedial cell

ablation. As the "J cells" contribute to Module 9 which has positive model coefficients for leftwards caudal tail bends, highly characteristic of J turns (McElligott and O'Malley, 2005), I expected to see that the production of these kinematics was affected post-ablation. Larvae would therefore have deficits in performing the careful reorientations towards prey that these kinematics would allow for, and show unusual reorientation during hunting routines, which might underlie what is seen in Figure 4.7B. The indication of pre- and post-ablation differences for this higher-level behavioural measure provides a foundation upon which to investigate changes at the kinematic level.

To illustrate the application of this analysis, I present some representative examples of "J cell" ablated larvae which show variations in the distributions of orientation change during the first bout of a hunting routine. These include: one larva which showed an increase in large angle orientation changes towards the ablated side ("Fish 1"), one larva with an increase in low angle orientation changes towards the ablated side ("Fish 2"), and a larva which showed no obvious difference in orientation change ("Fish 3"). I therefore applied this technique to these fish to try and identify alterations to behavioural output despite the variation in phenotype and small number of fish.

As "J cell" ablations contain cells which feature prominently in kinematic module 9, and only slightly in module 8, I expected to see a greater separation between the distributions of bouts projected onto module 9 than for module 8. Indeed, Fishes 1 and 2 which show a difference between pre-and post-ablation orientation changes also show a greater separation between their cos(θ) values for module 9 (Figure 4.8A,B). For these larvae, the distribution of cos(θ) values for Module 9 is shifted towards more negative values post-ablation. This would suggest an increase in the values of kinematics which have negative model coefficients, or a decrease in values with positive model coefficients. For module 9, kinematics with negative model coefficients include left and rightward segment velocities across all half beats, and rightward tail angles, whilst kinematics with positive model coefficients include leftward caudal tail angles and convergent eye positions. In support of this, I find that Fishes 1 and 2 show increases across left and right segment velocities, as well as some increases in rightward tail angles (Figure 4.7ABii). For the kinematic features with

positive weights, only Fish 2 showed a decrease in eye vergence angle, and interestingly neither larvae show decreases in features such as left caudal tail angles.

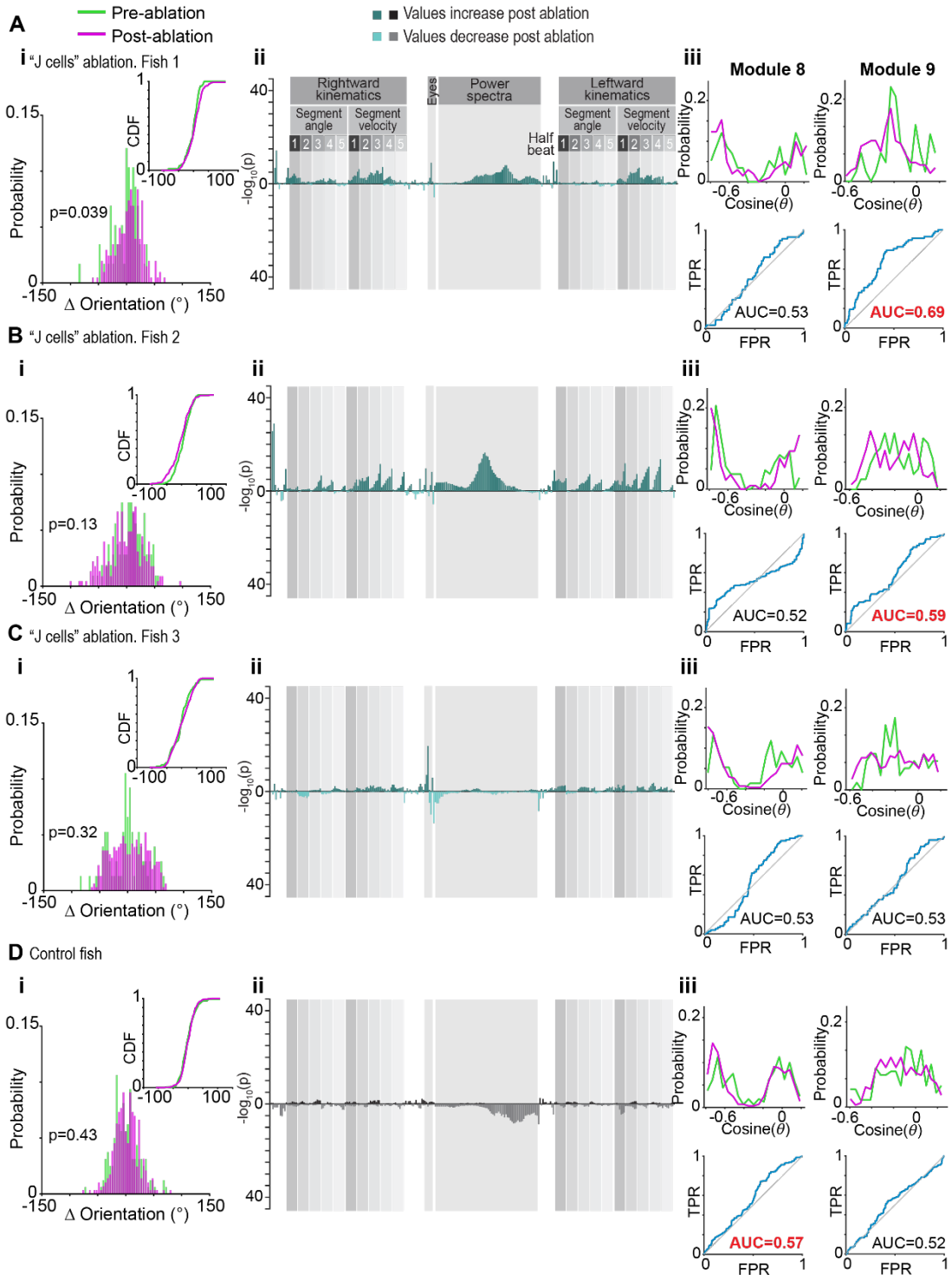

Figure 4.8 Kinematic and module projection analysis for "J cells" ablations
A. LHS ``J cells'' ablated fish with reduced high angle orientation changes
B. LHS ``J cells'' ablated fish with small increase in high angle orientation changes towards the ablated side
C. Fish with only minor differences in orientation changes.
D. Control fish.
i. Histograms with inset CDFs of orientation changes for pre- and post-ablation bouts.
ii. p-values from one-tailed Komologorov-Smirnov between pre- and post-ablation values for each

individual behavioural kinematic.
iii. . Top, pre- and post-ablation histograms of cos(θ) values for bouts projected onto module 8, which contains a large fraction of ventromedial cells, and module 9, which contains a large fraction of "J cells". Bottom, the corresponding ROC curves for these values.

This indicates how cells in modules do not simply encode the production of single kinematics, but may also be responsible for inhibiting the production of undesired behaviours.

For some of these example "J cell" ablations there is also a shift in the distribution of cos(θ) values for Module 8. I think this is because the caudal, lateral non-RS cells and large nMLF cells ablated here are cell types which also feature in module 8 (Figure 3.4). It is therefore possible that some kinematics are altered and the projection of bouts onto module 8 changed.

4.3 Discussion

I find that ablation of specific cells within modules can produce behavioural deficits at the level of large-scale behaviours, such as OMR turning and orientation during prey capture, as well as at the level of individual behavioural kinematics and in terms of the kinematic modules.

In addition to this, I suspect that the neurons within a module show context-specific activity, and so cannot easily compensate for each another. In these analyses, I only studied bouts produced in specific contexts where I would expect to see the ablated cells active (Chapter 2). For example: leftward optomotor gratings elicit a high fraction of left turn bouts, which in turn show high recruitment probability of left ventromedial cells, and the first bout in a hunting routine is typically a J turn bout (McElligott and O'Malley, 2005), which show high recruitment probabilities for "J cells". Under these specific conditions, I find that ablation of subgroups of cells within a module produce kinematic deficits, thus suggesting that the remaining cells within a module cannot compensate across all conditions. This could be tested further by continuing the analyses to extend across different contexts.

4.3.1 Limitations and selectivity of the laser ablation method

Studies of the RS system in larval zebrafish have frequently employed laser ablations of cells to test the roles of specific neurons in behaviour. Over the years, this protocol has been refined and authors have made an effort to examine the mechanism and selectivity of these methods.

Laser ablation methods frequently determine cell death by a loss of fluorescence from the targeted cell. One concern with this is the possibility that targeted cells are not visible due to photobleaching rather than cell death. This was addressed in Liu and Fetcho's study where they used a confocal microscope to focus a laser at high intensity on individual RS cells labelled with dextran conjugated dyes until the cell was no longer visible (Liu and Fetcho, 1999). To demonstrate that this profound loss of fluorescence was due to cell death and not simply a consequence of photobleaching, they found that targeted cells also showed signs of necrosis such as the formation of large vacuoles. In addition to this, the authors colabelled RS neurons with Texas red (excitation $\lambda = 568$ nm) and calcium green (excitation $\lambda = 488$ nm), and ablated cells by imaging Texas red. They found that while targeted cells were visible immediately after the ablation by calcium green, they could no longer be observed with either dye at 24 hours post-ablation. Overall this suggests that the loss of fluorescence following exposure to a prolonged, high-power laser is an indicator of cell death.

One way that laser ablations can cause cell death is through photothermal damage (Vogel and Venugopalan, 2003). In this case, cell death is often identified by the presence of a localised plasma or "cavitation bubble". These markers of cell death following high power laser irradiation were observed in the experiments described in this chapter (Figure 4.1C), as well as from other studies using a similar two-photon laser ablation technique in larval zebrafish (Orger *et al.*, 2008; Huang *et al.*, 2013; Dunn *et al.*, 2016; Henriques *et al.*, 2019). 2P photothermal ablations have also been found to remove the cell soma and produce a gradual degeneration of the axon, as demonstrated by 2P laser ablations of larval zebrafish Mauthner cells in a recent (Hecker *et al.*, 2020). This indicates that 2P laser ablations classified as thermal ablations are capable of killing neurons and producing a total loss of their projections.

Following a 2P thermal ablation, it is possible that surrounding tissue might be damaged, and that there are physiological responses by local glia which will result

in a more widespread trauma than anticipated (Hill *et al.*, 2017). To test the spatial selectivity of the 2P laser ablation technique, Orger et al. ablated retrogradely labelled RS neurons in transgenic larval zebrafish with pan-neuronal fluorophore expression (Orger *et al.*, 2008). They found that only the targeted cells showed signs of successful ablation, whilst the immediately neighbouring cells appeared unaffected. Similarly, Liu and Fetcho confirmed the spatial selectivity of their method by successfully ablating single cells in densely labelled spinal cord without damage to adjacent cells (Liu and Fetcho, 1999). While these studies provide evidence for spatial selectivity using the laser ablation approach, at present less is known about the local physiological or neuroprotective changes following damage, and the consequences of this response.

Laser ablations are likely to be spatially selective for targeted fluorescent cells due to photochemical effects where the impact of the laser depends on an interaction with the fluorophore. For example, Liu and Fetcho found that conducting the laser ablation protocol in the same brain regions of unlabelled fish did not produce the same behavioural phenotypes that they observed when the protocol was conducted on fish with fluorescently labelled neurons (Liu and Fetcho, 1999). This is likely to be due to photochemical damage caused by the generation of reactive oxygen species following high-power excitation of the fluorophore. Evidence for such photochemical damage has been described for chromophore-assisted laser inactivation of proteins (Liao, Roider and Jay, 1994). By compounding these increased photochemical effects with the photothermal effects described above, it is highly likely that targeted laser ablations are more likely to inflict damage limited to fluorescent cells than non-fluorescent surrounding tissue.

4.3.2 Comparisons to published results

The ventromedial cell ablations described here are the same as those conducted by Orger and Huang (Orger *et al.*, 2008; Huang *et al.*, 2013). I was able to reproduce the published phenotypes of impaired turning towards the side of ablation during the OMR (Orger *et al.*, 2008), reduced θ1 angles towards the ablated side (Huang *et al.*, 2013). I also found reduced turning towards the contralateral side during the OMR, which I hypothesise as being due to ablating nearby non-RS cells.

In my experiments I also studied behaviour across a wider range of contexts than other studies. Ablation experiments from other research groups typically only study a single behavioural context, whilst I collected data in response to optomotor gratings, looming spots, and live prey. I could therefore extend the analyses presented here to look at the effects of these cell ablations across different behavioural contexts. For example, from preliminary analysis discussed in this chapter, I can already identify a potential behavioural alteration during hunting routines following ventromedial cell ablations, which has not been examined in earlier studies (Huang *et al.*, 2013).

4.3.3 Variability in behaviour between fish

RS ablation experiments in larval zebrafish reveal variability in the behaviour of individual animals. Some studies have attributed this to variations in the number of cells ablated, or perhaps the ablation of different functional groups within a cell type (Orger *et al.*, 2008; Huang *et al.*, 2013). Due to the variability in labelling of RS neurons through spinal cord backfill and in using the Gal4/UAS system it is of course inevitable that different numbers of RS cells are ablated between fish. In the case of ventromedial cell ablations, I have not found an obvious strong relationship between the number of cells ablated and the published turn deficiency phenotype. I suspect that a source of variability in these experiments is that they were conducted over the course of many months, and involved the use of *KalTA4u504* larvae from different generations of fish.

4.3.4 Effects on hunting and prey capture

Ablation of cells associated with J turns would be expected to impair prey capture. To study changes in hunting, I also counted the number of *Paramecia* consumed by ablated larvae at different time points. However, these experiments were very preliminary and I found that the rate of prey capture was largely dependent on the number of *Paramecia* initially available. As I did not control for this, and also tested a range of time points, it means that I cannot reliably compare this data across my experiments. For future studies I would make use of the protocol developed by

Antinucci et al., where all fish are presented with the same number of *Paramecia* to hunt (Antinucci, Folgueira and Bianco, 2019).

Chapter 5 High-speed population imaging using AOL microscopy

5.1 Introduction

The RS population spans ~150 μm in depth, meaning that conventional raster-scanning 2P microscopy allows for sampling only the cells present on any single z-plane. Using this technique, I have been able to identify patterns of neuronal recruitment for different swim types, and develop encoding models which describe RS and non-RS activity in terms of behavioural kinematics. However, in order to gain a better insight into the activity patterns, and inter-neuron timing of RS and non-RS activity during behaviour, it would be useful to conduct calcium imaging of the entire population simultaneously. Inter-neuron timing will be useful in determining how the activity of different neurons active at similar times relate to behaviour, and provide insight into the coordination of RS and non-RS activity. In doing so, one could also develop "decoding models" of RS activity, which would ultimately use the combined activity of RS and non-RS cells to predict motor output.

Volumetric functional imaging of calcium indicators is an increasingly popular methodology to achieve large-scale population imaging. However, the maximal imaging speed of techniques where the objective or z-stage are physically moved, such as via a piezeoelectric device, are limited by these objects' inertia. To overcome this, researchers are using remote focusing technologies to achieve volumetric imaging. The aim of these techniques is to optically adjust the focal plane without movement of the objective or sample. These include the use of acousto-optic deflectors (AODs) and electrically tunable lenses (ETL) (Kirkby, Srinivas Nadella and Silver, 2010; Grewe *et al.*, 2011). These remote focusing techniques are able to

achieve high-speed sampling rates and can rapidly image across sparse and spatially disperse points of interest.

In this chapter I present the developments I have made in adapting a custom-built AOL 2P microscope for use with larval zebrafish and show preliminary data collected from this set up. This microscope and acquisition software were produced by Professor Angus Silver's laboratory. Adjustments to these systems were primarily implemented by Dr Victoria Griffiths and Dr Antoine Valera.

5.2 Results

5.2.1 RS Patch-scanning using an AOL microscope

AOL microscopy uses remote focussing to enable high-speed 3D imaging. The AOL itself consists of 4 acousto-optic deflector (AOD) crystals arranged in a series (Figure 5.1A). By driving each AOD with ultrasonic sound waves, a diffraction grating can be produced across the crystal, ultimately resulting in rapid remote focussing to different 3D locations. Each pair of AOD crystals formed a lens: one which enabled the focus and steering of the laser along the X-Z plane, and one for the Y-Z plane. The two orthogonally aligned pairs together (i.e. the AOL) thus enable the sequential focussing to different region within the volumetric field of view regardless of the distance between points.

The AOL microscope system allows a high degree of flexibility in the scan modes used to acquire data (Figure 5.1B). The total acquisition time of these different scan modes is dependent on the number of points scanned. It takes 24 µs for a sound wave to fill the AOD and enable focussing to a new point. Assuming a constant dwell time, usually 4 µs, this means that the main limiting factor to acquisition speed is the number of separate points that need to be scanned. Scanning a straight line along the X axis after refocussing to a new point does not require the 24 µs AOD fill time. Therefore, scan modes with lower numbers of separate lines/points can achieve higher acquisition speeds.

In order to observe differences in the relative timing of activity of neurons as determined by the rapid rise in fluorescence of calcium indicators, high imaging speeds are preferable to capture these events, which for GCaMP6f is between

50 – 75 ms (Chen *et al.*, 2013). To accommodate the distributed arrangement of RS and non-RS cells, the most suitable scan modes are either patch or point scans manually cantered on cell soma (Figure 5.1B). However, due to specimen movement (discussed below) I decided to use rectangular patch scans in order to determine if soma moved out of the scanning patch during fish swimming (Figure 5.1C). Although this scan mode is slower than point scanning, due to the limiting kinetics of GCaMP6f, it did not seem necessary to scan at rates at the level of kHz for these preliminary experiments. A series of 68 rectangular patches could achieve imaging rates of 48 Hz which could just capture the rise times for GCaMP6f (Figure 5.1C).

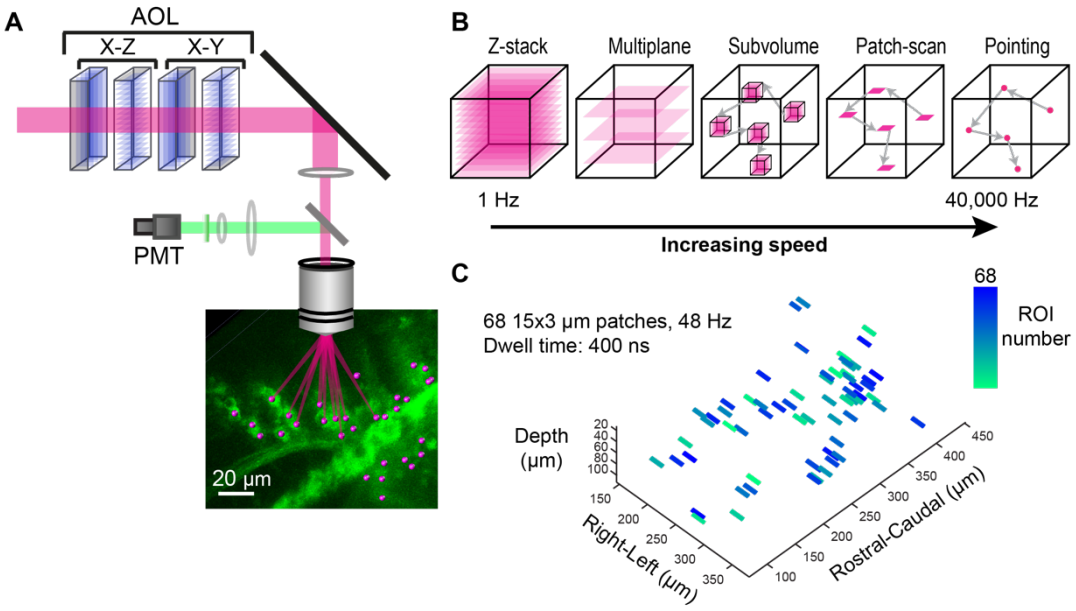

Figure 5.1AOL microscopy as a tool to study population activity of RS and non-RS neurons
A. Schematic of AOL and 3D random access point scanning. Cartoon illustrates the construction of the AOL and sampling of multiple points in a *KalTA4u508* larva.
B. Illustration of increased imaging speed across different scanning modes. Adapted from (Nadella *et al.*, 2016).
C. 15x3 µm patch scans centered around individual distributed across 3D space. Patches are coloured according to the order they were selected to improve patch visibility.

5.2.2 Online motion correction

As I was interested in studying RS population activity during swimming, movement produced by zebrafish swimming is a serious limitation for the consistent imaging of neurons. Although *post-hoc* processing techniques exist for correction of movement artefacts (Dombeck *et al.*, 2007), these can be slow and computationally intensive. Furthermore, with small patch sizes or even individual points, these cannot be easily implemented and will not account for axial movements in the Z-dimension. Due to locomotor outputs being repeatedly evoked during these experiments, there was therefore a need for a rapid online motion correction system.

This AOL microscope was primarily designed for *in vivo* calcium imaging of head-fixed rodents, and a motion correction system was developed to account for tissue displacements produced by animal movements, respiration, and heartbeats. This motion correction system involved the repeated tracking of a fluorescent object, such as a fluorescent bead, during functional imaging acquisition. Tracking consisted of imaging the reference object with a small X-Y patch followed by additional axial line scans in the Z dimension (Figure 5.2A). The 3D position of this object was computed and a movement "error" calculated by comparing this position with the original coordinates calculated from an initial reference image. This error was used to compute and apply an appropriate shift to the imaging field of view such that the functional scan positions were updated in line with the tissue movement (Figure 5.2B). As this periodic sampling of the reference object was interleaved with the functional point scans, this produced a trade-off between the time spent tracking the reference and the time available for imaging.

In order to apply this motion correction system to larval zebrafish I had to introduce a fluorescent structure into the volumetric field of view for use as a reference. For the system to work optimally, the reference object must be spherical and >4 μm in diameter. As visual stimuli were projected through a red filter to block green light affecting the signal PMT, this meant that imaging through the red channel was not possible. The fluorescent reference therefore had to be detectable under the green channel, and significantly brighter than GCaMP6f labelled neurons to prevent interference from neighbouring cells. I initially tried to label single neurons with a green dye via focal electroporation to use as a reference (data not shown), but

ultimately decided to use fluorescent beads due to their increased brightness, resistance to bleaching, and uniform shape.

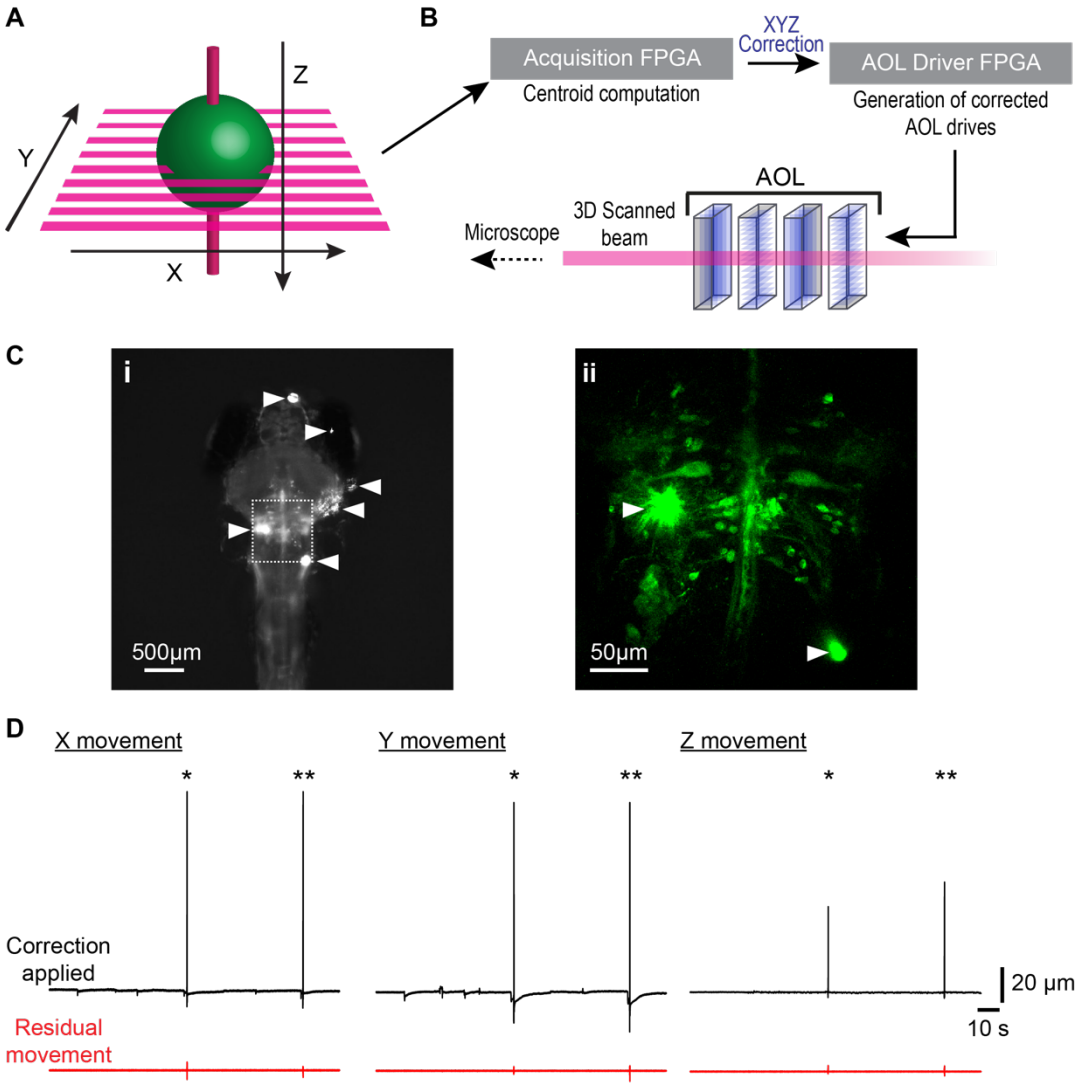

Figure 5.2 3D online motion correction
A. Cartoon of the XYZ tracking of a fluorescent reference (green).
B. Schematic depicting key parts of the motion correction system.
C. Fluorescent beads injected into a *KalTA4u508* larva. White arrowheads indicate fluorescent 5~um beads
i. Fluorescent micrograph of a fluorescent bead injected *KalTA4u508* larva at 6 dpf.
ii. Z-projection of area marked in i.
D. Detected and applied movement together with residual movement for X Y and Z dimensions. In black, the movement detected and correction applied by the system. In red, the residual movement that was not corrected. *, **, two large movements where the reference bead was ``lost" and the system reset to resume motion correction, producing a small residual movement.

Fish movement was found to be significantly greater than those recorded for *in vivo* experiments in mice. Implementation of the motion correction system using fluorescent beads in larval zebrafish identified displacements of up to 35 μm and speeds reaching up to 7 μm/ms during swim bouts (Griffiths et al., 2019, in preparation). To overcome this, the reference was sampled every 1 ms as opposed to every 2 ms, which was the typical sampling rate used for rodent experiments. This meant that achieving a working motion correction in larval zebrafish produced a 50% reduction in the duty cycle for functional imaging in comparison to rodent experiments.

These parameters produced a good motion correction of most swim bouts. High-speed tracking of the reference allowed for suitable corrections to be applied such that there was no residual movement for most swims (Figure 5.2D). We found that during particularly violent swims, the fluorescent bead was moved completely out of the reference field of view, which would cause the system to fail and the experiment to cease. To adapt for this, the motion correction system was paused when the bead moved out of the reference scan field of view, and resumed when it returned. This produced a small level of residual movement but meant that the experiment could still be continued without a total misalignment of imaging coordinates (* and **, Figure 5.2D).

This motion correction system relies on the assumption that the fluorescent reference does not drift in the specimen. This is because drift of the reference object would be detected by the system and result in the application of a similar shift to the functional imaging scans away from the true soma. We found that fluorescent reference drift did occur in some fish, and this drift varied between animals. We think that the severity of reference drift is related to where in the tissue the bead is placed, with dorsally located beads closer to the skin producing the most drift. To overcome this, we introduced a breakpoint between blocks of stimuli presentations where a cell within a patch could be registered to its original position at the start of the experiment. This adjustment could then be applied to all other patches such that cells remained in the field of view of functional imaging scans despite any minor changes to the position of the reference object.

5.2.3 RS population activity

Patches for functional imaging were manually positioned on cell soma. On average ~60 patches were used to sample RS and non-RS cells. This is a value significantly lower than the number of ROIs drawn in raster-scanning calcium imaging experiments. This is chiefly due to cells being singly marked rather than repeatedly if they occurred on a different z-planes. In addition, some patches contained more than one neuron. In these cases, patches were manually segmented into ROIs around individual cells after data acquisition. With the motion correction settings described above, this allowed me to conduct stable population imaging for ~1 hour together with visual stimulus presentation and behavioural recording (Figure 5.3A).

These fluorescence time series for individual neurons illustrate the different activity patterns of RS and non-RS neurons. Some neurons show highly synchronous activity, and there is also variation in which cells are active together (Figure 5.3). It is also possible to see occasions where the motion correction was paused and reset as small negative deflections in recorded fluorescence (red arrowheads Figure 5.3B). Overall, this reflects the ability to largely reproduce the calcium imaging experiments described in Chapter 2 using a high-speed microscope which can sample the activity of all neurons simultaneously.

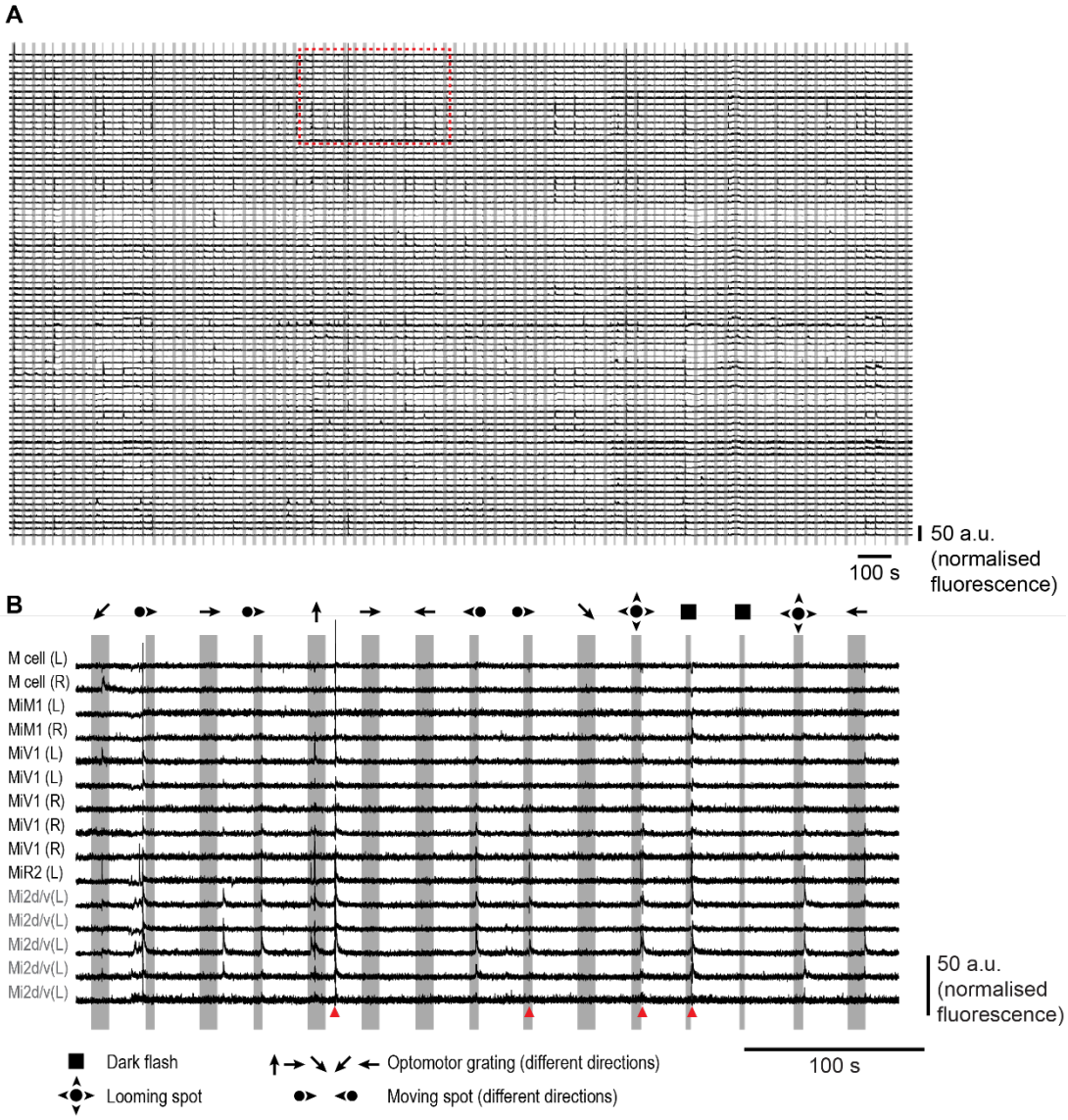

Figure 5.3 Stable recordings with online motion correction and patch scanning of soma
A. Population imaging of all ROIs from a single fish. Shaded regions indicate presentation of a visual stimulus. Neurons show different patterns of activity.
B. Close up view of marked region in A. Black cell labels indicate RS cells and grey labels non-RS cells Red arrowheads indicate periods where motion correction was paused and restarted

5.3 Discussion

In summary, this provides a methodology whereby calcium imaging can be conducted in larval zebrafish using an AOL microscope together with rapid, 3D online motion correction. This technique allows for high-speed calcium imaging of neuronal populations, which in turn could lead to the use of optical activity indicators with faster kinetics. Furthermore, the enhancements made to the online motion correction algorithm in order to account for the large and fast displacements observed in larval

zebrafish also serve to improve the algorithm's stability and usage in other model organisms.

5.3.1 Future technical developments

Due to complications with alignment of behavioural data to functional imaging data, tail tracking is not shown here. However, in future experiments it would be possible to identify the recruitment patterns for individual bout types and see how these compare to those developed from raster-scanning 2P experiments.

The increased temporal resolution achievable from AOL microscopy would allow calculation of the order and timing of activity between different RS and non-RS neurons during behaviour.

With fasters rates of scanning, one could also consider using fluorescent activity indicators with faster kinetics. New iterations of GECIs such as jGCaMP7 promise faster kinetics (Dana *et al.*, 2019), which could help in the calculation of timing between active neurons. However, preliminary attempts to use the jGCaMP7f variant in RS imaging experiments has identified a slower decay time than is measured for GCaMP6f, which could potentially mask the detection of subsequent spikes. Other rapid fluorescent activity indicators are genetically encoded voltage indicators (GEVIs) such as "Voltron" (Abdelfattah *et al.*, 2019). These would enable the identification of subthreshold events across neurons and provide insight into the true "linear drive" of neurons.

5.3.2 Decoding models

By sampling the activity of the whole RS population, one could develop predictive "decoding models". These would be models which use the activity of RS and non-RS neurons to predict the behavioural outcome. A first attempt to develop these models would be to use a linear classifier which predicts the bout type from neural activity. These decoding models would help to inform our understanding of the behavioural information represented across the RS/non-RS population.

Chapter 6 General Discussion

6.1 Summary

The aims of this thesis were to examine how locomotor outputs were encoded by the RS population and to develop new analytical and experimental tools with which to tackle this problem. My principal results are as follows:

1. Recruitment patterns of RS neurons to different bout types are distinct but partially overlapping, indicating that some neurons support kinematic features shared across bout types, while others support kinematic features unique to individual bout types. In addition, the recruitment probability of individual neurons for a particular bout type is not normally distributed, suggesting that neurons can show variable activity towards these behaviours.
2. The activity of individual neurons can be modelled using low-level kinematic features, and these can be used to identify kinematic modules. These modules represent the core kinematic combinations encoded by RS and non-RS activity, and combinations of these modules appear to support the production of various bout types.
3. RS and non-RS neurons within a cell label can contribute to multiple kinematic modules. This suggests that neurons within a group label can be functionally heterogeneous, and that singly-occurring neurons show broad kinematic tuning.
4. Selective ablation of a subgroup of neurons in a module can produce specific kinematic deficits for specific behavioural contexts where we expect these cells to be active. This suggests that neurons within a module cannot compensate fully compensate across all behavioural contexts.

5. Achievement of imaging tethered larval zebrafish, together with presentation of visual stimuli, using a high-speed 3D AOL microscope with rapid online 3D movement correction.

6.2 Reticulospinal neurons and locomotor control

6.2.1 Motor representation

The work presented in this thesis supports the developing view that larval zebrafish RS neurons are responsible for the production of specific kinematic features, as opposed to triggering entire locomotor behaviours or bout types. For example, there is currently strong evidence from various studies which are supported by this thesis, that the ventromedial (RoV3, MiV1, MIV2) neurons are key to ipsilateral turning by specifically affecting the θ1 kinematic feature (Orger *et al.*, 2008; Huang *et al.*, 2013). These neurons also show an increase in activity that corresponds with turn intensity (Figure 2.7B; Huang *et al.*, 2013). Studies in lamprey have identified RS neurons in the MRRN and rostral PRRN which show a similar functional role. In particular, RS neurons in these areas show an asymmetric bias in activity towards turn direction, and their activity level and fraction of recruited cells increases with turn amplitude (Fagerstedt *et al.*, 2001). While the exact kinematic contribution of these cells has not been investigated, it does appear likely that there are RS neurons which occupy similar functional roles across some vertebrate species. A low-level kinematic approach similar to that described here could therefore be beneficial to studies investigating motor control across different model organisms.

While this thesis has focused on the variety of kinematic outputs produced by RS neurons, an interesting avenue of research would be to examine any locomotor-halting RS neurons in the larval zebrafish hindbrain. “Stop” neurons have recently been identified in both rodents and lamprey (Bouvier *et al.*, 2015; Juvin *et al.*, 2016). These stop neurons have been identified in regions analogous to the inferior reticular nuclei: specifically the NRGi and NRMc in mice, and the PRRN in lamprey. Given their identification across these diverse vertebrate species, it is possible that there might exist similar neurons in larval zebrafish. In mice, these neurons have been identified as glutamatergic V2a neurons and so this population would act as a useful

starting point for this investigation. There currently exist transgenic zebrafish where V2a neurons can be selectively labelled (Kimura *et al.*, 2013), but it would be difficult to ascribe stop functions to neurons due to the slow imaging rates and GCaMP6f kinetics from our current 2P raster-scanning method.

6.2.2 Circuit architecture

The concept of a modular organisation to support rhythmic motor outputs has been put forward in the last few decades, and is exemplified by spinal cord CPGs (Büschges, 2005). Behavioural modules can be defined as groups of neurons which support distinct, coordinated motor outputs (Briggman and Kristan, 2008), and can thus be extended as a conceptual framework to be applied to other levels of the motor hierarchy, as well as to the production of patterned motor outputs across evolutionarily divergent species. For example, aside from spinal cord circuits (e.g. CPGs), modular circuits have also been identified in invertebrates, such as in the stomatogastric nervous system (STNS) of decapod crustaceans (Nusbaum and Beenhakker, 2002). The kinematic modules presented in Chapter 3 are a low-dimensional description of the combinations of kinematic features encoded by RS cell activity, and could provide an interesting perspective for a modular hindbrain circuit underlying motor output in a vertebrate species.

It is thought that these behavioural modules can be reconfigured and coordinated to ultimately produce distinct functional circuits and drive a wide range of behaviours. Studies in bullfrogs have identified topographically distinct spinal cord circuits (i.e. behavioural modules), associated with coherent activations of muscle groups or "muscle synergies", which in turn can be differentially combined and modulated to generate a range of kick behaviours (Saltiel, Tresch and Bizzi, 1998; Tresch, Saltiel and Bizzi, 1999; d'Avella, Saltiel and Bizzi, 2003). While this provides an example of how a modular organisation supports a variety of behaviours in spinal cord, it would be interesting to learn whether a similar principle is present in supraspinal descending pathways. Further studies in bullfrogs have attempted to investigate this by studying the motor outputs produced by stimulation of vestibular afferents (d'Avella and Bizzi, 1998). In this study, the authors found that the motor output produced by this stimulation was low-dimensional, and could therefore be a

product of combining multiple "primitive" spinal behavioural modules. While this supplied a promising start into the study of supraspinal behavioural modules, the work presented in this thesis provides evidence for behavioural modules in the reticulospinal pathway, and includes anatomical and kinematic descriptions for these modules. Furthermore, the preliminary analyses correlating these kinematic modules to bout types presented in Chapter 3 lends support to the idea that behavioural modules such as these can be differentially combined to produce diverse motor outputs.

Descriptions of modular circuits often feature neurons which participate in multiple modules. For example, in *Xenopus* embryos it has been found that many of the same spinal cord motorneurons and premotor interneurons are active for two kinematically distinct behaviours, swimming and struggling (Soffe, 1993). Similarly, studies in leeches have identified overlap in the networks which underlie the two mutually exclusive behaviours of swimming and crawling (Briggman and Kristan, 2006). Despite such behaviours being distinguishable from one another and even mutually exclusive, often they can involve the same muscle groups but activated in different patterns. It is therefore understandable that they might share some overlap in their motor instruction circuitry. The larval zebrafish RS system also shows a similar sharing of neurons for the production of distinct motor outputs, for example we find that recruitment maps for different bout types show some overlap (Chapter 2), and that RS neurons of the same cell type are often assigned to multiple different kinematic modules (Chapter 3).

Precisely how neurons achieve this flexible contribution to different behavioural modules, or how behavioural modules might be combined is not yet fully understood. Much of our present understanding about these phenomena has been learned from studies conducted in the STNS of lobsters and crabs, as it is possible to study most, if not all, stomatogastric ganglion neurons *in vitro*. Using these experimental preparations, it appears that behavioural modules can be reconfigured by many substances which can produce profound effects on motor outputs (Marder and Bucher, 2007). For example, a single hormone can convert two independent motor patterns into a different, conjoint rhythm by potentiating the synapses between neurons of the two original circuits (Dickinson, Mecsas and Marder, 1990). While such a level of detail is not yet known for the larval zebrafish RS pathway, this work on the STNS suggests that neuromodulators could have important effects on RS cell activity. One should note that there are likely to be some limits to how flexible

individual RS neurons are in contributing to different kinematic modules. This is due to RS cells having different morphologies and spinal cord targets, causing some restriction on which kinematic features could be produced. It would be interesting to learn both how neuromodulators might influence the kinematics encoded by a cell's activity, and thus explain our finding that RS neurons can contribute to multiple kinematic modules, and also how multiple kinematic modules could be deployed in a coordinated fashion.

Overall, the kinematic modules presented in this thesis provide an application of the modular circuit architecture described primarily for spinal and invertebrate circuits, to a vertebrate hindbrain population. The observations of these modular circuits described above, best resemble a reorganising circuit architecture (Morton and Chiel, 1994), as neurons can contribute to multiple kinematic modules and thus support a range of motor outputs. The approach of studying single cells and well-characterised, low-level behavioural measures used in this thesis can be applied to the study of locomotor control across species. Similarly, the growing focus on studying the functions of specific neurotransmitter classes, and the roles of neuromodulators on motor circuits for other model organisms will be an important area of study in larval zebrafish, and indeed one that has recently begun to be explored (Severi, Böhm and Wyart, 2018).

6.3 Future directions

Can we identify the putative local circuits which shape the coactivation of specific RS neurons? Volumetric calcium imaging using the AOL microscope would allow for simultaneous sampling of all RS and non-RS neurons. By using transgenic animals, we could also selectively image neurons of a particular neurotransmitter or transcription factor type, which would also allow us to consider these cells' morphology (Kinkhabwala *et al.*, 2011). Although calcium imaging would not allow us to confirm that cells are in synaptic contact with one another, it would still provide insight into the coordinated activity across neurons, which we could use to develop an understanding of potential hindbrain circuits.

With our understanding of RS encoding, could we construct a bout? For this effort, the information gained from AOL experiments with regard to inter-neuron timing and the development of decoding models would be most helpful. Through use of the KalTa4/UAS system, it is possible to express optogenetic activators (and inactivators) in RS and non-RS neurons. Patterned photostimulation, for example using a digital micromirror device or a spatial light modulator, could allow for spatially restricted photoactivation of specific neurons. By using targeted optogenetics, we could selectively stimulate the RS neurons we expect to underlie a certain behaviour and compare the outcome to our predictions.

How does reticulospinal encoding of kinematics change across development? While zebrafish larvae swim in discrete bouts, as they mature to adulthood, the motor outputs become more continuous. The RS population in adults is largely similar to that at larval stages, except for the addition of "tertiary" neurons (K. Lee and Eaton, 1991). It would be interesting to see how the RS neurons present in the larval stages might show alterations in activity and kinematic encoding to reflect this behavioural change, as well as study the functions of these tertiary neurons. However, there are many complications associated with imaging zebrafish beyond ~10 dpf such as: difficulty in tethering the animal, the need to supply oxygenated water to the animal, and increased scattering produced from a larger brain and increased overlaying tissue. To address the latter problem, developments in 3-photon microscopy techniques could allow for the improved imaging of juvenile or adult zebrafish brain structures.

Chapter 7 Materials & Methods

7.1 Animals

Zebrafish larvae were raised in fish facility water at 28°C on a 14/10 h light/dark cycle and fed *Paramecia* from 4 dpf. All larvae carried the *mitfa-/-* skin- pigmentation mutation (Lister *et al.*, 1999). All larvae were *Tg(- 2.5pvalb6:KalTA4)*^{u508Tg} (also known as *KalTA4u508*) and *Tg(UAS:GCaMP6f,cryaa:mCherry)*^{icm06Tg} (Knafo *et al.*, 2017). The *KalTA4u508* line was developed previously by the lab and is a putative enhancer trap generated by Tol2 transgenesis (Suster, Sumiyama and Kawakami, 2009). All experiments were conducted in accordance with the United Kingdom Animals (Scientific Procedures) Act, 1986.

7.2 Reticulospinal labelling by spinal cord injection

Larvae at 3-5 dpf were anaesthetised using MS222 (Sigma) and placed on a sylgard dish. Dextran-conjugated Texas Red dye (D3328, Invitrogen) dissolved in distilled water (0.04 mg/ul) was pressure injected into the spinal cord at somite 12 in order to label the majority of RS neurons as well as maximise survival following the procedure. Fish were allowed to recover for 12 hours before 2P imaging.

7.3 Raster-scanning two-photon microscopy

Two-photon (2P) imaging and targeted cell ablations were performed using a custom-built 2P microscope [Olympus XLUMPLFLN 20x 1.0 NA objective, 580 nm PMT dichroic (Semrock), 510/84 nm and 641/75 nm bandpass filters (Semrock),

Coherent Chameleon II ultrafast laser]. GCaMP6f was either imaged at an excitation wavelength of 920 nm for calcium imaging experiments (10.8 mW at sample), or at 800 nm for anatomical imaging with dextran-conjugated Texas Red (6.5 mW at sample).

7.3.1 Calcium imaging experiments

As the RS population spans over 100 μm in depth, calcium imaging was conducted at a range of successive focal planes ("z-planes") each separated by 5 μm. The imaging field of view was 369.6 μm by 231.54 μm. Imaging rate was 4.8 Hz, and scanning dwell time was 2.4 μs.

7.3.2 Calcium imaging post-processing and analysis

All calcium imaging analysis was performed using custom-written MATLAB (MathWorks) scripts. To correct for motion artefacts caused by animal movements and specimen drift, each frame was aligned to the mean time-series image for that specific z-plane as per (Bianco and Engert, 2015). Frames with more than a 5 μm shift were discarded and replaced with the mean image, and the entire epoch itself was discarded if it required more than 5 such replacements. Motion-corrected data was used for all further analysis. All ROIs were manually drawn and the appropriate RS or non-RS label assigned.

The fluorescence time series for each cell was extracted by computing the mean value of all pixels within the corresponding ROI binary mask for each time point. To calculate the inferred spiking of each ROI, I used the OASIS deconvolution algorithm (Friedrich, Zhou and Paninski, 2017). This also provided a binary measure of whether or not a cell was active during individual bouts.

7.3.3 Precise laser ablations

Control and ablated fish were mounted together on the same slide in 3% low melting point agarose. All fish underwent a pre-ablation anatomical z-stack at 6 dpf

to assess the completeness of the expression pattern. If expression was not complete, larvae were kept for use as controls. Targeted soma in ablated fish were individually spiral scanned for 140 ms at 800 nm, 150-200 mW (power at sample). Following this, an additional z-stack was taken to record the presence of an auto-fluorescent cavitation bubble which is a typical marker of a successful ablation. After recovery and behavioural testing at 7 dpf, ablated larvae received additional post-ablation anatomical z-stacks to confirm the absence of targeted cells.

7.4 Two-photon acousto-optic lens microscopy

A custom-built compact AOL 3D 2P microscope designed by Professor Angus Silver's lab at UCL was used for these experiments [Olympus XLUMPLFLN 20x 1.0 NA objective, 520/70 nm bandpass filter (Semrock), GaAsP PMTs (H7422, Hamamatsu), 80 MHz pulsed Ti:Sapphire laser (Coherent Chameleon)] (Kirkby, Srinivas Nadella and Silver, 2010; Nadella *et al.*, 2016). The AOL consisted of two orthogonally arranged pairs of acousto-optic deflectors (Gooch and Housego) and was controlled by a field-programmable gate array control board (FPGA; Xilinx VC707). To block red light from the projectors affecting the red PMT, an opaque disc was used. GCaMP6f was imaged at an excitation wavelength of 920 nm (15 mW at sample).

ROIs were manually marked together with their anatomical RS/non-RS ID as individual 3D points on cell soma using Vaa3D software (Peng *et al.*, 2010). For calcium imaging experiments, each point was used as the centre for a single XY scanned "patch". Patch size could be flexibly adjusted for each experiment but was roughly 15x3 μm in size. After acquisition, each patch was manually segmented into individual ROIs around cell soma. A fluorescence time series for each ROI was produced by taking the mean fluorescence for all pixels in that ROI for each time point.

7.4.1 Hindbrain injections of fluorescent beads

Larvae at 3 dpf were anaesthetised and mounted upright in 3% low-melting point agarose (Sigma-Aldrich). A small piece of agarose was cut away with an ophthalmic scalpel to expose an area of the larvae's head around the hindbrain

ventricle. Yellow-green fluorescent beads with a diameter of 5 μm (Invitrogen) were suspended in Ringer's solution (123 mM NaCl, 1.53 mM CaCl2, 4.96 KCl, pH 7.4), and pressure injected into the hindbrain ventricle. Once the presence of fluorescent beads in the hindbrain was confirmed, fish were unmounted from the agarose and left to recover until AOL calcium imaging experiments at 6-7 dpf. Fluorescent beads were used in rapid online movement correction during AOL microscopy.

7.4.2 Online motion correction

Rapid, online 3D motion correction was achieved using a movement correction system designed and implemented by Professor Angus Silver's lab (Griffiths et al., 2019, in preparation). In this system, a green fluorescent bead was used as a reference. An initial reference image of this bead and its 3D position was collected. During functional imaging, the reference bead was scanned every 1 ms in a small X-Y "patch" followed by a several axial scans. An FPGA calculated the 3D position of the object and computed an "error" between the current position and the coordinates from the original reference image. An appropriate coordinate shift was estimated, and this information was sent to the FPGA controlling the AOL 3D laser. This allowed for the AOL drives to be calculated such that the imaging field of view was adjusted in concert with the 3D bead movement.

7.5 Presentation of stimuli and behavioural tracking during two-photon microscopy

All stimuli presentation and behavioural tracking was implemented using custom LabVIEW and MATLAB software.

7.5.1 Stimulus presentation

A similar visual stimulus presentation and behavioural tracking system was used for both raster-scanning and AOL microscopy. All visual stimuli were designed using Psychophysics Toolbox (Brainard, 1997) and presented in a pseudo-random

order. Optomotor gratings had a period of 10 mm and moved at 1 cycle/s. A range of grating directions were shown to elicit a variety of different amplitude turns. Prey-like stimuli consisted of dark spots with a Weber contrast of -1 which moved at 30°/s either from left->right or right->left across ~200° of the frontal visual field. Looming stimuli were presented in front of the fish with an L/V ratio of either 255 or 490 ms. A 3 s whole-field dark flash was also presented. Frontal visual stimuli were back-projected (Optoma ML750ST) onto a curved screen placed in front of the larvae at a viewing distance of ~7 mm. A sub-stage projector (P2 Jr Pico Projector) was used to project stimuli onto a diffusive screen directly below the mounted larva via a cold mirror. Filters (Number 29 Wratten filter (Kodak)) were placed in front of all projectors to block green light from the PMT. The water-puff stimulus was only presented during raster-scanning 2P microscopy and was controlled by a solenoid valve (MHE2-MS1H-3/2G-QS-4-K, Festo), using a circuit design adapted from "Openspritzer" (Forman *et al.*, 2017).

For raster scanning microscopy, the visual stimuli were presented 3-5 times in a pseudo-random order for each z-plane. Stimuli were presented in successive 30.2 s "epochs" consisting of 145 imaging frames. The stimulus was presented on the 38th frame, thus allowing a reasonable number of frames for calculations of baseline fluorescence.

For AOL microscopy, the visual stimuli were presented in successive 30 s epochs. Visual stimuli were presented in a pseudo-random. The stimulus was presented 8 s after the start of the epoch.

7.5.2 Tethered behavioural tracking

For raster-scanning microscopy, the fish's eyes were illuminated at 720 nm and recorded at 60 Hz using an FL3-U3-13Y3M-C camera (Point Grey). Eye position was calculated online as the angle between the long axis of an ellipse fit to each eye and the midline of the fish's head. Positive angles describe movements clockwise from the midline, and negative angles for counterclockwise movements. The tail was illuminated by a single 850 nm LED, and imaged at 400-420 Hz by a sub-stage GS3-U3-41C6NIR-C camera (Point Grey). The tail was tracked online by using machine vision algorithms to describe it with 11 points, and the angles between the resulting

10 adjacent segments were calculated (Bianco et al., 2011). Positive angles describe rightward tail bends, and negative angles describe leftward bends.

7.5.3 Identification of bouts and extraction of kinematic features

Swim bouts were first identified using velocity thresholds (800°/s for bout onset, 200°/s for bout offset) applied to the smoothed absolute tail angular velocity traces. Any identified bouts with a duration <61 ms were removed. Tail beat frequency was calculated as the reciprocal of the mean full cycle period during a swim bout. Tail vigour was calculated by integrating the absolute tail angular velocity during a swim bout. Bout asymmetry measures the degree to which tail curvature during a bout shows the same laterality as that determined from the first half beat. Half-beats were identified as the peaks in the angular velocity trace of a bout and the peak angle along different segments of the tail (θ1), peak velocity (vel1), and period between each half beat was calculated. Fraction of curvature for the first half beat was calculated for rostral, middle and caudal parts of the tail.

For a list of kinematic features see Appendix A.

7.5.4 Clustering of tethered bouts (in collaboration with Dr Isaac Bianco)

Unsupervised clustering of tethered behaviour was performed using the data from 51 fish. Swim bouts were determined by calculating the tail velocity, and identifying periods where the velocity exceeded a particular threshold. All bouts were then described by a range of kinematic features (Appendix A), and PCA was performed to create a representation of bouts in terms of the first 20 principal components. The bouts from each fish in this principal component space were clustered separately using a hierarchical agglomerative clustering algorithm with Pearson's correlation distance metric (Bianco and Engert, 2015). In this procedure, the Pearson's correlation between all pairs of bouts were calculated. The two bouts with the highest correlation coefficient were joined into a cluster and the process repeated until no pairwise correlation exceeded a threshold of 0.7. These clusters were

themselves subjected to hierarchical clustering using the correlation distance between their centroids to produce a set of "superclusters". Individual bouts were reassigned if they were closer to the centroid of a different supercluster. Ultimately this produced 9 clusters or "bout types" which were assigned a name and laterality. To add bouts collected from subsequent fish to this classification, the correlation coefficient was calculated between each new bout and the bout type centroids. Bouts were assigned to the cluster with which they had the highest correlation coefficient. However, if bouts had < 0.85 correlation coefficient to any cluster centroid they were marked as unclassified.

7.6 Encoding model and kinematic module development (in collaboration with Dr Isaac Bianco and Dr James Fitzgerald)

Bouts from 61 fish were described in terms of 154 kinematic features (see Appendix A). For each fish, SVD was applied to the bouts sampled from a single imaging plane to produce orthogonal "kinematic modes". These modes were used as the input features for a generalised linear model. The model outputs were the inferred spike rates for each cell on that z-plane. As this took the form of a rate, these generalised linear models used the natural logarithm as a link function (Poisson regression). We used elastic-net regularised regression to improve the interpretability of these models (Zou and Hastie, 2005). Elastic-net models were fit using the "glmnet" package for MATLAB (Qian *et al.*, 2013). Parameters controlling the ratio of L1 vs L2 penalty (α) and degree of regularisation (λ) were selected to minimise cross-validated Poisson deviance. For each cell this produced a set of model coefficients corresponding to the kinematic modes. These were then transformed to produce model coefficients in terms of the original 154 kinematic features.

Cells were clustered according to their linear drive, computed by the multiplication of their model coefficients, to the kinematic features of 5,596 bouts. The range of bouts used to calculate this linear drive was produced by sampling <=100 bouts from 61 fish across the different bout types. Clustering was achieved by using a pairwise correlation clustering algorithm (Bianco and Engert, 2015).

7.7 Free-swimming behaviour

The behavioural tracking system used infrared illumination at 850 nm and larvae were tracked at 700 fps by camera (MC1362, Mikrotron). Larvae at 6-7 dpf were placed in 3.5 ml of system water in a 35 mm Petri dish. Fish were allowed to acclimatise for at least 5 min before behavioural recordings began and *Paramecia* were added to the Petri dish just before recordings started. Visual stimuli were presented beneath the fish using a projector (P2 Jr Pico Projector). If the fish moved within 11 mm from the edge of the dish, an inward moving concentric grating was presented to encourage the fish to return to the centre. Visual stimuli were only presented when the larva was in this central region and were presented in egocentric coordinates to the larva's position. The stimuli consisted of leftward and rightward optomotor gratings (period 10 mm moving at 1 cycle/s), and a left or a right looming spot with an L/V ratio of 255 ms. Gratings and looms were presented in alternation with an interval of 60 s. Each experiment typically lasted ~1 hour.

7.7.1 Analyses of free-swimming behaviour

Data analysis was performed using custom software written in LabView (National Instruments) and MATLAB (MathWorks). Eye and tail kinematics were tracked online. Images were first background-subtracted using a continuously updated background model. Images were then thresholded and the body centroid found by a particle detection routine for binary objects within a set area limit. Eye centroids were detected using a second threshold and particle detection procedure to identify centroids close to the body centroid. Body and eye orientations were computed using second- and third-order image moments. Eye orientation was calculated as the angle between the major axis of the eye and the body orientation vector, vergence angles were in turn calculated as the difference between left and right eye angles. To track the tail, consecutive annular line-scans were performed starting from the body centroid towards the tip of the tail to define 9 equidistant X-Y coordinates along the tail. Inter-segment angles were calculated between the 8 resulting segments.

Cumulative tail angle was calculated as the sum of these inter-segment angles. Positive tail angles indicate rightward tail bends and negative tail angles indicate leftward tail bends. Hunting routines were defined as periods of high ocular vergence. Periods of high ocular vergence were used to define hunting routines. As the vergence angle distribution was bimodal, a two-term Gaussian model was fit to this distribution. The threshold used to define hunting periods was calculated as being one standard deviation below the centre of the higher angle Gaussian.

Projection of individual bouts onto modules was achieved by describing bouts in terms of the same kinematic features as the kinematic modules and computing the normalised dot product.

7.8 Statistical analyses

To compare pre- and post-ablation metrics of gross behavioural measures, I used paired t-tests. One-tailed Kolmogorov-Smirnov tests were used to compare the distributions of individual kinematics between pre- and post-ablation conditions. p-values are stated in all cases. Values in figures represent mean ± standard deviation unless stated otherwise.

The normalised dot product between pre- and post-ablation bouts to an individual module was computed to produce cos(θ) values describing the separation between bouts and modules. ROC analysis was run to provide an AUC value indicating how well-separated these cos(θ) values are between pre- and post-ablation conditions. To determine the significance of these AUC values, I used a permutation test inspired by Britten *et al.*, 1993, where the ROC analysis was repeated 1000 times using shuffled class labels (pre or post ablation conditions). If the AUC value calculated from the real data lay outside the central 95% of the AUC values collected from the shuffled data, this value was considered to be significant.

References

Abdelfattah, A. S. *et al.* (2019) 'Bright and photostable chemigenetic indicators for extended in vivo voltage imaging.', *Science (New York, N.Y.)*. American Association for the Advancement of Science, 365(6454), pp. 699–704. doi: 10.1126/science.aav6416.

Ahrens, M. B. *et al.* (2012) 'Brain-wide neuronal dynamics during motor adaptation in zebrafish.', *Nature*. Europe PMC Funders, 485(7399), pp. 471–7. doi: 10.1038/nature11057.

Antinucci, P., Folgueira, M. and Bianco, I. H. (2019) 'A pretectal command system controls hunting behaviour', *bioRxiv*. Cold Spring Harbor Laboratory, p. 637215. doi: 10.1101/637215.

Bhattacharyya, K., McLean, D. L. and MacIver, M. A. (2017) 'Visual Threat Assessment and Reticulospinal Encoding of Calibrated Responses in Larval Zebrafish', *Current Biology*. doi: 10.1016/j.cub.2017.08.012.

Bianco, I. H. and Engert, F. (2015) 'Visuomotor Transformations Underlying Hunting Behavior in Zebrafish', *Current Biology*, 25(7), pp. 831–846. doi: 10.1016/j.cub.2015.01.042.

Bianco, I. H., Kampff, A. R. and Engert, F. (2011) 'Prey capture behavior evoked by simple visual stimuli in larval zebrafish', *Frontiers in Systems Neuroscience*, 5, p. 101. doi: 10.3389/fnsys.2011.00101.

Borla, M. A. *et al.* (2002) 'Prey capture by larval zebrafish: Evidence for fine axial motor control', *Brain, Behavior and Evolution*, 60(4), pp. 207–229. doi: 10.1159/000066699.

Bouvier, J. *et al.* (2015) 'Descending Command Neurons in the Brainstem that Halt Locomotion.', *Cell*. Cell Press, 163(5), pp. 1191–203. doi: 10.1016/j.cell.2015.10.074.

Brainard, D. H. (1997) 'The Psychophysics Toolbox', *Spatial Vision*, 10(4), pp. 433–436. doi: 10.1163/156856897X00357.

Briggman, K. L. and Kristan, W. B. (2006) 'Imaging dedicated and multifunctional neural circuits generating distinct behaviors.', *The Journal of neuroscience : the official journal of the Society for Neuroscience*. Society for Neuroscience, 26(42), pp. 10925–33. doi: 10.1523/JNEUROSCI.3265-06.2006.

Briggman, K. L. and Kristan, W. B. (2008) ‘Multifunctional Pattern-Generating Circuits’, *Annual Review of Neuroscience*. Annual Reviews , 31(1), pp. 271–294. doi: 10.1146/annurev.neuro.31.060407.125552.

Britten, K. H. *et al.* (1993) ‘A relationship between behavioral choice and the visual responses of neurons in macaque MT.’, *Visual neuroscience*, 13(1), pp. 87–100. Available at: http://www.ncbi.nlm.nih.gov/pubmed/8730992 (Accessed: 10 September 2019).

Brodin, L. *et al.* (1988) ‘Reticulospinal neurons in lamprey: transmitters, synaptic interactions and their role during locomotion.’, *Archives Italiennes de Biologie*. Pisa University Press, 126(4), pp. 317–345. Available at: http://www.architalbiol.org/index.php/aib/article/view/126317/860 (Accessed: 2 September 2019).

Brownstone, R. M. and Chopek, J. W. (2018) ‘Reticulospinal Systems for Tuning Motor Commands’, *Frontiers in Neural Circuits*. Frontiers Media SA, 12, p. 30. doi: 10.3389/FNCIR.2018.00030.

Budick, S. A. and O’Malley, D. M. (2000) ‘Locomotor repertoire of the larval zebrafish: swimming, turning and prey capture’, *Journal of Experimental Biology*, 203(17), pp. 2565–2579. Available at: http://jeb.biologists.org/content/203/17/2565 (Accessed: 10 June 2015).

Burgess, H. A. and Granato, M. (2007) ‘Modulation of locomotor activity in larval zebrafish during light adaptation.’, *The Journal of experimental biology*, 210(Pt 14), pp. 2526–39. doi: 10.1242/jeb.003939.

Büschges, A. (2005) ‘Sensory Control and Organization of Neural Networks Mediating Coordination of Multisegmental Organs for Locomotion’, *Journal of Neurophysiology*. American Physiological Society, 93(3), pp. 1127–1135. doi: 10.1152/jn.00615.2004.

Buss, R. R. and Drapeau, P. (2001) ‘Synaptic Drive to Motoneurons During Fictive Swimming in the Developing Zebrafish’, *Journal of Neurophysiology*. American Physiological SocietyBethesda, MD , 86(1), pp. 197–210. doi: 10.1152/jn.2001.86.1.197.

Cabelguen, J.-M., Bourcier-Lucas, C. and Dubuc, R. (2003) ‘Bimodal locomotion elicited by electrical stimulation of the midbrain in the salamander Notophthalmus viridescens.’, *The Journal of neuroscience : the official journal of the Society for Neuroscience*. Society for Neuroscience, 23(6), pp. 2434–9. doi:

10.1523/JNEUROSCI.23-06-02434.2003.

Caggiano, V. *et al.* (2018) 'Midbrain circuits that set locomotor speed and gait selection', *Nature*. Nature Publishing Group, 553(7689), pp. 455–460. doi: 10.1038/nature25448.

Capelli, P. *et al.* (2017) 'Locomotor speed control circuits in the caudal brainstem', *Nature*. Nature Publishing Group, 551(7680), p. 373. doi: 10.1038/nature24064.

Chen, T.-W. *et al.* (2013) 'Ultrasensitive fluorescent proteins for imaging neuronal activity.', *Nature*. Nature Publishing Group, a division of Macmillan Publishers Limited. All Rights Reserved., 499(7458), pp. 295–300. doi: 10.1038/nature12354.

d'Avella, A. and Bizzi, E. (1998) 'Low dimensionality of supraspinally induced force fields.', *Proceedings of the National Academy of Sciences of the United States of America*. National Academy of Sciences, 95(13), pp. 7711–4. doi: 10.1073/pnas.95.13.7711.

d'Avella, A., Saltiel, P. and Bizzi, E. (2003) 'Combinations of muscle synergies in the construction of a natural motor behavior', *Nature Neuroscience*. Nature Publishing Group, 6(3), pp. 300–308. doi: 10.1038/nn1010.

Daghfous, G. *et al.* (2016) 'Sensory Activation of Command Cells for Locomotion and Modulatory Mechanisms: Lessons from Lampreys', *Frontiers in Neural Circuits*, 10, p. 18. doi: 10.3389/fncir.2016.00018.

Dale, N. and Roberts, A. (1984) 'Excitatory amino acid receptors in Xenopus embryo spinal cord and their role in the activation of swimming.', *The Journal of Physiology*. John Wiley & Sons, Ltd (10.1111), 348(1), pp. 527–543. doi: 10.1113/jphysiol.1984.sp015123.

Dana, H. *et al.* (2019) 'High-performance calcium sensors for imaging activity in neuronal populations and microcompartments', *Nature Methods*. Nature Publishing Group, 16(7), pp. 649–657. doi: 10.1038/s41592-019-0435-6.

Deliagina, T. G. *et al.* (1992) 'Vestibular control of swimming in lamprey', *Experimental Brain Research*. Springer-Verlag, 90(3), pp. 499–507. doi: 10.1007/BF00230932.

Dickinson, P. S., Mecsas, C. and Marder, E. (1990) 'Neuropeptide fusion of two motor-pattern generator circuits', *Nature*. Nature Publishing Group, 344(6262), pp. 155–158. doi: 10.1038/344155a0.

Dombeck, D. A. *et al.* (2007) ‘Imaging large-scale neural activity with cellular resolution in awake, mobile mice.’, *Neuron*. NIH Public Access, 56(1), pp. 43–57. doi: 10.1016/j.neuron.2007.08.003.

Dunn, T. W. *et al.* (2016) ‘Neural Circuits Underlying Visually Evoked Escapes in Larval Zebrafish’, *Neuron*, 89(3), pp. 613–628. doi: 10.1016/j.neuron.2015.12.021.

Eaton, R. C., DiDomenico, R. and Nissanov, J. (1991) ‘Role of the Mauthner Cell in Sensorimotor Integration by the Brain Stem Escape Network’, *Brain, Behavior and Evolution*. Karger Publishers, 37(5), pp. 272–285. doi: 10.1159/000114365.

Esposito, M. S., Capelli, P. and Arber, S. (2014) ‘Brainstem nucleus MdV mediates skilled forelimb motor tasks’, *Nature*. Nature Publishing Group, 508(7496), pp. 351–356. doi: 10.1038/nature13023.

Fagerstedt, P. *et al.* (2001) ‘Lateral Turns in the Lamprey. II. Activity of Reticulospinal Neurons During the Generation of Fictive Turns’, *Journal of Neurophysiology*. American Physiological SocietyBethesda, MD , 86(5), pp. 2257–2265. doi: 10.1152/jn.2001.86.5.2257.

Forman, C. J. *et al.* (2017) ‘Openspritzer: an open hardware pressure ejection system for reliably delivering picolitre volumes’, *Scientific Reports*. Nature Publishing Group, 7(1), p. 2188. doi: 10.1038/s41598-017-02301-2.

Friedrich, J., Zhou, P. and Paninski, L. (2017) ‘Fast online deconvolution of calcium imaging data’, *PLOS Computational Biology*. Edited by J. Vogelstein. Public Library of Science, 13(3), p. e1005423. doi: 10.1371/journal.pcbi.1005423.

Gahtan, E., Tanger, P. and Baier, H. (2005) ‘Visual Prey Capture in Larval Zebrafish Is Controlled by Identified Reticulospinal Neurons Downstream of the Tectum’, *The Journal of Neuroscience*, 25(40), pp. 9294–9303. doi: 10.1523/JNEUROSCI.2678-05.2005.

Georgopoulos, A., Schwartz, A. and Kettner, R. (1986) ‘Neuronal population coding of movement direction’, *Science*, 233(4771).

Graham Brown, T. (1911) ‘The Intrinsic Factors in the Act of Progression in the Mammal’, *Proceedings of the Royal Society B: Biological Sciences*. The Royal Society London, 84(572), pp. 308–319. doi: 10.1098/rspb.1911.0077.

Grewe, B. F. *et al.* (2011) ‘Fast two-layer two-photon imaging of neuronal cell populations using an electrically tunable lens’, *Biomedical Optics Express*, 2(7), p. 2035. doi: 10.1364/BOE.2.002035.

Grienberger, C. and Konnerth, A. (2012) ‘Imaging calcium in neurons.’, *Neuron*, 73(5), pp. 862–85. doi: 10.1016/j.neuron.2012.02.011.

Griffiths, V. A. *et al.* (2019) *Real-time 3D movement correction for two-photon imaging in behaving animals*.

Grillner, S. *et al.* (1987) ‘Transmitters, membrane properties and network circuitry in the control of locomotion in lamprey’, *Trends in Neurosciences*. Elsevier, 10(1), pp. 34–41. doi: 10.1016/0166-2236(87)90123-8.

Grillner, S. *et al.* (2007) ‘Modeling a vertebrate motor system: pattern generation, steering and control of body orientation’, *Progress in Brain Research*, 165, pp. 221–234. doi: 10.1016/S0079-6123(06)65014-0.

Grillner, S. and Wallén, P. (1984) ‘How does the Lamprey Central Nervous System make the Lamprey Swim?’, *Journal of Experimental Biology*, 112(1).

Hecker, A. *et al.* (2020) ‘Removing a single neuron in a vertebrate brain forever abolishes an essential behavior.’, *Proceedings of the National Academy of Sciences of the United States of America*. National Academy of Sciences, 117(6), pp. 3254–3260. doi: 10.1073/pnas.1918578117.

Henriques, P. M. *et al.* (2019) ‘Nucleus Isthmi Is Required to Sustain Target Pursuit during Visually Guided Prey-Catching’, *Current Biology*. Cell Press, 29(11), pp. 1771-1786.e5. doi: 10.1016/J.CUB.2019.04.064.

Higashijima, S., Hotta, Y. and Okamoto, H. (2000) ‘Visualization of cranial motor neurons in live transgenic zebrafish expressing green fluorescent protein under the control of the islet-1 promoter/enhancer.’, *The Journal of neuroscience : the official journal of the Society for Neuroscience*. Society for Neuroscience, 20(1), pp. 206–18. Available at: http://www.ncbi.nlm.nih.gov/pubmed/10627598 (Accessed: 27 July 2016).

Hill, R. A. *et al.* (2017) ‘Targeted two-photon chemical apoptotic ablation of defined cell types in vivo’, *Nature Communications*. Nature Publishing Group, 8(1), p. 15837. doi: 10.1038/ncomms15837.

Huang, K.-H. *et al.* (2013a) ‘Spinal projection neurons control turning behaviors in zebrafish.’, *Current biology : CB*. Elsevier, 23(16), pp. 1566–73. doi: 10.1016/j.cub.2013.06.044.

Huang, K.-H. *et al.* (2013b) ‘Spinal projection neurons control turning behaviors in zebrafish.’, *Current biology : CB*, 23(16), pp. 1566–73. doi: 10.1016/j.cub.2013.06.044.

Huang, K. H. *et al.* (2013) 'Spinal projection neurons control turning behaviors in zebrafish', *Current Biology*. Elsevier, 23(16), pp. 1566–1573. doi: 10.1016/j.cub.2013.06.044.

Josset, N. *et al.* (2018) 'Distinct Contributions of Mesencephalic Locomotor Region Nuclei to Locomotor Control in the Freely Behaving Mouse', *Current Biology*, 28(6), pp. 884-901.e3. doi: 10.1016/j.cub.2018.02.007.

Juvin, L. *et al.* (2016) *A Specific Population of Reticulospinal Neurons Controls the Termination of Locomotion*, *Cell Reports*. Cell Press. Available at: https://www.sciencedirect.com/science/article/pii/S221112471630612X?via%3Dihub (Accessed: 17 June 2016).

K. Lee, R. K. and Eaton, R. C. (1991) 'Identifiable reticulospinal neurons of the adult zebrafish,Brachydanio rerio', *The Journal of Comparative Neurology*. Wiley Subscription Services, Inc., A Wiley Company, 304(1), pp. 34–52. doi: 10.1002/cne.903040104.

Kashin, S. M., Feldman, A. G. and Orlovsky, G. N. (1974) 'Locomotion of fish evoked by electrical stimulation of the brain', *Brain Research*. Elsevier, 82(1), pp. 41–47. doi: 10.1016/0006-8993(74)90891-9.

Kimmel, C. B., Patterson, J. and Kimmel, R. O. (1974) 'The development and behavioral characteristics of the startle response in the zebra fish.', *Developmental psychobiology*, 7(1), pp. 47–60. doi: 10.1002/dev.420070109.

Kimmel, C. B., Powell, S. L. and Metcalfe, W. K. (1982) 'Brain neurons which project to the spinal cord in young larvae of the zebrafish.', *The Journal of comparative neurology*, 205(2), pp. 112–27. doi: 10.1002/cne.902050203.

Kimura, Y. *et al.* (2013) 'Hindbrain V2a Neurons in the Excitation of Spinal Locomotor Circuits during Zebrafish Swimming', *Current Biology*. Cell Press, 23(10), pp. 843–849. doi: 10.1016/j.cub.2013.03.066.

Kinkhabwala, A. *et al.* (2011) 'A structural and functional ground plan for neurons in the hindbrain of zebrafish', *Proceedings of the National Academy of Sciences of the United States of America*, 108(3), pp. 1164–1169. doi: 10.1073/pnas.1012185108.

Kirkby, P. A., Srinivas Nadella, K. M. N. and Silver, R. A. (2010) 'A compact Acousto-Optic Lens for 2D and 3D femtosecond based 2-photon microscopy.', *Optics express*. Europe PMC Funders, 18(13), pp. 13721–45. Available at: http://www.ncbi.nlm.nih.gov/pubmed/20588506 (Accessed: 20 October 2018).

Knafo, S. *et al.* (2017) ‘Mechanosensory neurons control the timing of spinal microcircuit selection during locomotion.’, *eLife*. eLife Sciences Publications, Ltd, 6. doi: 10.7554/eLife.25260.

Koyama, M. *et al.* (2016) ‘A circuit motif in the zebrafish hindbrain for a two alternative behavioral choice to turn left or right’, *eLife*. eLife Sciences Publications Limited, 5, pp. 451–465. doi: 10.7554/eLife.16808.

Kriegeskorte, N. and Douglas, P. K. (2019) ‘Interpreting encoding and decoding models’, *Current Opinion in Neurobiology*. Elsevier Current Trends, 55, pp. 167–179. doi: 10.1016/J.CONB.2019.04.002.

Kupfermann, I. and Weiss, K. R. (1978) ‘The command neuron concept’, *Behavioral and Brain Sciences*, 1(01), p. 3. doi: 10.1017/S0140525X00059057.

Lau, J. Y., Bianco, I. H. and Severi, K. E. (2019) ‘Cellular-level understanding of supraspinal control: what can be learned from zebrafish?’, *Current Opinion in Physiology*. Elsevier, 8, pp. 141–145. doi: 10.1016/J.COPHYS.2019.01.013.

Lee, A. M. *et al.* (2014) ‘Identification of a Brainstem Circuit Regulating Visual Cortical State in Parallel with Locomotion’, *Neuron*. Cell Press, 83(2), pp. 455–466. doi: 10.1016/J.NEURON.2014.06.031.

Lein, E. S. *et al.* (2007) ‘Genome-wide atlas of gene expression in the adult mouse brain’, *Nature*. Nature Publishing Group, 445(7124), pp. 168–176. doi: 10.1038/nature05453.

Liao, J. C., Roider, J. and Jay, D. G. (1994) ‘Chromophore-assisted laser inactivation of proteins is mediated by the photogeneration of free radicals.’, *Proceedings of the National Academy of Sciences of the United States of America*. National Academy of Sciences, 91(7), pp. 2659–63. doi: 10.1073/pnas.91.7.2659.

Lister, J. A. *et al.* (1999) ‘nacre encodes a zebrafish microphthalmia-related protein that regulates neural-crest-derived pigment cell fate.’, *Development (Cambridge, England)*, 126(17), pp. 3757–67. Available at: http://www.ncbi.nlm.nih.gov/pubmed/10433906 (Accessed: 11 September 2019).

Liu, K. S. and Fetcho, J. R. (1999) ‘Laser Ablations Reveal Functional Relationships of Segmental Hindbrain Neurons in Zebrafish’, *Neuron*, 23(2), pp. 325–335. doi: 10.1016/S0896-6273(00)80783-7.

Marder, E. and Bucher, D. (2007) ‘Understanding Circuit Dynamics Using the Stomatogastric Nervous System of Lobsters and Crabs’, *Annual Review of Physiology*. Annual Reviews, 69(1), pp. 291–316. doi:

10.1146/annurev.physiol.69.031905.161516.

Marquart, G. D. *et al.* (2015) 'A 3D Searchable Database of Transgenic Zebrafish Gal4 and Cre Lines for Functional Neuroanatomy Studies', *Frontiers in Neural Circuits*. Frontiers, 9, p. 78. doi: 10.3389/fncir.2015.00078.

Marques, J. C. *et al.* (2018) 'Structure of the Zebrafish Locomotor Repertoire Revealed with Unsupervised Behavioral Clustering', *Current Biology*. Cell Press, 28(2), pp. 181-195.e5. Available at: https://www.sciencedirect.com/science/article/pii/S0960982217316044?via%3Dihub (Accessed: 5 January 2018).

McClenahan, P., Troup, M. and Scott, E. K. (2012) 'Fin-tail coordination during escape and predatory behavior in larval zebrafish.', *PloS one*, 7(2), p. e32295. doi: 10.1371/journal.pone.0032295.

McElligott, M. B. and O'Malley, D. M. (2005) 'Prey tracking by larval zebrafish: axial kinematics and visual control.', *Brain, behavior and evolution*. Karger Publishers, 66(3), pp. 177–96. doi: 10.1159/000087158.

Mearns, D. S. *et al.* (2019) 'Deconstructing hunting behavior reveals a tightly coupled stimulus-response loop', *bioRxiv*. Cold Spring Harbor Laboratory, p. 656959. doi: 10.1101/656959.

Metcalfe, W. K., Mendelson, B. and Kimmel, C. B. (1986) 'Segmental homologies among reticulospinal neurons in the hindbrain of the zebrafish larva.', *The Journal of comparative neurology*, 251(2), pp. 147–59. doi: 10.1002/cne.902510202.

Morton, D. W. and Chiel, H. J. (1994) 'Neural architectures for adaptive behavior', *Trends in Neurosciences*, 17(10), pp. 413–420. doi: 10.1016/0166-2236(94)90015-9.

Murakami, Y. and Kuratani, S. (2008) 'Brain segmentation and trigeminal projections in the lamprey; with reference to vertebrate brain evolution', *Brain Research Bulletin*. Elsevier, 75(2–4), pp. 218–224. doi: 10.1016/J.BRAINRESBULL.2007.10.057.

Nadella, K. M. N. S. *et al.* (2016) 'Random-access scanning microscopy for 3D imaging in awake behaving animals', *Nature Methods*. Nature Publishing Group, 13(12), pp. 1001–1004. doi: 10.1038/nmeth.4033.

Nakamura, Y. *et al.* (1989) 'Monosynaptic nigral inputs to the pedunculopontine tegmental nucleus neurons which send their axons to the medial reticular formation in the medulla oblongata. An electron microscopic study in the

cat', *Neuroscience Letters*. Elsevier, 103(2), pp. 145–150. doi: 10.1016/0304-3940(89)90566-1.

Nusbaum, M. P. and Beenhakker, M. P. (2002) 'A small-systems approach to motor pattern generation', *Nature*. Nature Publishing Group, 417(6886), pp. 343–350. doi: 10.1038/417343a.

O'Malley, D. M., Kao, Y.-H. and Fetcho, J. R. (1996) 'Imaging the Functional Organization of Zebrafish Hindbrain Segments during Escape Behaviors', *Neuron*, 17(6), pp. 1145–1155. doi: 10.1016/S0896-6273(00)80246-9.

Orger, M. B. *et al.* (2008) 'Control of visually guided behavior by distinct populations of spinal projection neurons.', *Nature neuroscience*. Nature Publishing Group, 11(3), pp. 327–33. doi: 10.1038/nn2048.

Peng, H. *et al.* (2010) 'V3D enables real-time 3D visualization and quantitative analysis of large-scale biological image data sets', *Nature Biotechnology*. Nature Publishing Group, 28(4), pp. 348–353. doi: 10.1038/nbt.1612.

Pnevmatikakis, E. A. A. *et al.* (2016) 'Simultaneous Denoising, Deconvolution, and Demixing of Calcium Imaging Data', *Neuron*. Elsevier, 89(2), pp. 285–299. doi: 10.1016/j.neuron.2015.11.037.

Qian, J. *et al.* (2013) *Glmnet for Matlab*. Available at: https://web.stanford.edu/~hastie/glmnet_matlab/ (Accessed: 31 August 2019).

Ray, D. Le *et al.* (2010) 'A neuronal substrate for a state-dependent modulation of sensory inputs in the brainstem', *European Journal of Neuroscience*. John Wiley & Sons, Ltd (10.1111), 32(1), pp. 53–59. doi: 10.1111/j.1460-9568.2010.07276.x.

Roseberry, T. K. *et al.* (2016) 'Cell-Type-Specific Control of Brainstem Locomotor Circuits by Basal Ganglia', *Cell*. Elsevier, 164(3), pp. 526–537. doi: 10.1016/j.cell.2015.12.037.

Saltiel, P., Tresch, M. C. and Bizzi, E. (1998) 'Spinal Cord Modular Organization and Rhythm Generation: An NMDA Iontophoretic Study in the Frog', *Journal of Neurophysiology*. American Physiological SocietyBethesda, MD , 80(5), pp. 2323–2339. doi: 10.1152/jn.1998.80.5.2323.

Severi, K. E. *et al.* (2014) 'Neural Control and Modulation of Swimming Speed in the Larval Zebrafish', *Neuron*, 83(3), pp. 692–707. doi: 10.1016/j.neuron.2014.06.032.

Severi, K. E., Böhm, U. L. and Wyart, C. (2018) 'Investigation of hindbrain

activity during active locomotion reveals inhibitory neurons involved in sensorimotor processing.', *Scientific reports*. Nature Publishing Group, 8(1), p. 13615. doi: 10.1038/s41598-018-31968-4.

Sherrington, C. S. (1911) *The integrative action of the nervous system.* New Haven: Yale University Press. doi: 10.1037/13798-000.

Shik, M. L., Severin, F. V and Orlovsky, G. N. (1969) 'Control of walking and running by means of electrical stimulation of the mesencephalon.', *Electroencephalography and clinical neurophysiology*, 26(5), p. 549. Available at: http://www.ncbi.nlm.nih.gov/pubmed/4181500 (Accessed: 6 October 2018).

Sirota, M. G., Di Prisco, G. V. and Dubuc, R. (2000) 'Stimulation of the mesencephalic locomotor region elicits controlled swimming in semi-intact lampreys', *European Journal of Neuroscience*. Wiley/Blackwell (10.1111), 12(11), pp. 4081–4092. doi: 10.1046/j.1460-9568.2000.00301.x.

Skinner, R. D. and Garcia-Rill, E. (1984) 'The mesencephalic locomotor region (MLR) in the rat.', *Brain Research*. Elsevier, 323(2), pp. 385–9. doi: 10.1016/0006-8993(84)90319-6.

Soffe, S. R. (1993) 'Two distinct rhythmic motor patterns are driven by common premotor and motor neurons in a simple vertebrate spinal cord.', *The Journal of neuroscience : the official journal of the Society for Neuroscience*. Society for Neuroscience, 13(10), pp. 4456–69. doi: 10.1523/JNEUROSCI.13-10-04456.1993.

Steeves, J. D. and Jordan, L. M. (1980) 'Localization of a descending pathway in the spinal cord which is necessary for controlled treadmill locomotion', *Neuroscience Letters*. Elsevier, 20(3), pp. 283–288. doi: 10.1016/0304-3940(80)90161-5.

Steeves, J. D. and Jordan, L. M. (1984) 'Autoradiographic demonstration of the projections from the mesencephalic locomotor region', *Brain Research*. Elsevier, 307(1–2), pp. 263–276. doi: 10.1016/0006-8993(84)90480-3.

Suster, M. L., Sumiyama, K. and Kawakami, K. (2009) 'Transposon-mediated BAC transgenesis in zebrafish and mice.', *BMC genomics*. BioMed Central, 10, p. 477. doi: 10.1186/1471-2164-10-477.

Takakusaki, K. *et al.* (2016) 'Brainstem control of locomotion and muscle tone with special reference to the role of the mesopontine tegmentum and medullary reticulospinal systems.', *Journal of neural transmission (Vienna, Austria : 1996)*. Springer, 123(7), pp. 695–729. doi: 10.1007/s00702-015-1475-4.

Temizer, I. *et al.* (2015) 'A Visual Pathway for Looming-Evoked Escape in Larval Zebrafish', *Current Biology*, 25(14), pp. 1823–1834. doi: 10.1016/j.cub.2015.06.002.

Thiele, T. R., Donovan, J. C. and Baier, H. (2014) 'Descending control of swim posture by a midbrain nucleus in zebrafish', *Neuron*, 83(3), pp. 679–691. doi: 10.1016/j.neuron.2014.04.018.

Tresch, M. C., Saltiel, P. and Bizzi, E. (1999) 'The construction of movement by the spinal cord', *Nature Neuroscience*. Nature Publishing Group, 2(2), pp. 162–167. doi: 10.1038/5721.

Valverde, F. (1961) 'Reticular formation of the pons and medulla oblongata. A Golgi study', *The Journal of Comparative Neurology*. John Wiley & Sons, Ltd, 116(1), pp. 71–99. doi: 10.1002/cne.901160105.

Vladimirov, N. *et al.* (2018) 'Brain-wide circuit interrogation at the cellular level guided by online analysis of neuronal function', *Nature Methods*. Nature Publishing Group, 15(12), pp. 1117–1125. doi: 10.1038/s41592-018-0221-x.

Vogel, A. and Venugopalan, V. (2003) 'Mechanisms of Pulsed Laser Ablation of Biological Tissues', *Chemical Reviews*. American Chemical Society, 103(2), pp. 577–644. doi: 10.1021/CR010379N.

Wiersma, C. A. G. and Ikeda, K. (1964) 'Interneurons commanding swimmeret movements in the crayfish, Procambarus clarki (girard)', *Comparative Biochemistry and Physiology*. Pergamon, 12(4), pp. 509–525. doi: 10.1016/0010-406X(64)90153-7.

Yaksi, E. and Friedrich, R. W. (2006) 'Reconstruction of firing rate changes across neuronal populations by temporally deconvolved Ca2+ imaging', *Nature Methods*. Nature Publishing Group, 3(5), pp. 377–383. doi: 10.1038/nmeth874.

Zompa, I. C. and Dubuc, R. (1996) 'A mesencephalic relay for visual inputs to reticulospinal neurones in lampreys', *Brain Research*. Elsevier, 718(1–2), pp. 221–227. doi: 10.1016/0006-8993(96)00131-X.

Zottoli, S. J. and Faber, D. S. (2000) '■ Review : The Mauthner Cell: What Has it Taught us?', *The Neuroscientist*. Sage PublicationsSage CA: Thousand Oaks, CA, 6(1), pp. 26–38. doi: 10.1177/107385840000600111.

Zou, H. and Hastie, T. (2005) 'Regularization and Variable Selection via the Elastic Net', *Journal of the Royal Statistical Society. Series B (Statistical Methodology)*, 67(2), pp. 301–320. Available at:

https://www.jstor.org/stable/3647580?seq=1#metadata_info_tab_contents (Accessed: 1 August 2019).

Appendix A. Kinematic features

Kinematic feature	Brief description
vig120	Swim vigour for first 120 ms of bout
vigmax	Maximum vigour for bout
intcum60ms*	Laterality for first 60 ms of bout
morphAI*	Tail asymmetry index
morphAI2*	Tail asymmetry index
prepeak	Maximum cumulative angle "prepeak" preceding the first half beat
max TBF	Maximum tail beat frequency of bout
mean TBF	Mean tail beat frequency of bout
max angle	Maximum cumulative tail angle of bout
max vel	Maximum tail velocity of bout
θ1 segment *n**	Maximum tail angle during the first half beat for segments *n* = 5,6,7,8,9,10,11
θ2 segment *n**	Maximum tail angle during the second half beat for segments *n* = 5,6,7,8,9,10,11
θ3 segment *n**	Maximum tail angle during the third half beat for segments *n* = 5,6,7,8,9,10,11
θ4 segment *n**	Maximum tail angle during the fourth half beat for segments *n* = 5,6,7,8,9,10,11
vel1 segment *n**	Maximum velocity during the first half bout for segments *n* = 5,6,7,8,9,10,11
vel2 segment *n**	Maximum velocity during the second half bout for segments *n* = 5,6,7,8,9,10,11
vel3 segment *n**	Maximum velocity during the third half bout for segments *n* = 5,6,7,8,9,10,11

vel4 segment *n**	Maximum velocity during the fourth half bout for segments *n* = 5,6,7,8,9,10,11
period 1	Time between peak angle of first and second half beats
period 2	Time between peak angle of second and third half beats
period 3	Time between peak angle of third and fourth half beats
period 4	Time between peak angle of fourth and fifth half beats
fcR1	Fraction of tail curvature for first half beat of bout in rostral parts of tail (segment 5)
fcM1	Fraction of tail curvature for first half beat of bout in middle parts of tail (segment 8)
fcC1	Fraction of tail curvature for first half beat of bout in caudal parts of tail (segment 11)
ratio tp1*	First half beat trough divided by first half beat θ1 segment 11
ratio period 2v1	period 2 divided by period 1
ratio theta 2v1*	θ2 segment 11 divided by θ1
Lpost*	Left eye angle at end of bout
Ldelta*	Change in left eye angle between bout start and end
Rpost*	Right eye angle at end of bout
Rdelta*	Change in right eye angle between bout start and end
Vpost*	Vergence angle at end of bout
Vdelta*	Change in vergence angle between bout start and end
duration	Duration of bout
fft spectra *n*	Fast Fourier transform of cumulative tail angle, power at *n* = 1-70 Hz

* Kinematics which are separated into left and rightward values for use in the development of encoding models (Chapter 3), and for single feature and kinematic module projection analysis (Chapter 4).

Appendix B. Review 1

Title: Cellular-level understanding of Supraspinal control: what can be learned from zebrafish?

Journal: Current Opinions in Physiology

Year: 2019

Authors: Joanna YN Lau[1], Isaac H Bianco[1] & Kristen E Severi[2]

1 Department of Neuroscience, Physiology & Pharmacology, University College London, WC1E 6BT, United Kingdom
2 Federated Department of Biological Sciences, New Jersey Institute of Technology, University Heights, Newark, NJ, 07102, USA

DOI: 10.1016/j.cophys.2019.01.013